

## Distribution Agreement

In presenting this thesis or dissertation as a partial fulfillment of the requirements for an advanced degree from Emory University, I hereby grant to Emory University and its agents the non-exclusive license to archive, make accessible, and display my thesis or dissertation in whole or in part in all forms of media, now or hereafter known, including display on the world wide web. I understand that I may select some access restrictions as part of the online submission of this thesis or dissertation. I retain all ownership rights to the copyright of the thesis or dissertation. I also retain the right to use in future works (such as articles or books) all or part of this thesis or dissertation.

Signed by:  
Signature:   
7DD4CD88FDF34BA...

Christine Bowen  
Name

8/28/2024 | 11:57 AM EDT  
Date

**Title** Kv1.3 potassium channel regulation of microglial inflammatory response

**Author** Christine Bowen

**Degree** Doctor of Philosophy

**Program** Biological and Biomedical Sciences  
Biochemistry, Cell and Developmental Biology

**Approved by the Committee**

Signed by:  Srikant Rangaraju  
092221B60AD5439... *Advisor*

DocuSigned by:  Nicholas Seyfried  
4DDA20DAD30547B... *Advisor*

DocuSigned by:  Victor Faundez  
8525D8A9E8FE4A0... *Committee Member*

DocuSigned by:  Yue Feng  
337F8F9625844A4... *Committee Member*

Signed by:  Michael Koval  
0E321480F386404... *Committee Member*

DocuSigned by:  Jennifer Kwong  
3694F1918F48472... *Committee Member*

**Accepted by the Laney Graduate School:**

---

Kimberly Jacob Arriola, Ph.D, MPH  
Dean, James T. Laney Graduate School

---

Date

**Kv1.3 potassium channel regulation of microglial inflammatory response**

By

Christine Alyssia Bowen

B.S. Appalachian State University 2017

Advisors: Srikant Rangaraju, MBBS, MS and Nicholas Seyfried, PhD

An abstract of

A dissertation submitted to the Faculty of the James T. Laney School of Graduate Studies of  
Emory University

in partial fulfillment of the requirements for the degree of

Doctor of Philosophy

in Biochemistry, Cellular, and Developmental Biology

2024

## ABSTRACT

### **Kv1.3 potassium channel regulation of microglial inflammatory response**

By: Christine Alyssia Bowen

Microglia are the resident macrophages in the brain. During the lifespan, microglia have a distinct heterogeneity, where microglia can transition to different states over time. In disease conditions, like Alzheimer's Disease, microglia shift toward a disease associated state, referred to as disease associated microglia (DAM). DAM have distinct expression profiles, where there is an activation of the TLR2 response, resulting an increase in inflammatory cytokines (*e.g.* TNF- $\alpha$ , IL-1 $\beta$ , STAT1). The transition to this state reduces the ability to clear A $\beta$  plaques and promote brain homeostasis, while increasing the detrimental effects of AD. Our lab shows that the Kv1.3 potassium channel is highly present on the cell surface of these DAM. Treatment via blockade of the channel results in a reduction of the detrimental components of DAM. However, it remains unclear how Kv1.3 influences the inflammatory response of microglia. We hypothesize that Kv1.3 directly interacts with key signaling proteins during a microglial immune response. To test this hypothesis, we utilized proximity-labeling and mass spectrometry to evaluate proteins interacting with Kv1.3. We determined that around 200 proteins interact with the N-terminus of Kv1.3 and is largely responsible for protein processing and trafficking Kv1.3 to the mitochondria. During an immune response, the C-terminus of Kv1.3 interacts with key immune signaling proteins (*e.g.* TLR2, STAT1, C3). Some of the C-terminal interactors (around 70 proteins) are dependent on the PDZ-binding domain, such that these proteins no longer interact with Kv1.3 when the PDZ-binding domain is removed. Overall, we highlight that Kv1.3 directly interacts with key immune signaling proteins during a microglial inflammatory response. This thesis will enable better understanding for how Kv1.3 influences microglial response and can be used to evaluate how targeting Kv1.3 could be beneficial for the treatment of neuroinflammatory diseases.

**Kv1.3 potassium channel regulation of microglial inflammatory response**

By

Christine Alyssia Bowen

B.S. Appalachian State University 2017

Advisors: Srikant Rangaraju, MBBS, MS and Nicholas Seyfried, PhD

A dissertation submitted to the Faculty of the James T. Laney School of Graduate Studies of  
Emory University

in partial fulfillment of the requirements for the degree of

Doctor of Philosophy

in Biochemistry, Cellular, and Developmental Biology

2024

## ACKNOWLEDGEMENTS

Research from this publication was supported by the National Institute of Aging and the National Institute of Neurological Disease and Stroke of the National Institute of Health: 5T32GM135060-03 (CAB), 1F31AG074665-01 (CAB), R01NS114130 (SR), R01AG075820 (SR, NTS, LBW), R01 ES034796 (EW), and 1RF1AG060285 (VF). NS100294 (HW). In addition, this work was also supported National Scientific Fund: NSF CAREER 1944053 (LBW). This research was supported by the Viral Vector Core of the Emory Center for Neurodegenerative Disease Core Facilities, the Emory Flow Cytometry Core (EFCC), the Custom Cloning Core Division of Emory Integrated Genomics Core (EIGC), and the Integrated Cellular Imaging Core (ICI) all at Emory University. The author appreciates Christina Ramelow for helping design a figure, and Biorender for software to create images. Upasna Sirivastava assisted with uploading and preparing data files for PRIDE. Eric Dammer assisted with annotation of one hit wonders using this github: <https://github.com/edammer/MQ1pepAnnotate/>

There are many people I would like to thank for assisting me during these past several years of my graduate studies. First, I'd like to thank my friends and family, who supported me during the most difficult times in my studies as well as my personal life. I'd next like to thank my mentors: Srikant Rangaraju and Nicholas Seyfried. Dr. Seyfried offered support for many of my mass spectrometry experiments as well as welcomed me into his lab. He provided professional support on all of my experiments and guided me during career development. Dr. Rangaraju was instrumental in support as well. He guided me in all of my writing, experimental design, as well as offering support throughout my career. From the Wulff lab in UCSD, I'd like to thank Heike Wulff and Hai Nguyen. Dr. Wulff offered support and guidance throughout my project. Dr. Nguyen offered support through completing the electrophysiology and analysis. I

have the greatest appreciation for both of my students, Hollis Zeng and Young Lin, for providing support and allowing me to teach them throughout my experiments. I also would like to acknowledge the efforts of Brendan Tobin in the Wood lab at GA Tech. Brendan processed the Luminex samples and Dr. Wood provided guidance on interpretation of results. I'd like to thank Pritha Bagchi for teaching me how to process and analyze mass spectrometry data and for Duc Duong for running the mass spectrometry machine. Aditya Natu was instrumental with analysis and figure development. I'd like to thank Dr. Espinosa-Garcia for completing the mitochondrial fractions and running western blots on the material as well as Dr. Werner in the Faundez lab for teaching and supporting her. For the completion of the pSTAT1 assays, I'd like to thank Dr. Kumari and Amanda Brandelli. I'm especially grateful to Hailian Xiao for offering support throughout all of my thesis work. I'd like to thank my fellow graduate students in the lab: Dr. Juliet Santiago, Dr. Sydney Sunna, Christina Ramelow, and Sarah Shapley for offering all forms of support during my career.

## TABLE OF CONTENTS

I.	INTRODUCTION.....	1
i.	Microglia are the immune cells of the brain.....	1
a.	Microglia are derived from macrophage progenitors in early development.....	2
b.	Molecular and functional heterogeneity of microglia.....	2
c.	Microglia nomenclature and terminology.....	5
d.	Microglia during inflammation have a distinct phenotype.....	7
e.	<i>In vitro</i> models for microglial activation and induction of inflammatory response.....	8
f.	Lipopolysaccharide (LPS) as a model for inflammation.....	11
g.	Microglia in Neuroinflammatory disease and inflammation.....	12
h.	Immune Cells contribute significantly to the disease progression of Alzheimer’s Disease.....	13
i.	Microglia have a distinct disease-associated state in AD.....	14
j.	Mouse models of AD have similar features to human AD.....	16
ii.	Kv1.3 potassium channel influences microglial response.....	18
a.	The Kv1.3 potassium channel is highly expressed by microglia in neuroinflammatory states.....	18
b.	The Kv1.3 potassium channel allows for efflux of potassium in immune cells.....	19
c.	Kv1.3 is present in the mitochondria and alters metabolism in cells...20	

d. Kv1.3 activity increases in T-lymphocyte and macrophage inflammatory responses.....	22
e. Kv1.3 channels in the brain .....	23
f. Knock out (KO) of Kv1.3 in mouse models highlights a reduction of inflammatory response.....	24
g. Blockade of Kv1.3 alters inflammatory responses.....	25
h. KV1.3 interactors in immune cells.....	26
i. Kv1.3 as a potential for the treatment of AD.....	27
j. Current knowledge gaps related to Kv1.3 channels in microglia.....	27
k. Central Hypothesis: Kv1.3 directly interacts with immune signaling proteins in microglia during neuroinflammatory diseases.....	31

II. CHAPTER II: Proximity labeling proteomics reveals Kv1.3 potassium channel

immune interactors in microglia.....	31
i. Abstract.....	32
ii. Graphical Abstract.....	33
iii. Introduction.....	33
iv. Experimental Procedures.....	36
v. Results.....	59
a. Validation of N and C terminus TurboID fusion constructs for mapping the Kv1.3 interactome in HEK-293 cells.....	59
b. Kv1.3 Amino and Carboxyl terminal fusions with TurboID identifies distinct domain-interacting proteins in HEK-293 cells.....	63

c.	Generation and validation of stably transduced BV-2 microglial lines expressing N and C term Kv1.3-TurboID fusions.....	67
d.	Identification of Kv1.3 channel domain-specific protein interactors and molecular pathways in BV-2 microglia.....	70
e.	Pro-inflammatory activation preferentially modifies the C-terminal interactome of Kv1.3 channels in microglia.....	74
f.	Kv1.3 C-terminal inflammatory interactors dependent on the PDZ binding domain.....	75
g.	Kv1.3 channel is present in mitochondria-enriched fractions in microglia .....	78
h.	Verification of interactions of Kv1.3 with C3 and pSTAT1 via the C terminal domain.....	79
vi.	Discussion.....	85
vii.	Conclusion.....	90
viii.	Supplemental Figures.....	91
III.	CHAPTER III: DISCUSSION AND FUTURE DIRECTIONS.....	99
i.	Kv1.3 interacting proteins.....	100
a.	Kv1.3 is associated with cell signaling in HEK-293 cells.....	101
b.	Proximity labeling shows that Kv1.3 interacts with many endoplasmic reticulum associated proteins.....	102
c.	Proximity labeling of proteins interacting with Kv1.3 highlight the presence of Kv1.3 in the mitochondria.....	103

d.	Kv1.3 interactome contains proteins that are dependent on the PDZ-binding domain to interact with Kv1.3.....	105
e.	The C-termini of Kv1.3 interacts with key immune signaling during LPS stimulation in microglia.....	106
f.	Implications of Kv1.3 interactors in microglia.....	107
g.	Limitations of TurboID-based proximity labeling for Kv1.3 channel interactome studies.....	107
ii.	Future Applications.....	108
a.	Establishing Kv1.3 Potassium Channel interactors in T-cells.....	108
b.	Utilizing the Split-TurboID method to further evaluate interactors with the Kv1.3 complex in microglia.....	109
c.	Pharmacological blockade of Kv1.3 influences Microglial inflammatory response.....	109
d.	Developing a microglial-specific Kv1.3 conditional Knock Out.....	111
IV.	CHAPTER IV: REFERENCES.....	112

## **I. CHAPTER I: INTRODUCTION:**

### **i. Microglia are the primary immune cells of the brain**

Macrophages are formed during embryogenesis and assimilate into many different tissue types. There exist many tissue-specific macrophages throughout the body, including the brain. Beyond inflammation, macrophages are essential to organogenesis and the maintenance of homeostasis [1]. The resident tissue-specific macrophage in the brain is the microglia. Microglia were first characterized by Rio-Hortega in 1932 [2]. Microglia largely differ from other macrophages in that they are located primarily in the nervous system. Specifically, when the blood brain barrier (BBB) forms, they become trapped and remain in the Central Nervous System (CNS) [3]. Similar to macrophages, microglia express MHCII, and both release cytokines in response to inflammatory stimuli [4]. Compared to other tissue specific macrophages, microglia express several genes that encode receptors that allow them to constantly sense and survey their microenvironment, and respond to cues from other cells including neurons, astrocytes and other microglia. Some of these unique microglial genes include CX3CR1 and SiglecH [5]. Using cell surface markers, one can identify microglia as CD11b high and CD45 intermediate, a phenotype that allows one to distinguish them from non-microglial macrophages that enter the brain from the blood, or reside in perivascular spaces [3]. CD11b acts as an integrin in immune cells and CD45 is a receptor tyrosine phosphatase, both of which are frequently used as tools to look for macrophages because they are located on the cell surface and there are good antibodies to both. Distinguishing microglia from other tissue-derived macrophages is necessary to determine how immunity behaves differently in the brain from other tissue types. These markers also allow one to isolate and phenotype microglia in contrast to other macrophage populations in the brain, using transcriptomic, proteomic and flow cytometry-based approaches.

### **Microglia are derived from macrophage progenitors in early development.**

In order to understand how microglia change their states in disease condition, it is important to consider the origins of microglia in the brain. Microglia are derived from the yolk-sac early in development [6]. Macrophage progenitors cross into the embryo from the yolk sac around embryonic day (E)8.5 [7]. Fate-mapping highlights that these progenitors for macrophages gradually transition into microglia as the mouse embryo develops and mature into microglia by post-natal day (PN) 20 [3]. During early development microglia rely on CSF-1 for formation during embryogenesis and the first two weeks postnatal [8, 9]. Over the first few weeks postnatal, the abundance of CSF-1 decreases in the brain whereas IL-34 increases, both of which bind to and activate the microglial CSF1R [9]. As this increase occurs, IL-34 becomes necessary for microglial maintenance in the adult brain [9]. The presence of TGF- $\beta$ 1 and TGF- $\beta$ R in developing microglia is high but is maintained in adult homeostatic microglia [10]. Not only does identifying the markers for adult and embryonic microglia help differentiate different states of microglia, but these markers can also change the outcome of other cell types during different stages of life. Identification of the differences between the embryonic and adult microglia is necessary for understanding how microglia transition to different states.

### **Molecular and functional heterogeneity of microglia**

Looking at heterogeneity of cell types within the brain, glia consist of 90%, whereas neurons consist of 10% of the brain's cell population. Within glia cell populations, 45-75% are oligodendrocytes, 19-40% are astrocytes, 10% are microglia, and less than 1% are the remaining cell types. In the healthy brain, there is a low presence of lymphocytes compared to other tissue

types such as spleen or liver. Thus, microglia act as the primary immune cell. During homeostasis, microglia primarily clear dying neurons, contribute to synaptic pruning and phagocytize any potentially harmful foreign material [11]. Microglia in homeostasis have a distinct phenotype, with a small cell body and thin, surveying processes [12]. Mass spectrometry and RNAseq show homeostatic microglia contain markers, such as P2RY12, TGF- $\beta$  and TMEM119 [13]. In addition to those markers, the chemoreceptor CX3CR1 is essential to microglia and macrophages [14]. Increased phagocytosis occurs when the CX3CR1 is blocked [14]. In the healthy brain, microglia utilize the C1q and C3 complement system to bind to synapses for synapsis remodeling [15]. When microglia transition away from a homeostatic state, their morphology transitions to enlargement of the cell body and thickened processes [16]. Microglia in this state often have the capacity to phagocytize debris [16]. As aging occurs the phenotype and expression of microglia change where there is an age dependent increase in the MTOR pathway as mice age [17].

During myelination, Microglia regulate growth of axons and synapses during post-natal development, by expressing Spp1 and Igf1 [18]. Presence of Spp1+ microglia are located along the axonal tracks [18]. This presence of microglia at the axonal tracks is hypothesized to assist in guiding cells toward myelination or pruning excessively myelinated material.

It is well classified that microglia infiltrate the brain prior to vascularization during development and macrophages as a whole are known for assisting in tracking of blood vessels [19]. In retinal angiogenesis, microglia release Notch1, Dll4, and Jag1 to interact with endothelial cells to promote vascular development [20]. Microglia are attracted toward vascularization in the brain via chemoreceptors like Cx3cr1 and P2RY12 [19]. However, perivascular macrophages in the

brain are often classified distinctly from microglia due to their different expression profiles, specifically, the expression of Lyve1 and absence of Sal1 [21].

During homeostasis microglia strengthen the blood brain barrier (BBB) through forming tight junctions with endothelial cells [22]. During an inflammatory responses microglia utilize CCR5 dependent migration to the cerebral vascular system [22]. There is strong evidence that microglial dysfunction contributes to BBB permeability during neurodegenerative disease [23].

Microglia gene expression changes depending on the role that they perform. Heterogeneity of microglia within the brain highlights that different populations of microglia can be carrying out different functions within the brain at any given moment in time. Many of the roles of microglia, when dysregulated can contribute to the disease conditions of neuroinflammatory disease. Some of roles, such as phagocytosis of dead cells or infectious material, which can assist microglia in clearing debris and protecting the brain from damage. Other microglial functions can become overactive and further contribute to the pathology of many neurodegenerative diseases. There is a distinct immune phenotype that increases in microglia during neurodegenerative diseases.

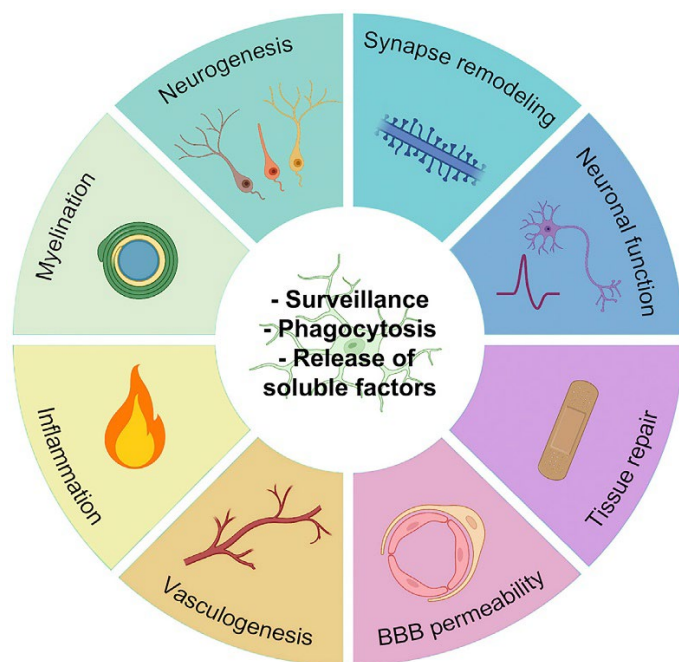


**Figure 1. Microglial functions in the healthy brain.** [24] Microglia cells act as the immune regulators in the brain. In addition, they also regulate neuronal and axonal growth, BBB development and vasculogenesis. During an inflammatory response, microglia phenotypes change and heterogeneity of microglia increases, allowing them play a diverse array of functional roles which are contextualized to brain region, cell type they interact with as well as stage of disease. The heterogeneity within microglia is also highly dynamic, such that microglial states can rapidly transform, rather than remain fixed.

### **Microglia nomenclature and terminology**

Similar to other tissue-derived macrophages, microglia can also adopt various molecular and functional states. In an attempt to provide proper nomenclature for the various microglial states, a group of microglial experts met in 2022 to evaluate terminology. They determined that microglia states cannot be split into activated and resting microglial states, because this would

imply that when microglia are in a homeostatic state that they are no longer active [24]. In addition, the dichotomy of M1 (meaning proinflammatory) and M2 (meaning anti-inflammatory), while initially based on trying to identify microglia at different states, is overly simplified and does not reflect the heterogeneity of microglial states observed *in vivo* [24]. In an effort to highlight microglial heterogeneity, terminology in the field has transitioned to integrating expression and abundance rather than a dichotomic categorization. In this paper, we'll primarily use Disease Associated Microglia (DAM) to describe the microglial phenotype during neuroinflammatory diseases like AD, PD, or, stroke. We will also highlight the importance of microglia during development and homeostasis, where the change in homeostasis contributes to the transition to the DAM state of microglia.

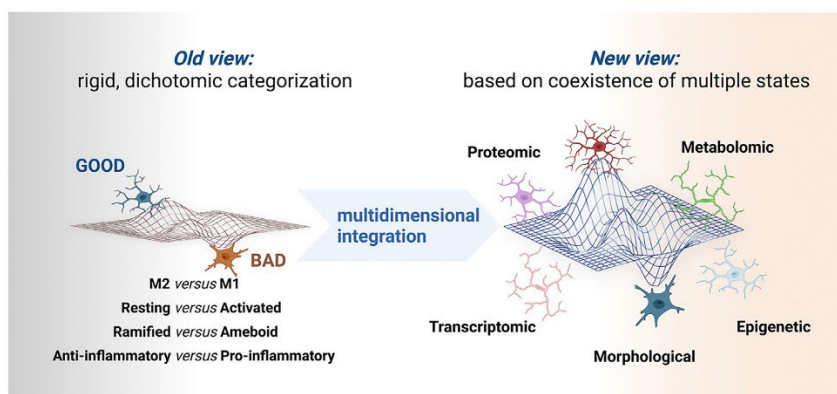


**Figure 2 Nomenclature of microglia has transitioned away from a binary perspective towards focusing on the heterogeneity and complexity of different microglial states [24].**

Microglial heterogeneity exists throughout the lifespan but changes based on conditions in the brain. In this article we'll be referring to microglia primarily in the context of the types of proteins and RNA that are active during a change in the homeostatic state of the microglia. This means that we need to avoid terminology that limits microglial states as a binary, and instead focus on overall changes in state across a continuum.

### **Microglia during inflammation have a distinct phenotype.**

The heterogeneity of microglia can vary depending on the type of neurodegenerative disease; however, the consistent presence of microglia producing an inflammatory response has been well categorized across many disease conditions. Describing microglia during the traditional classification of inflammation, allows for us to describe similarities and differences between microglia in different neurological diseases. Lipopolysaccharide (LPS), a small fragment of gram-negative bacterial membrane, is traditionally used as a treatment to induce inflammation in microglia. This inflammatory signaling cascade is typically started with stimulation of TLR4 in microglia [25]. During TLR4 activation of microglia, particularly in the presence of A $\beta$  or LPS, microglia release a series of inflammatory mediators such as IL-1 $\beta$ , TNF- $\alpha$ , and IL-6 [25]. On the cellular surface of microglia, TLR4 can dimerize with TLR2 or TLR6, resulting in activation of different immune signaling responses. Inhibition of the TLR4 signaling cascade results in a reduction of the NF $\kappa$ B pathway and ERK1/2 phosphorylation [25]. Microglia during an immune response have a localized depolarization that occurs. Microglial activation during an inflammatory response normally is characterized by depolarization due to inwardly rectifying channel activity [26]. The presence of outwardly rectifying K<sup>+</sup> channels allows for reestablishment of the electrical gradient across the membrane of the microglial cell [26]. In addition, microglia typically have a change in phenotype, where the cell bodies become significantly larger and their processes become thickened and shortened [27]. These phenotypes allow for scientists to classify microglia as being more inflammatory and many times is shared across multiple disease conditions. In an effort to better understand inflammation mediated by microglia, it is necessary to model these diseases *in vivo* and *in vitro*.

### ***In vitro* models for microglial activation and induction of inflammatory response.**

There are multiple ways to model microglia *in vitro*, this ranges from isolating primary microglia from mice, utilizing iPSCs to grow microglia-like cells, and growing either mouse or human cell lines. One of the many benefits of cell culture are cost and effort. In general, cell culture is lower cost than *in vivo* work. In addition, sample sizes can be larger *in vitro* with more uniformity across each group. In addition, the statistical power of experiments can be greatly increased due to the ability for experiments to be larger in size *in vitro*. However, overall, cultured microglia often display slightly different phenotypes than cells in the brain of humans or mice. There are strengths and weaknesses to each culture process for studying microglia.

#### Primary culture

Primary microglia can be isolated by either mechanical dissociation and growth on astrocytes, CD11b magnetic column isolation, FACS, or immunopanning [28]. One of the earliest methods developed for isolating primary microglia is the ‘shake off’ method, where microglia are mechanically agitated until they lift off an astrocytic bed. These cells are typically isolated via mechanically dissociation from the mouse brain [29]. These primary cultures usually are collected from day 0 – 3 mouse cortex prior to the formation of the meninges. The Barres’ lab determined that part of maintaining a homeostatic state, such as the maintenance of the TMEM119 marker, in these primary cultures is the presence of TGF- $\beta$  and cholesterol [30]. The microglial homeostatic phenotypes is best maintained when microglia can remain in the presence of other cell types, primarily astrocytes in a serum-free environment [30]. During an LPS

challenge, primary microglia produce an TLR2-dependent response, which results in the release of proinflammatory cytokines, such as iNOS and IL-6 [31].

### Immortalized BV-2 microglia

BV-2 (BV2 retroviral-immortalized microglia) cells are a stabilized cell line designed by Baise et al. in 1990. They isolated microglia cells from 1-week old mouse cortex that were then transduced utilizing a v-raf/v-myc oncogenes to allow for immortalization of the cell line[32]. BV-2 cells produce a similar immune response to primary microglia, where there are numerous transcriptomic and proteomic overlaps between BV-2 cell responses and primary microglial responses, including production of inflammatory cytokines (such as IL-1 $\beta$  and TNF- $\alpha$ ), activation of the NF- $\kappa$ B pathway, and release of NO [32-34]. This makes them beneficial for studying various inflammatory diseases including Alzheimer's Disease and Stroke. In culture, BV-2 cells mimic many of the shifts in heterogeneity seen in AD. A $\beta$ <sub>1-42</sub>, whose over abundance is a significant marker for AD, exposure of BV-2 cells results in activation of TLR4 as well as the NLRP3 inflammasome [35]. In Ischemic stroke, microglia have very similar iNOS behavior as BV-2 cells in neuroinflammatory models [36]. In BV-2 cells experience an increase in the phagocytic response to A $\beta$  during regulation of the TLR-2 pathway [37]. However, due to being transduced with an oncogene, there are several changes in BV-2 cells from primary microglia, primarily in that they proliferate more rapidly, have increased adhesion, and have some transcriptional and proteomic responses that are distinct from primary microglia [33, 38]. In addition, BV-2 cells have lower expression of key homeostatic markers such as TMEM119 and P2RY12 [39].

### Immortalized mouse microglial cells (MMCs)

Mouse microglia cells (MMCs) are another cell line that was developed transducing by C57BL/6 primary microglia with the J6 retrovirus [40, 41]. MMCs are more similar to primary microglia cell culture as far as iNOS production and release of pro-inflammatory cytokines than BV-2 cells [40]. IL-1 $\beta$  and TNF- $\alpha$ , as well as other cytokines were significantly higher in BV-2 cells than MMCs or primary microglia [40].  $\alpha$ -synuclein exposure of MMC cells, shows activation of the NLRP3 inflammasome and activation of RNA-binding proteins [42]. MMC cells also express the Kv1.3 potassium channel, whereas BV-2 cells do not.

### Immortalized human microglial cells (HMCs)

In 1995, human microglial cell lines were created from human embryonic microglia via the SV40 T-antigen [43]. These cells show key microglial morphologies [44]. They also have similar markers to primary cultures of microglia, such as CD11b and CD68 and can produce [43]. They produce similar cytokine response to A $\beta$  as other microglia, including IL-1 $\beta$  and TNF- $\alpha$ .

### Induced pluripotent stem cells (iPSCs)

Microglial like cells are often derived from human pluripotent stem cells through exposure to maturation signals like CSF1 and IL-34 [45]. A combination of these signals allow for iPSCs to take a microglial like state where they express markers such as P2RY12, TMEM119, and HEXB [45]. iPSC formed microglia, developed from human AD patients, when exposed to LPS mimic mouse models of AD (*e.g.* expression of CCL3, STAT1, IL-6) [46]. Co-culture of these cells with neurons also helps retain the microglial morphology and function, which allows for visualization of cell to cell interactions between neurons and microglia [47]. In addition, when put into a more endogenous mouse brain microenvironment, human iPSCs retain their identity

and function and allows for scientists to evaluate how the periphery can influence microglial function [48]. Experimentally, iPSCs are impractical for high throughput experiments and more research needs to be completed to determine the physiological relevance of the model [49].

*In vitro* cultures can be a valuable tool to describe the response of microglia during different states. Each of these cultures have advantages and disadvantages. *In vitro* models of microglia often are used as a way to evaluate the signaling processes of microglia during an immune response.

### **Lipopolysaccharide (LPS) as a model for inflammation:**

LPS is often used as a mechanism to mimic an immune response in microglia.

Lipopolysaccharide is an endotoxin that consists of a piece of the outer membrane of a gram-negative bacterium, usually isolated from *E. coli*. LPS primarily targets the TLR4, which is primarily expressed by glia and neurons in the brain [50]. Activation of TLR4 occurs in many neuroinflammatory diseases, including AD, PD, and ischemic stroke [51]. In monocytes and microglia, LPS induces the release of cytokines, such as, TNF- $\alpha$ , IL-6, and IL-1 [50]. These cytokines are often expressed by microglia in neuroinflammatory diseases such as AD or stroke. In patients suffering from AD, LPS is often found in the brain due to degradation of the blood brain barrier (BBB) [52]. There are genes that overlap with A $\beta$  overexpression mouse models, these include *Tlr2*, *Il1*, and *Kcna3*; however there are many genes that are unique to A $\beta$  overexpression mouse models that are absent in LPS model mice, including *ApoE*, *Cxcr4*, and *Timp2* [27]. Thus, LPS acts as a good model for neuroinflammatory diseases but doesn't completely model the A $\beta$  response. Microglial response in neuroinflammatory diseases is more

complicated than the LPS model can capture. Despite this, aspects of LPS-induced microglial activation *in vitro* and *in vivo* recapitulate some molecular changes that are of relevance in disease models; therefore, LPS is an important tool for investigating specific mechanisms in microglia *in vitro* and *in vivo*.

### **Microglia in Neuroinflammatory disease and inflammation**

In many neurodegenerative and neuroinflammatory diseases, microglia play a key role in the pathogenesis and disease conditions. The heterogeneity of microglia distinctly transition during inflammation, which can drastically alter the function of the microglia. Notably, some microglia undergo a transition from a homeostatic expression to a disease associated expression which can be highlighted in a distinct shift in the RNA expression. The expression patterns, both in the presence of RNA and the release of cytokines for microglia differ depending on the disease, but the presence of many inflammatory components remain consistent in many of these diseases [53, 54]. Another common theme in neurodegenerative diseases includes microglia actively killing otherwise healthy neurons. Microglia utilize both direct pathways, by release of metalloproteases, and indirect pathways, through release of TNF- $\alpha$ , BDNF, and IGF, to kill neurons [53, 54]. Another major transition is changes in interactions between microglial Cx3cr1 and fractalkine, which is released by neurons [53, 54]. Dying neurons release fractalkine, which attract microglial cxe3cr1 and promote the eat me signals for phagocytosis. In disease conditions, increased fractalkine and Cx3cr1 interactions can shift of microglia toward an inflammatory and injurious response [53].

In addition to signaling for phagocytosis and cellular death the NLRP3 inflammasome contributes to microglial functional changes during AD. In AD patients and in Tau22 mice, there is a high expression of the NLRP3 inflammasome [55]. The NLRP3 inflammasome is a known component of the immune response, which typically forms and cleaves proIL-1 $\beta$  [56]. This cleavage of proIL-1 $\beta$  allows for IL-1 $\beta$  to leave the cell and signal an immune response to surrounding cells [56]. Blockade of the NLRP3 activations results in a reduction in the hyperphosphorylation of Tau [55]. Tau overproduction and packaging occurs in the exosome of microglia [57]. Tau overproduction does not occur in healthy microglia. This indicates that signaling associated with Tau overproduction likely contributes to changes in the NLRP3 inflammasome in microglia. Inflammatory responses are not just present in AD; other neurodegenerative diseases, such as stroke, have similar shifts in immune response.

In Stroke, there are also populations of proinflammatory microglia that exhibit proinflammatory cytokines, *e.g.* TNF- $\alpha$  and IL-1 $\beta$  [58, 59]. Microglia have a high expression of STAT1, a known inflammatory marker, that can be regulated by Fingolimod, an approved treatment for stroke [60]. The proinflammatory state of microglia in stroke has also been regulated by the flux of ions that regulate microglial pH [59, 61]. The disease conditions of microglia in neurodegenerative diseases directly contribute to progression of the disease. This can be highlighted specifically in Alzheimer's Disease.

### **Immune Cells contribute significantly to the disease progression of Alzheimer's Disease.**

Alzheimer's Disease (AD) is a neurodegenerative disease that affects millions of people each year. AD is marked by neurotoxicity and dementia [62]. This primary markers for AD is the

accumulation of Amyloid- $\beta$  ( $A\beta$ ) and Tau a misfolded protein thought to promote the disease progression [62]. However, presence of  $A\beta$  and Tau misfolding, as well as synaptic changes occurs years before the noticeable disease conditions appear [63]. Furthermore, some patients have a large accumulation of Tau without progression of AD or dementia [64]. This indicates that the presence of  $A\beta$  and Tau is not the only factor contributing to AD. Microglial activation in patients with AD occurs before the onset of dementia, suggesting that activation of microglia contributes to the behavioral changes associated with memory [65]. The proinflammatory contributions of microglia have a damaging effect on neurons and overall neurological function, by promoting premature cellular death and failing to clear  $A\beta$  [66]. Evaluation of WT and  $A\beta$  overexpression mouse models highlights the heterogeneity of microglia during AD [27]. In the presence of  $A\beta$ , microglia present a decrease of key homeostatic genes, which are largely associated with cellular metabolism and biosynthetic machinery, including *Tmem119* and *P2ry12* [27]. This is in concert with an increase in interferon signaling, and increases in proteins like *Kcna3* and *Tlr2* in one population of disease associated microglia [27]. Another population of disease associated microglia (DAM), has higher phagocytic and protective properties, including *Cxcr4* and *ApoE* [27]. These distinct disease associated states show the transition of microglial heterogeneity during disease. However, some of these DAM may contribute to disease conditions more than others, depending on their gene expression.

### **Microglia have a distinct disease-associated states in AD.**

In Alzheimer's Disease, microglia shift towards a disease-associated state referred to as Disease Associated Microglia (DAM) [13]. DAM have a high presence of APOE and TREM2, it is likely that there are multiple states of DAM within the brain, with varying levels of contributions

to the disease conditions in AD [13]. Microglia in AD often have higher proteostasis, phagocytosis, and protein clearance associated with overexpression of Amyloid and pTau [67]. Particularly, Laser-captured early onset datasets show A $\beta$  plaques promote show a higher expression of AXL, APOE, and TREM2, known markers expressed in microglia [68]. snRNAseq of 5xFAD and human AD patients shows a TREM2-dependant transition of DAM in AD [69]. The presence of TREM2 and APOE leads to a reduction of the expression of key homeostatic genes such as P2ry12, Tmem119, and Smad3 [70]. The APOE expression clusters with key microglial complement signaling proteins such as C1QA, C1QB [67]. Increased expression of the AD risk gene CD33, results in a reduction of the ability for microglia to clear A $\beta$  in mouse models of AD [71]. The proinflammatory properties of DAM release excessive cytokines, fail to clear A $\beta$  accumulation, and promote further neurotoxicity which likely contributes to the disease progression of AD. Proinflammatory DAM primarily express factors such as TLR1, Il1 $\beta$ , and Kv1.3[72]. Furthermore, DAM and activated astrocytes signal to promote infiltration of T-cells and other immune cells.

The dichotomy of microglial DAM possessing both protective and detrimental effects highlight the complexity of immune responses during disease. This leads to necessary evaluation of how each of these disease states may contribute to the disease condition. While analysis of DAM in human AD is preferable, the conditions for this are not always favorable. Human studies are expensive and minimally accessible. Many times, scientists utilize mouse models as a way to evaluate microglia in disease-like conditions.

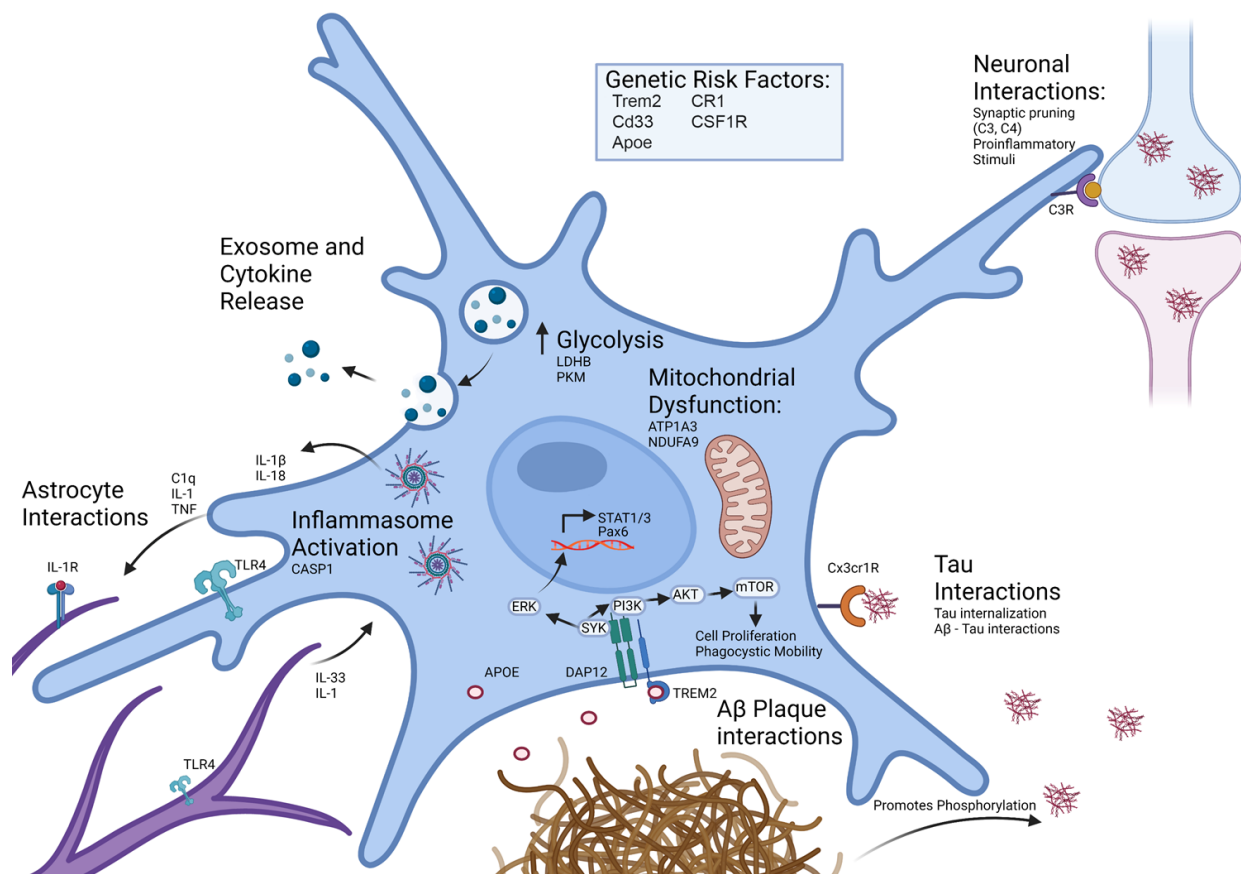


**Figure 3. Microglia in Alzheimer's Disease.** Adapted from Sunna et al. 2023.[73]

### Mouse models of AD have similar features to human AD.

There are several mouse models for AD, I will be highlighting two in this section. 5XFAD transgenic mice, which overexpress human amyloid beta (A4) precursor protein 695 (APP) with the Swedish (K670N, M671L), Florida (I716V), and London (V717I) and human PS1 containing two mutations, M146L and L286V [74]. These Familial Alzheimer's Disease (FAD) mutations enable mice to overproduce A $\beta$  and produce AD-like conditions [74]. The other mouse model is APP mice, which is mouse that expresses a chimeric mouse/human amyloid precursor protein (Mo/HuAPP695swe) and a mutant human presenilin 1 (PS1-dE9) [75]. Both of these models

overproduce A $\beta$  and produce some similar features to the disease. As described earlier, A $\beta$  models do not account for all disease conditions. In addition to A $\beta$ , Tau is largely abundant and is absent from these models. There are some models that include Tau and A $\beta$  but those models are newer and not fully evaluated yet. Both the 5xFAD and APP mouse models discussed highlight similar microglial functions as AD patients.

Similar to AD patients, microglial activation in 5xFAD mice occurs prior to the formation of A $\beta$  plaques [76]. Inhibition of microglial immune function in 5xFAD mice alleviates the disease progression of AD, therefore there is a need to establish therapeutics that target the proinflammatory properties of DAM while preserving the properties of protective DAM [77]. Gene-expression profiles of 5xFAD microglia surrounding A $\beta$  plaques shows a higher expression of proinflammatory genes, such as Cxcr4 and CCL3; these features are very similar to the expression in patients with AD [68]. In 5xFAD mice, removal of the Bace-1 gene results in a reduction of the microglial DAM phenotype at the transcriptional level [37]. In patients with AD and APP mice, there appears to be higher transduction of NF $\kappa$ B into the nucleus of astrocytes and microglia and activation of C3, which activates the C3aR in neurons [78]. This signaling pathway is associated with age-dependent synaptic and neuronal loss. Deficits in C3 in APP mice result in a reduction of A $\beta$  plaques and a reduction of synaptic and neuronal loss [79]. While these similarities are important, comparison between microglia in human AD compared to AD mouse models show that mouse models have a distinct reduction in response [80]. That being said, DAM in both mice and humans overlap with many aging genes [80].

There is a clear transition of microglia to a disease associated state during AD. Some of the conditions can be reproduced in vivo and in vitro to assist in studying microglial roles in AD.

There remain some larger gaps in the knowledge of the field, such as how much of a detrimental

role do microglia play in AD? In this sectioned, I highlighted both beneficial and detrimental roles of microglia. It appears that these roles may be dependent on how much of a response is produced. If we reduce the cellular response of AD, does this truly limit the disease? The discovery of AD started with the overproduction of A $\beta$  and Tau; however, it is clear that many cell types, including microglia, contribute to the disease. How can we regulate the function of microglia during a diseased response? We see that modifying microglial function can have beneficial effects on mouse models [77, 81], but can that transfer to human AD patients? Mitigation of microglia likely contribute to regulation of the disease.

## **ii. Kv1.3 potassium channel influences microglial response**

### **The Kv1.3 potassium channel is highly expressed by microglia in neuroinflammatory states**

The Kv1.3 potassium channel is implicated in a number of neuroinflammatory diseases. The overexpression of Kv1.3 in T-cells in multiple sclerosis (MS) and during inflammatory responses has been well described [82]. Blockade of these channels results in a reduction of the inflammatory response of T cells [82]. In addition to peripheral neuroinflammatory diseases, Kv1.3 expression increases in AD, PD and stroke [72, 83, 84]. Within these neuroinflammatory diseases, microglia appear to be the primary expressors of Kv1.3 in the brain [72, 83, 84]. Where about 2-4% of microglia express the Kv1.3 channel, however during disease conditions the expression increases [85]. The increased presence of Kv1.3 channels in immune cells during neuroinflammatory diseases suggests that Kv1.3 plays a role in transition of immune cells to an inflammatory response.

### **The Kv1.3 potassium channel allows for efflux of potassium in immune cells.**

Kv1.3 is a potassium channel that is expressed on the cellular surface of immune cells. This is a voltage-dependent channel that allows for potassium to flow out of the cell. Each Kv1.3 monomeric sub-unit contains six transmembrane domains, with both the N and C termini facing the cytosol [86-88]. The N-terminus of Kv1.3 contains domains responsible for channel tetramerization, sub-unit assembly and localization to the membrane. Particularly, the S1 region of the N-terminus allows for caveolin-1 to bind to Kv1.3 and targets it toward lipid rafts [89]. The C-terminus contains a PDZ-binding domain that binds to PSD-95 that could recruit other signaling proteins which form scaffolds for ERK signaling [90]. Truncation of the PDZ-binding domain in T-cells indicates changes in Kv1.3 function without effects on the ability of the channel to localize to the cell membrane [91]. It is likely that the PDZ-binding domain is important for the function and interactions with Kv1.3. The Kv1.3 channel interacts with a homotetramer of Kv $\beta$  proteins (Kv $\beta$ 1-3), which is necessary for the channel to function.

Due to Kv1.3 being a channel, interactions with other proteins are not the only contributions to the function of the channel. Voltage has a large role in whether the Kv1.3 channel is active. During homeostasis, the Kv1.3 potassium channel remains closed. During an inflammatory response in microglia calcium channels, such as P2X7 and P2X4, allow calcium to flow into the cell and promoting depolarization across the cell [92]. Depolarization of -20mV promotes the activation of Kv1.3 and the outward flux of potassium to reestablish the membrane potential [93]. The outward flow from Kv1.3 is hypothesized to allow for more calcium influx to promote early calcium signaling in microglia. Kv1.3 activity is not exclusive to the cell membrane. Kv1.3 is processed in the endoplasmic reticulum and then packaged via the Golgi apparatus to the

surface membrane. There is also biophysical evidence that Kv1.3 may be present on the inner mitochondrial membrane[94].

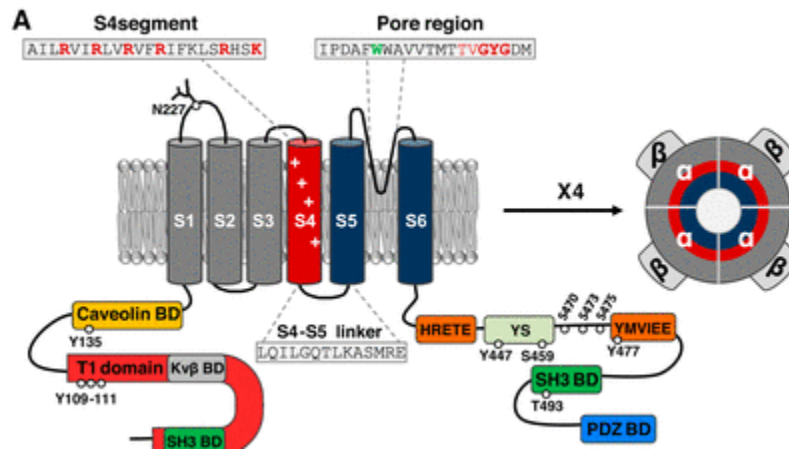


**Figure 4: Kv1.3 Potassium Channel Structure.** Kv1.3 consists of six transmembrane domains with both the N-terminus and the C-terminus located inside the cytoplasm. The N-terminus is largely responsible for Kv1.3 localization. Whereas, the C-terminus has a PDZ-binding domain that may interact with key immune signaling proteins. Four Kv1.3 monomers form together along with Kv $\beta$ 2 to form a potassium channel that allows for potassium to flow out of the cell. Adapted from Pérez-García, *et al.* [95].

### **Kv1.3 is present in the mitochondria and alters metabolism in cells.**

Electrophysiology, immunohistochemistry, and electron microscopy identify Kv1.3 on the inner membrane of the mitochondria [96]. In addition to the biophysical evidence of Kv1.3 being present in the mitochondria, the N-terminus interacts with the TIM23 complex, which translocates Kv1.3 to the inner mitochondrial membrane [94]. During normal lymphocyte apoptosis, Bax blocks Kv1.3 in mitochondria, resulting in hyperpolarity of the inner

mitochondrial membrane and increases release of reactive oxygen species and cytochrome C [97]. Increases in Kv1.3 channel function results in an increase in cellular respiration and reactive oxygen species [98]. There are quite a few gaps in knowledge regarding the function and topology of the channel in mitochondria. Further studies are necessary to evaluate the functional implications of Kv1.3 in the mitochondria and how alteration of the channel may influence the mitochondrial function in cellular respiration. However, these current studies indicate that Kv1.3 is both present in the mitochondria and Kv1.3 activity and function may change mitochondrial functions.

In addition to being present in the mitochondria, Kv1.3 can change systematic metabolism. There are several studies that indicate Kv1.3 can contribute to insulin resistance and obesity. External blockade of the Kv1.3 channel utilizing the peptide ShK-186 in mice with a high fat diet results in a reduction of weight gain, decreased blood sugar levels, and enhanced peripheral insulin [99]. Kv1.3 KO mice show a reduction in weight gain as well as an increase in their metabolic rate [100]. Within obese mice, olfactory bulb cell sensing and metabolism is reduced; blockade of the Kv1.3 channel utilizing ShK-186 results in a maintenance of the metabolism and sensing capabilities of the olfactory bulbs [101]. Knock out of the Kv1.3 channel results in a hyper sensitivity to smell, referred to as “super-smeller” mice [102]. Overall, these studies highlight the important roles Kv1.3 plays in metabolism both at the systematic and cellular level. At a cellular level, Kv1.3 can change the immune signaling and mitochondrial function of cells, in particular immune cells.

**Kv1.3 activity increases in T-lymphocyte and macrophage inflammatory responses.**

Kv1.3 activity is increased in immune cells during inflammation and likely influences the response of immune cells. T-lymphocytes have two major features: inducing apoptosis in infected cells and release of cytokines to recruit other immune cells. In T-lymphocytes, Kv1.3 is directly linked to  $\beta 1$  integrin adhesion of the T-cell during an inflammatory response and a blockade of the channel changes that adhesion [103]. The ability for T-cells to alter adhesion allows for them to attach to infected or damaged cells to induce apoptosis. During inflammatory responses, T-lymphocytes have increased calcium influx. This calcium influx is necessary for early immune signaling in T-cells to induce a release of cytokines. The calcium dependent channels, such as IKCa1, and voltage-dependent channels like Kv1.3 assist in regulation of the inflammatory response and calcium influx [104]. By inhibition of the potassium channel, the influx of calcium can be reduced, thus decreasing an immune response. This can be highlighted by blockade studies of Kv1.3. Blockade of the Kv1.3 channel reduces the activation of the NLRP3 inflammasome and increased cytokine expression, IL-1 $\beta$ , some clear signs of T-lymphocyte activation in inflammation [105]. Highlighting a clear reduction of an inflammatory response in T-cells when there is inhibition of the Kv1.3 potassium channel.

Similar to T-cells, macrophages are another type of immune cell that express Kv1.3.

Macrophages are part of the innate immunity and act as the body's main phagocytic cell during an immune response. Similar to microglia and T-cells, they also release cytokines as part of an immune response. During a macrophage inflammatory response, Kv1.3 hetero-oligomerizes with a similar Kv channel, Kv1.5 to allow for potassium to flow out of the cell [106]. However, increases in inflammation using TNF- $\alpha$  exposure, results in an increase in Kv1.3 without a change in Kv1.5 [106]. Blockade of the Kv1.3 potassium channel shows a reduction of the

inflammatory response of macrophages, including the reduction of inflammatory cytokines such as IL-6 and IL-1 $\beta$  [107]. Regulation of the Kv1.3 channels in cultured macrophages, show a reduction in Erk activation, a key component in inflammatory responses [108]. This clearly shows that Kv1.3 activity directly alters macrophage activation of an immune response.

Microglia, act as the macrophage of the brain and express Kv1.3 in a similar manner.

### **Kv1.3 channels in the brain**

Within the brain, Kv1.3 is primarily present in microglia but is present in all glia as well as neurons. During chronic inflammation, infiltrating monocytes and T-cells also express Kv1.3 [72]. While Kv1.3 (Kcna3) mRNA is present in oligodendrocytes, Kv1.3 does not contribute to the whole cell conductance [109]. In development, Kv1.3 is highly expressed in oligodendrocyte progenitor cells, which decrease with maturity [110]. However, during myelin injury, Kv1.3 activity increases in oligodendrocytes [110, 111]. Blockade of the Kv1.3 channel reduces myelin injury [111].

In astrocytes, Kv1.3 appears to primarily located in the Golgi apparatus, unlike other cell types where it's expressed on the cell surface [112]. Animal models of MS show high expression of Kv1.3 in inflammatory astrocytes, microglia, and infiltrating macrophages [113]. Blockade of the Kv1.3 channel decreases the inflammatory modulators of astrocytes [113]. This indicates that the inflammatory response may have some astrocytic contributions. Future studies evaluating how astrocyte and oligodendrocyte expression of Kv1.3 will be quite valuable.

During proliferation, microglial Kv channels transition from a mix of Kv1.5 and Kv1.3 to primarily expressing Kv1.3, whereas the non-proliferative microglia have a higher expression of

Kv1.5 [114]. Both Kv1.3 and Kv1.5 regulate in the immune functions of microglia [115]. Recent cell culture studies show similar features, where BV-2 cells and primary microglial cultures that are mobile have a higher Kv1.3 open channels present on the cell surface than Kv1.5 [116]. Kv1.3 activity is noticeably increased during an inflammatory response in microglia [117]. Kv1.3 expression is present in microglia that have a high interferon response and activation of the MCH II mechanism [27]. Microglia that express Kv1.3 have increased ability to release nitric oxide (NO), which actively kills neurons whereas blockade of the channel results in reduction of the NO release [118]. In addition, the channel is activated in concert with increases in proinflammatory cytokines, such as IL-1 $\beta$  and TNF- $\alpha$  [119]. This highlights that Kv1.3 is integral in the production of an inflammatory response in microglia in the brain. Regulation of Kv1.3 via knock out (KO) or blockade changes disease conditions and microglial function.

**Knock out (KO) of Kv1.3 in mouse models highlights a reduction of inflammatory response.**

Kv1.3 KO mice were designed by Fadool *et al.* in 2004 [102]. These mice are often characterized by their reduced metabolism, super smelling ability, and reduction of proinflammatory response [100, 102, 119]. T-lymphocytes of mice with a KO of Kv1.3 show a reduction in C4<sup>+</sup> T-cell differentiation possibility due to the reduction of their proliferation [120]. Microglia of Kv1.3 KO mice show a reduction of their proinflammatory response to LPS [119]. This includes a reduction of many proinflammatory cytokines, such as TNF- $\alpha$  and IL-1 $\beta$  [119]. These mice are quite valuable in evaluating Kv1.3 activity *in vivo*; however, due to the fact that the KO is active throughout the life-span of the mouse and active in all cell types, it can be difficult to determine how much age and cell type contributes to these reductions in

metabolism and inflammatory response. Establishing a cre-lox system that is inducible and promoter specific will likely highlight the importance of microglial Kv1.3 in the brain more distinctly. Knock out models are not the only way to evaluate Kv1.3 influence in inflammatory responses. In addition to KO, blockade of the channel can evaluate how Kv1.3 regulates immune function in the brain.

### **Blockade of Kv1.3 alters inflammatory responses.**

A peptide from sea anemone, Shk-223, was derived as a blockade that is high selective to Kv1.3 [121]. This 35 amino acid long peptide, with an  $IC_{50}$  of 200pM binds to the external portion of the active channel, blocking the flow of potassium out of the cell [121]. While ShK-223 is highly selective the amount of the peptide that actually enters the brain is widely unknown. On the other hand, a small molecule, referred to as Phenoxyalkoxypsoralen-1 (PAP-1), blocks the internal portions of Kv1.3 in a use dependent manner, meaning that PAP-1 binds to active Kv1.3 and increases binding the more Kv1.3 is present [122]. The  $EC_{50}$  of PAP-1 is 2nM with a 23 fold selectivity for Kv1.3 over Kv1.5 [122]. It is evident that PAP-1 crosses the blood brain barrier due to its smaller size, however, it's affinity for Kv1.3 is lower than Shk-223. Both of these blockades provide relevant information on how Kv1.3 works since both influence Kv1.3 differently. Blockade of Kv1.3 with either ShK-223 or PAP-1 results in a reduction of inflammatory responses in both 5xFAD mice and LPS induced mice.

In mice that are prone to postoperative decline, blockade of Kv1.3 utilizing PAP-1, reduces microglial neuroinflammatory responses [123]. In the 5xFAD model of AD, blockade using the ShK-223 molecule resulted in a change in the microglial phenotype [85]. Blockade resulted in an increase in the proinflammatory genes, such as *Il1b*, *Trem3*, while increasing phagocytic and signaling genes, such as *P2ry12*, *c1qa*, and *Tmem119* [85]. Stroke models additionally show a

reduction infarct size in the transient middle cerebral artery occlusion (tMCAO) model when blocking Kv1.3 with ShK-223 [84]. PAP-1 blockade of the channel shows similar features in reducing an inflammatory response with a reduction of IL-1 $\beta$  and IFN- $\gamma$  in MCAO models [124]. *In vitro* models of inflammation utilizing BV-2 cells, show a similar feature, where ShK-223 blockade of Kv1.3 increases the phagocytic capacity of cells while decreasing the release of proinflammatory cytokines [117]. PAP-1 blockade of BV-2 cells results in a decrease of Key proinflammatory cytokines such as IL-1 $\beta$ , TNF- $\alpha$ , IL-6, and iNOS [119]. This section highlights that Kv1.3 influences microglial function but how is Kv1.3 influencing immune signaling. Evaluation of potential interactors of Kv1.3 in immune cells will help determine how Kv1.3 alters immune function.

### **KV1.3 interactors in immune cells.**

There are several Kv1.3 interactors that are specific to immune cells. Kv1.3 activity is highly dependent on the activity of receptor tyrosine kinases, which is likely due to the phosphorylation of the channel itself [125]. Two known receptor tyrosine kinases, toll-like receptor I and II are known to phosphorylate proteins in early microglial immune signaling. Changes in the TLR I and II activity alters the activity of Kv1.3 in microglia, suggesting that physical interaction between these proteins at the cell membrane occurs [119]. Activation of TLR I and II are important component of microglial response to immune stimuli, such as LPS. These interactions between Kv1.3 and TLRs likely occur with the c-terminus of Kv1.3, where phosphorylation of Kv1.3 occurs [90]. The PDZ-binding domain of Kv1.3, located on the c-terminus has been shown to interact with PSD-95 and other signaling proteins necessary for Erk activation [90]. Thus, it appears that the PDZ-binding domain is necessary for the C-terminus to interact with key immune signaling proteins. The N-terminus of Kv1.3 is largely responsible for signaling to

proteins regarding localization of Kv1.3, either to the cell surface via caveolin-1 or to the mitochondria by TIMM23 [89, 94]. The majority of these studies are completed through co-immunoprecipitation, which is a great technique for evaluating which proteins could interact with Kv1.3, but does not always capture proteins interacting with each other *in vivo*. In addition, these studies miss any proteins that may be transiently interacting with Kv1.3.

### **Kv1.3 as a potential for the treatment of AD.**

Based on the cellular hypothesis of Alzheimer's Disease, it is likely that microglia are a major contributor of AD disease conditions. A growing question in the field is how to we increase the beneficial effects of microglia (*i. e.* phagocytosis of A $\beta$  and clearing of dying cells) while decreasing some of the detrimental effects of microglia (*i.e.* inability of phagocytose material and excessive production of cytokines). Kv1.3 has been shown to be present on the surface of DAM that increase inflammation, have existing drug treatments that are highly specific to the channel, and preliminary data highlighting reduction of Kv1.3 reducing the inflammatory response of microglia in AD models. This makes Kv1.3 an excellent option for targeting and potentially treating AD, as well as other neuroinflammatory diseases such as stroke.

### **Current knowledge gaps related to Kv1.3 channels in microglia**

While Kv1.3 blockade reduces the disease conditions, it remains unclear how much of this is microglial specific. This means that studies need to be completed to determine how much microglial Kv1.3 influences the disease compared to global reduction of Kv1.3. We suggest future studies where Kv1.3 is conditionally knocked out in microglia alone and compared to

global KO. This would help highlight how much of the disease condition is Kv1.3 microglial specific.

Another way at grasping the cell-type specificity is utilizing the blockade model and evaluating single nuclear RNAseq. This will establish which cell types are altered by regulation of the Kv1.3 channel. This would be particularly valuable in AD and stroke mouse models.

Another gap in the field that remains is how peptide vs. small molecule blockade changes the function of microglia. Further evaluation comparing PAP-1 and Shk-223 should help determine the influence of small molecule vs. peptide blockade. Additionally, PAP-1 blocks internal portion of Kv1.3 and Shk-223 blocks external portion of Kv1.3. This will enable researchers to evaluate Kv1.3 influence at the cell surface compared to Kv1.3 located on other organelles, such as mitochondria.

As a potential drug target, how Kv1.3 regulates immune function is widely unknown. To understand the process of regulation of inflammatory signaling, it would be useful to further determine what the interactors of the Kv1.3 channel. The purpose of this project was to evaluate the interacting proteins with Kv1.3 to determine how Kv1.3 regulates immune response. In order to evaluate the potential physical interactors with Kv1.3 during an immune response, we fused Kv1.3 to TurboID [126]. TurboID is a biotin-ligase derived from BioID that can add biotin at a faster rate, 10 minutes compared to BioID requiring closer to 24 h [126]. TurboID can add biotin the proximal proteins within a 10 nm distance [126]. After proximal proteins are biotinylated, streptavidin pull-downs can capture all biotinylated proteins for evaluation via Mass Spectrometry [126]. We utilized the TurboID approach to answer two questions, what are the physical interactors of Kv1.3 and how does that change in microglia during an immune

response? Our hypothesis is that Kv1.3 physically interacts with immune signaling proteins during an immune response in microglia.

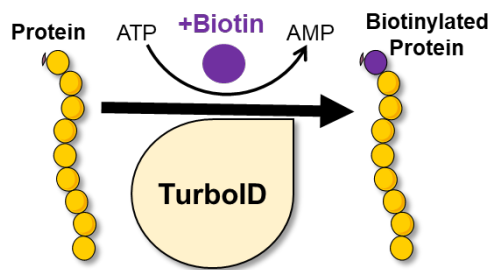


**Figure 5: TurboID biotinylation of proximal proteins.** TurboID can add biotin to proximal proteins at a 10nm radius by utilizing ATP and exogenous biotin to add biotin to proteins within 10 minutes of exposure. This method was utilized by our group to determine which proteins interact with Kv1.3 and how that changes during an immune response in microglia. Adapted from Sydney Sunna.

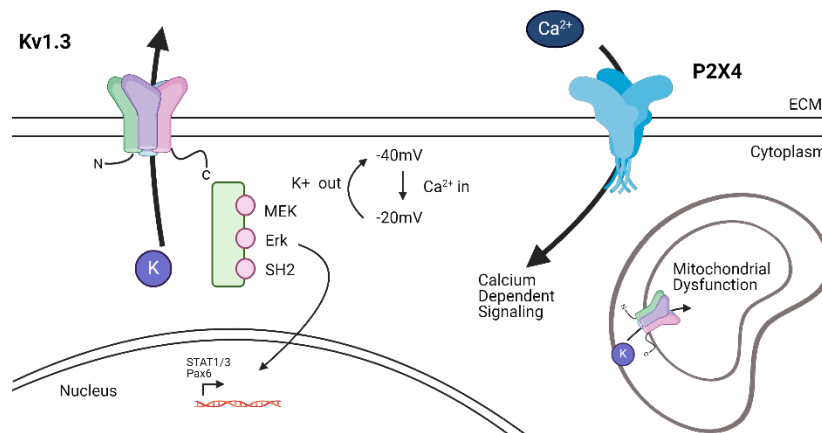


**Figure 6: Kv1.3 interactions with immune signaling may be beyond activation of the channel.**

During an immune response, there is a large influx of calcium via the P2X4 channel [93]. The calcium is necessary for calcium dependent signaling that promotes an inflammatory response in microglia. This leads to localized depolarization across the cell membrane, which then activates Kv1.3 allowing for potassium to flow out of the cell [93]. There are two standing hypotheses in the field, The first is that Kv1.3 is regulating immune signaling by gauging how much potassium flows out of the cell. If a blockade or change in Kv1.3 prevents flow of K<sup>+</sup> out of the cell then more calcium cannot enter the cell because the depolarization is too great. However, this hypothesis does not account for physical interactions with the channel. Our lab focused on an alternative hypothesis, that the presence of key binding domains, such as the PDZ-binding domain, may interact with immune signaling proteins, such as Ras, and alter the downstream signaling of those proteins. Our secondary goal was to evaluate the localization of proteins interacting with Kv1.3. This was to determine how much Kv1.3 influenced the functions of organelles, particularly that of mitochondria. To evaluate this, we utilized TurboID to biotinylate proteins proximal to Kv1.3. We determined that Kv1.3 interacts with key immune signaling proteins in microglia during an immune response and that interaction is altered during truncation or blockade of the channel. Our results suggest that Kv1.3 physically interacts with proteins during an immune response, which have not been previously described. This allows the field to be closer to understanding how Kv1.3 could influence microglial function in AD, getting us closer to utilizing Kv1.3 as a potential drug target for the treatment of AD.

**Central Hypothesis: Kv1.3 directly interacts with immune signaling proteins in microglia during neuroinflammatory diseases.**

The objectives of this dissertation are to establish a proximity-labeling technique to identify the Kv1.3 protein-protein interactome, examine how the interactome of the N and C domains of Kv1.3 differ, identify the importance of the C-terminal PDZ domain in shaping the Kv1.3 interactome, and lastly, understanding whether pro-inflammatory stimulation of microglia re-organizes the Kv1.3 interactome.

## **II. CHAPTER II: Proximity labeling proteomics reveals Kv1.3 potassium channel immune interactors in microglia.**

\*Original findings are published in a first author publication in the journal *Molecular & Cellular Proteomics*. Supplemental figures and datasheets can be found online at:

Bowen, C. A., Nguyen, H. M., Lin, Y., Bagchi, P., Natu, A., Espinosa-Garcia, C., Werner, E., Kumari, R., Brandelli, A. D., Kumar, P., Tobin, B. R., Wood, L., Faundez, V., Wulff, H., Seyfried, N. T., & Rangaraju, S. (2024). Proximity Labeling Proteomics Reveals Kv1.3 Potassium Channel Immune Interactors in Microglia. *Molecular & Cellular Proteomics*, 23(8).

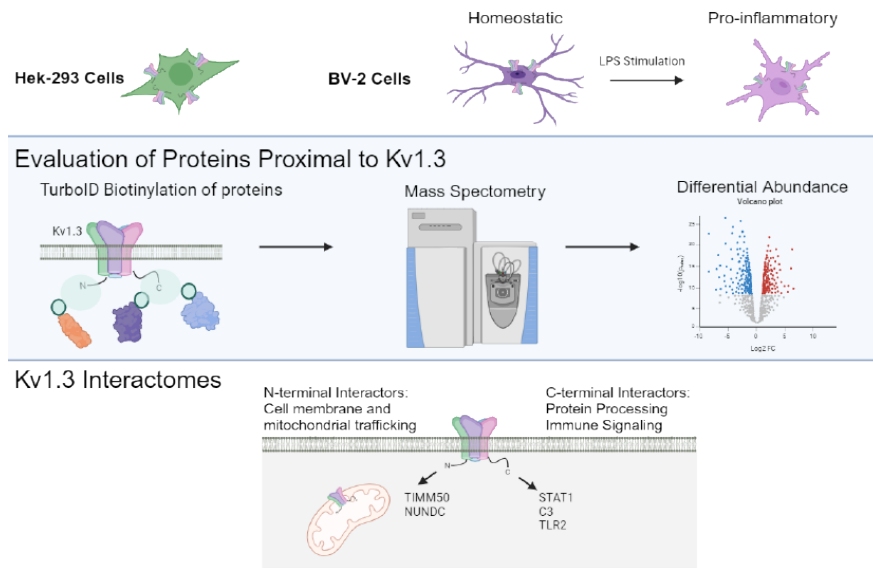
<https://doi.org/10.1016/j.mcpro.2024.100809>

## i. ABSTRACT

Microglia are resident immune cells of the brain and regulate its inflammatory state. In neurodegenerative diseases, microglia transition from a homeostatic state to a state referred to as disease associated microglia (DAM). DAM express higher levels of proinflammatory signaling molecules, like STAT1 and TLR2, and show transitions in mitochondrial activity toward a more glycolytic response. Inhibition of Kv1.3 decreases the proinflammatory signature of DAM, though how Kv1.3 influences the response is unknown. Our goal was to identify the potential proteins interacting with Kv1.3 during transition to DAM. We utilized TurboID, a biotin ligase, fused to Kv1.3 to evaluate potential interacting proteins with Kv1.3 via mass spectrometry in BV-2 microglia following TLR4-mediated activation. Electrophysiology, western blotting, and flow cytometry were used to evaluate Kv1.3 channel presence and TurboID biotinylation activity. We hypothesized that Kv1.3 contains domain-specific interactors that vary during a TLR4-induced inflammatory response, some of which are dependent on the PDZ-binding domain on the C-terminus. We determined that the N-terminus of Kv1.3 is responsible for trafficking Kv1.3 to the cell surface and mitochondria (*e.g.* NUDC, TIMM50). Whereas, the C-terminus interacts with immune signaling proteins in an LPS-induced inflammatory response (*e.g.* STAT1, TLR2, and C3). There are 70 proteins that rely on the C-terminal PDZ-binding domain to interact with Kv1.3 (*e.g.* ND3, Snx3, and Sun1). Furthermore, we used Kv1.3 blockade to verify functional coupling between Kv1.3 and interferon-mediated STAT1 activation. Overall, we highlight that the Kv1.3 potassium channel functions beyond conducting the outward flux of potassium ions in an inflammatory context and that Kv1.3 modulates the activity of key immune signaling proteins, such as STAT1 and C3.

## ii. GRAPHICAL ABSTRACT

Expression of Kv1.3-TurboID



## iii. INTRODUCTION

Microglia are the resident myeloid immune cells of the central nervous system and are recognized to play critical roles in the pathogenesis of several neurological disorders. Microglia are involved in synaptic pruning, phagocytosis and clearance of cellular debris and protein aggregates, release of trophic and toxic factors and extracellular vesicles [1, 2]. Recent advances in transcriptomic profiling have revealed heterogeneity within microglia, where some homeostatic microglia adopt a disease-associated microglia (DAM) signature [3, 4]. DAM signatures appear to be conserved across several chronic neuroinflammatory and neurodegenerative disorders including Alzheimer's disease (AD), Parkinson's disease (PD), multiple sclerosis, and ischemic stroke [5-7]. Within the DAM population, functional

heterogeneity is also present, such that a sub-set of DAM phenotypes may have detrimental effects via increased synaptic phagocytosis and release of neurotoxic factors that have damaging effects on neurons and overall neurological function, by promoting premature cellular death and impaired pathological protein clearance [8]. Regulators of these pro-inflammatory DAM functions in neurological diseases, therefore, represent potential therapeutic targets for neuro-immunomodulation. The Kv1.3 potassium channel has emerged as a regulator of pro-inflammatory functions of DAM. Pharmacological blockade of Kv1.3 channels has also been shown to reduce neuropathology in mouse models of AD, PD and stroke models [5, 9-11]. However, the molecular mechanisms that allow Kv1.3 channels to regulate immune functions of microglia are not fully understood.

The *Kcna3* gene encodes the Kv1.3 potassium channel protein, which homotetramerizes to form functional voltage-activated outward-rectifying K<sup>+</sup> channels [12, 13]. K<sup>+</sup> efflux via Kv1.3 fine tunes membrane potential following membrane depolarization, which in turn regulates calcium flux in immune cells such as effector memory T cells and microglia [14]. Beyond the cell surface, there is also biophysical evidence for the presence of Kv1.3 channels in the inner mitochondrial membrane, which may allow intracellular Kv1.3 channels to regulate metabolism, apoptosis and immune functions [15, 16]. While Kv1.3 channels can regulate membrane potential and calcium flux, Kv1.3 channels may also regulate immune pathways via direct protein-protein interactions at the plasma membrane [9, 17]. Based on the observed co-localization of Kv1.3 channels with integrins, receptors and immune signaling proteins in T cells, there is a strong possibility that Kv1.3 also regulates immune signaling in microglia through directly interacting with proteins associated with immune function [18, 19].

Each Kv1.3 monomeric subunit contains six transmembrane domains, with both the N- and C-termini facing the cytosol [12, 20, 21]. The N-terminus of Kv1.3 contains domains responsible for channel tetramerization, subunit assembly and localization to the membrane. The C-terminus contains a PDZ-binding domain, which can interact with PSD-95 and signaling proteins which form scaffolds for ERK signaling [17, 22]. Removal of the PDZ-binding domain results in changes of Kv1.3 function and localization [23]. The Kv1.3 channel also interacts with a homotetramer of Kv $\beta$  proteins (Kv $\beta$ 1-3), which further extends the breadth of potential interactors of Kv1.3 channels [22]. Many mechanistic aspects of Kv1.3 channel interactors and function have been investigated in T cells. However, the protein interactions with the N and C termini of Kv1.3 channels in microglia are less well characterized. Given the molecular and functional heterogeneity in microglial responses within DAM, it is also possible that the protein-protein interactome of Kv1.3 channels may vary, based on the activation context of microglia.

To test this hypothesis, we investigated the N and C terminal interactomes of Kv1.3 channels in microglia, and their relationship to the activation state of microglia. We hypothesized that Kv1.3 contains domain-specific interactors, some of which are dependent on the PDZ binding domain on the C-terminus, and shift toward immune function annotated proteins during an LPS-response in microglia. To accomplish this, we utilized proximity-dependent biotinylation of Kv1.3 by fusing the biotin ligase TurboID to the N or C terminus of Kv1.3 in HEK-293 and BV-2 microglial cell lines [24]. Utilizing the BV-2 microglia cell line is more efficient than primary microglia for stable cell line transduction and generating sufficient material for proteomics studies [25]. Biotinylated proteins were then enriched and quantified using mass spectrometry-based proteomics. After verifying that these TurboID-Kv1.3 fusions did not impact channel localization and function, we identified N and C terminal protein-protein interactomes,

highlighting several novel domain-specific associations between Kv1.3 channels and immune function. We also imposed an inflammatory challenge with lipopolysaccharide (LPS) to induce a pro-inflammatory microglial state which mimics the TLR activation that occurs in AD and PD [26, 27]. We assessed the relationship between microglial pro-inflammatory activation, and the Kv1.3 channel interactomes. Our studies identified several novel domain-specific immune protein interactions of Kv1.3 channels in microglia, including STAT1 and C3 at the C-terminus and TIMM50 at the N-terminus, which may explain how microglial Kv1.3 channels participate in regulating diverse immune mechanisms of neurological diseases.

#### **iv. EXPERIMENTAL PROCEDURES**

##### **PLASMID and LV design:**

Five plasmid constructs were designed through the Emory University custom cloning core using cloning strategies summarized in Table 1.

The TurboID construct was previously described in Sunna et al. [28]. The V5-TurboID-NES plasmid (Addgene, #107169) was transformed using a competent *E. coli* strain DH5 $\alpha$  according to the manufacturer protocols. QIAfilter Plasmid kits (Midi prep kit; Qiagen; catalog no.: 12243) were utilized to purify plasmid DNAs following the manufacturer's protocol. Restriction sites were introduced via the PCR primers and the V5-TurboID-NES sequence was subcloned into pCDH-EF1-MCS-BGH-PGK-GFP-T2A-Puro (CD550A-1) and sequenced (Table 1). This construct was utilized as a positive control for biotinylation of proteins.

The construct utilized for a transfection control comprised of an overexpression of methionine-tRNA synthetase (MeTRS) (AddGene, pMarsL274G) were created and sequenced using protocol described above.

Each of the Kcna3 based constructs was on a FUGW backbone with Kcna3 isolated from cDNA with a GS rich 15 amino acid linker (5'-GGCGGAGGGGGCTCA-3'<sup>x3</sup>), a V5 tag, and TurboID either on the 3' or 5' end of the Kcna3 gene. These constructs were formed via protocols described in Sunna et al. [29].

The Kv1.3 C-term Fusion $\Delta$ PDZ construct had a truncated Kcna3. The deletion of TDV, which are the last 3 amino acids are described as essential to Kv1.3 function and localization [23]. This truncated Kcna3 was fused with the same 15 amino acid linker, a V5 tag, and TurboID.

Puromycin resistance was used as a selection marker at a separate location of the plasmid. DNA sequencing was used to confirm plasmid orientation and correct insertion.

Plasmids were packaged into lentivirus (LV) by the Emory University Viral Vector Core and purified as described below. HEK-293FT (Invitrogen) cells were maintained in complete medium (4.5 g/L Glucose and L- Glutamine containing DMEM supplemented with 10% FBS and 1% Pen-Strep) and incubated at 37 °C, 5% CO<sub>2</sub>. One day before transfection, HEK-293FT cells were seeded onto five 150 mm plates at a density of 1x10<sup>7</sup> cells per plate in 20 mL of complete medium. The cells were approximately 70-80% confluent at the time of transfection.

The day of transfection, the DNA mixture prepared as the following: 53  $\mu$ g of lentiviral plasmid, 35  $\mu$ g of pCMV $\Delta$  8.9 and 17.5  $\mu$ g of pVSVG in 4.5 mL of ddH<sub>2</sub>O, 0.5 mL of 1.5 M NaCl. The polyethylenimine (PEI) mixture prepared as the following: 0.84 mL of 7.5 mM PEI, 0.5 mL of 1.5 M NaCl in 3.66 mL of ddH<sub>2</sub>O. The DNA mixture and PEI mixture were then combined. This

10 mL solution was vortexed 20 s and incubated for 20 min at room temperature. Then 2 mL of the mixture was added drop wise to each dish then incubated for 48 h before harvesting.

For plasmid purification, the supernatants (media) containing lentivirus were collected 48 h and 72 h post-transfection, combined and then centrifuged at 500 x g for 5 min at 4 °C, followed by passage through a 0.45 µm low protein binding filter. The total 200 mL of supernatant was centrifuged at 28,000 rpm for 2 h at 4 °C in a 45Ti rotor (Beckman), which can sustain faster speeds. The virus pellets were resuspended in 500 µL of PBS, incubated on ice for 30 min, resuspended virus particles were combined and loaded into a 12 mL of SW 41 tube, 3 mL of 20% sucrose cushion, and centrifuged at 28,000 rpm for 2 h at 4 °C in a SW 41 rotor (Beckman). The virus pellet was resuspended in 60 µL of PBS, then stored at -80 °C.

For transduction of BV-2 cells, purified virus was added to cells at a multiplicity of infection (MOI) of 10 along with 8 µg/mL polybrene for 24 h. Remaining LV media was then removed, and cells were allowed to grow in DMEM-F12 (10% FBS, 1% Penicillin/streptomycin) for 5 days. Puromycin was then added at 2 µg/mL for 7 days. Presence of Kcna3 gene was confirmed with qPCR.

### **Cell Culture and Maintenance:**

Mycoplasma free HEK-293 cells (obtained from Seyfried Lab) were grown in DMEM-F12 (10% FBS, 1% Penicillin/streptomycin) and plated at 1 million cells in a 10cm dish for protein lysis and 100,000 cells/well on Poly-L-lysine coated coverslips (coating protocol followed via manufacturer's procedure) in 24 well plates for immunofluorescence. Mycoplasma free BV-2 cells (Obtained from Tansey lab) were grown in DMEM-F12 (10% FBS, 1% Pen/strep) at 1

million cells in a 10 cm dish. Cells were allowed to adhere to the plate for 24 h prior to experiments.

### **Dosing and Immune Stimulation:**

HEK-293 cells were transfected with plasmids using the JETPRIME transfection reagent for 24 h according to the manufacture's protocol. For biotinylation, HEK-293 cells underwent a full media change with the addition of 200  $\mu$ M Biotin in DMEM-F12 (10%FBS, 1%P/S) for 24 h.

BV-2 cells were treated with either 100 ng/mL LPS or PBS for 24 h. At 23 h of LPS or PBS incubation, 200  $\mu$ M Biotin was added in without a media change for 1 h. In contrast to 24 h of biotinylation used in HEK-293 studies, we limited the biotinylation duration to 1 h, to increase the stringency of the interactomes of Kv1.3.

### **Electrophysiology**

Electrophysiological experiments were conducted on transfected HEK-293 and transduced BV-2 cells that were plated on poly-Lysine-coated glass coverslips. The cells were allowed to attach for 10 min at 37°C before starting the electrophysiological measurements using the whole-cell configuration of the patch-clamp technique at room temperature with an EPC-10 HEKA amplifier. Transfected HEK-293 cells were visualized by epifluorescence microscopy of green fluorescent protein by eGFP-C1 plasmid cotransfection (Addgene, 2487, discontinued). The Ringer solution used contained 160 mM NaCl, 4.5 mM KCl, 2 mM CaCl<sub>2</sub>, 1 mM MgCl<sub>2</sub>, 10 mM HEPES, pH 7.4, and had an osmolarity of 300 mOsm. Patch pipettes were made from soda lime glass (micro-hematocrit tubes, Kimble Chase, Rochester, NY) and had resistances of 2-3 M $\Omega$  when submerged in the bath solution. The pipettes were filled with an internal solution

containing 145 mM KF, 1 mM HEPES, 10 mM EGTA, 2 mM MgCl<sub>2</sub>, pH 7.2, 300 mOsm. Series resistance and whole-cell capacitance compensation were used as quality criteria for electrophysiology. Current amplitudes were recorded in voltage-clamp mode and elicited using a 200-ms voltage step from -80 to +40 mV at a frequency of 0.1 Hz. Use-dependency was determined using the same protocol but with a pulse frequency of 1 Hz for 10 pulses. The fractional current of the last pulse was normalized to the first pulse to determine the extent of cumulative (use-dependent) inactivation. Whole-cell patch-clamp data are presented as mean ± S.D., and statistical significance was determined using a paired Student's t-test for direct comparison between WT and TurboID-fusion constructs.

The voltage dependence of activation was examined using a step protocol where cells were depolarized for 200 ms from a holding potential of -80 mV to a range of potentials from -80 to +40 mV in 10-mV increments, with an interpulse duration of 30 s. The peak currents were normalized to the maximum peak current and plotted against the voltage. The reversal potential was calculated by individually fitting the resulting I-V curve of each data set with the equation:  $I = z * (V - V_r)$ , where I is the normalized current amplitude, z is the apparent gating charge, V is the potential of the given pulse, and V<sub>r</sub> is the reversal potential. Conductance was then directly calculated using the equation:  $G = I/(V - V_r)$ , where G is conductance and I, V, and V<sub>r</sub> are as described above. The conductance values were fit with the two-state Boltzmann equation:  $G = [1 + \exp(-0.03937 \times z \times (V - V_{1/2}))]^{-1}$ , where z is the apparent gating charge and V is the potential of the given pulse, and V<sub>1/2</sub> is the potential for half-maximal activation.

The activation and inactivation kinetics were examined using currents elicited by the same step protocol used for determining the current amplitude at +40 mV above. The activation and inactivation time constants were calculated using the Chebyshev method to fit the activating

phase and inactivating phase, respectively, of each trace with a single exponential equation:  $I = A \times \exp[-(t - K) / \tau] + C$ , where  $I$  is the current,  $A$  represents the relative proportions of current activating with the time constants  $\tau$ ,  $K$  is the time shift, and  $C$  is the steady-state asymptote. Only the constants  $\tau$  are reported.

### **Quantitative Real Time Polymerase Chain Reaction (qRT-PCR):**

#### RNA extraction:

BV-2 cells were washed 2x with cold 1x PBS, then incubated in Trizol for 5 min. A chloroform/phenol extraction was performed according to manufacturer's protocol (Invitrogen). RNA was suspended in 50  $\mu$ L of DPEC treated water. Purity and quantity of RNA was evaluated using a Nanodrop 2000 (Thermo scientific).  $A_{260}/_{280}$  above 1.3 and  $A_{260}/_{230} \geq 2.0$  were considered acceptable purity levels for RNA.

#### cDNA Synthesis:

2  $\mu$ g of RNA was mixed with 5  $\mu$ L 10x RT buffer, 2.5  $\mu$ L Multiscribe reverse transcriptase, 2  $\mu$ L dNTP mix, 5  $\mu$ L 10x RT random Primers, and DPEC H<sub>2</sub>O for a 50  $\mu$ L reaction and incubated in an Applied Biosystems 2720 Thermocycler according to Applied Biosystems Protocol. cDNA was diluted 1:10 prior to qRT-PCR.

#### Real-Time Quantitative Reverse Transcription PCR (qRT-PCR):

A 20  $\mu$ L reaction was utilized with 10  $\mu$ L Taqman Universal Master Mix II, 1  $\mu$ L designated primer (listed in Table 2), 4  $\mu$ L DPEC H<sub>2</sub>O, and 5  $\mu$ L cDNA (diluted 1:10) according to the Applied Biosystems protocol in the MicroAmp Fast-96-well Reaction Plate sealed with MicroAmp Optical Adhesive Film. The Applied Biosystems 7500 Fast Real-Time PCR System

was utilized. cDNA was probed with either *Kcna3* or the housekeeping gene *Gapdh*. Fold Change was calculated on CT values and normalized to housekeeping genes and negative control. Statistical significance was calculated based on unpaired t-test and graphed on PRISM (Version 10.1.0).

### **Immunofluorescence microscopy:**

Cells were washed in plate twice with 1x PBS prior to fixing with 4% PFA for 30 min at room temperature then washed three times with 1x PBS for 5 min (n=2). Cells were permeabilized in 0.1% Triton X100 + 2% horse serum (HS) in 1x PBS for 30 min at room temperature. Cells were incubated with rabbit anti-V5 (1:500) in 2% HS in 1x PBS for 1 h at room temperature and then washed three times with 1x PBS for 5 min at room temperature. Cells were further incubated with a secondary antibody mix consisting of 1:500 Donkey anti-Rabbit FITC, and 1:500 Streptavidin-594 for 1 h at room temperature followed by three 1x PBS 5 min washes at room temperature. Coverslips were mounted on slides using mounting media (Prolong Diamond) and dried for 48 h. Slides were sealed with clear nail polish for 24 h and imaged using a Nikon A1R HD25 inverted confocal microscope using a 60x objective lens using NIS-Elements Imaging software. Image analysis and processing was completed via ImageJ.

### **Flow Cytometry:**

Cells (BV-2 or HEK-293) were scraped and collected using ice-cold PBS in a centrifuge tube and washed by adding extra PBS (n=3). To determine Kv1.3 presence, the cells were transferred into a flow tube and incubated with ShK-F6CA at a concentration of 5.5  $\mu$ M in 100  $\mu$ L PBS on ice for 30 min in the dark, followed by 3 PBS washes [30]. For each PBS washing step, 1 mL of

PBS was added to the flow tube and centrifuged at 2200 rpm for 3 min, followed by the removal of the supernatant. The cells were kept in the dark on ice until flow cytometry was performed.

To determine biotin presence in BV-2 cells, cells were first fixed in 1x fixation buffer for 30 min on ice, then washed thrice with cold 1x PBS. Cells were then permeabilized for 30 min using 1x permeabilization buffer on ice. To determine the presence of biotin, fixed and permeabilized cells were incubated with Streptavidin-488 (1:500 in permeabilization buffer) and incubated for 1 h on ice in the dark. After incubation, the cells were washed, as mentioned above. After the last wash, 200  $\mu$ L of PBS was added, vortexed and kept on ice in the dark until flow cytometry was performed. Unstained OneComp beads and beads stained with Alexa fluoro-488, ShK-F6CA and unstained cells were used as a control. All flow cytometry data was collected on the BD Aria II instrument and analyzed using the Flow Jo software.

### **Cell Lysis and protein processing:**

BV-2 and HEK-293 cells were rinsed twice with 1x PBS prior to scraping in PBS then spun at 800xg for 5 min at RT (n=3). Cells were lysed in 8 M urea in Tris-NaH<sub>2</sub>PO<sub>4</sub> with Halt Protease inhibitor (1:100). Lysates were probe sonicated at 30% amplitude three times for 5 s on 10 s off. Lysates were centrifuged at 15000xg for 15 min. Supernatants, containing solubilized proteins were processed for affinity purification (AP) and Mass Spectrometry (MS).

### **Western Blot:**

Protein amount in each cell lysate was quantified using a BCA colorimetric assay (n=3). To confirm protein biotinylation 10 µg of protein were added to 4x Laemmli buffer (1:50 beta-mercaptoethanol) and boiled for 10 min at 95°C and resolved on a BOLT 4%-12% Bis-Tris Gel at a current of 80 V for 15 min followed by 120 V for 40 min along with a 250 kDa Ladder. Proteins were transferred to a nitrocellulose membrane using the iBLOT mini stack system. Ponceau staining for 2 min were used to confirm equal loading. The membrane was washed using 1x TBS for 15 min and blocked for 30 min using StartingBlock T20 (TBS) blocking buffer. at room temperature. Blots were then incubated with streptavidin-680 (1:10000 in Blocking Buffer) for 1 h at room temperature protected from light. Blots were washed twice in TBS-T for 10 min at room temperature and twice in TBS for 5 min at room temperature. Membranes were then imaged using the Odyssey Li-COR system.

#### **Affinity purification of biotinylated proteins:**

83 µL of Pierce streptavidin magnetic beads (Thermo-scientific, 83817) were washed with 1 mL RIPA buffer for 2 min on rotation at room temperature. Protein lysates, 1 mg for HEK-293 Cells and 0.5 mg for BV-2, were brought up in 500 µL RIPA buffer and incubated with magnetic beads on rotation at 4°C for 1 h. Beads were washed twice with 1 mL of RIPA buffer for 8 min followed by one wash with 1 mL of 1 M KCl for 8 min on rotation at room temperature. Beads were then washed with 1 mL of 0.1 M Na<sub>2</sub>CO<sub>3</sub> for 10 s and 1 mL of 2 M Urea in tris-HCl buffer (10 mM, pH:8) for 10 s at room temperature. The beads were then washed twice with RIPA buffer for 8 min followed by 2 PBS washes for 2 minutes each. For each wash, samples were spun down and incubated on magnetic rack for 2 min to allow full attachment of beads to the magnet. After the final PBS wash PBS was removed completely and the beads were dissolved in 80 µL of PSB. 8 µL of beads (10% of total) were resuspended in 30 µL of 2x Laemmli buffer

supplemented with 2 mM biotin and 20 mM DTT and boiled at 95°C for 15 min. Western blot and silver stain were used to check for streptavidin labeling and protein abundance post-AP.

Protein bound beads were stored at 20°C until on-bead digestion.

### **Protein Digestion and Peptide Clean Up:**

For mass spectrometry protein were digested from cell lysates (Input; represents protein present in whole cell) and on protein attached to the beads (represents; biotin enriched proteins). To prepare biotin enriched samples for mass spectrometry, protein bound streptavidin beads were washed three times with 1x PBS and then resuspended with 150 µL 50 mM ammonium bicarbonate (ABC,  $\text{NH}_4\text{HCO}_3$ ). 1 mM dithiothreitol (DTT) was added to reduce samples for 30 mins on a rotor (800 rpm) at room temperature. 5 mM iodoacetamide (IAA) was added to alkylate cysteines for 30 min on a rotor at room temperature, protected from light. Proteins were digested overnight with 0.5 µg of lysyl endopeptidase on rotation (800 rpm) at room temperature. Proteins were further digested by 1 µg trypsin overnight on rotation (800 rpm) at room temperature. Samples were acidified to 1% Formic Acid (FA) and 0.1% trifluoroacetic acid (TFA), desalted using an HLB column, and dried using cold vacuum centrifugation (SpeedVac Vacuum Concentrator).

To prepare cell lysates for mass spectrometry different concentrations were optimized for digestion. 100 µg of pooled cell lysates were reduced with 1 mM DTT for 30 min and alkylated with 5 mM IAA for 30 min protected from light. Samples were diluted two-fold in ABC and digested with 2 µg of lysyl endopeptidase overnight on rotation at room temperature. Samples were further diluted to a final urea concentration of 1 M and digested by 4 µg trypsin overnight on rotation at room temperature. Samples were acidified to 1% Formic Acid (FA) and 0.1% trifluoroacetic acid (TFA), desalted using an HLB column, and dried down using cold vacuum

centrifugation (SpeedVac Vacuum Concentrator). Digestion protocol also outlined in outlined in Sunna, et al. and Rayaprolu et al. [28, 31].

### **Mass Spectrometry:**

Derived peptides were resuspended in the loading buffer (0.1% trifluoroacetic acid, TFA) and were separated on a Waters Charged Surface Hybrid (CSH) column (150  $\mu\text{m}$  internal diameter (ID) x 15 cm; particle size: 1.7  $\mu\text{m}$ ). HEK-293 and BV-2 samples were run on the same mass spectrometer with similar chromatography settings, only differing by number of samples run. BV-2 cell samples were run on an EVOSEP liquid chromatography system using the 15 samples per day preset gradient (88 min) and were monitored on a Q-Exactive Plus Hybrid Quadrupole-Orbitrap Mass Spectrometer (ThermoFisher Scientific). Whereas, HEK-293 cell samples were run on an EVOSEP liquid chromatography system using the 30 samples per day preset gradient (44 min) and were monitored on a Q-Exactive Plus Hybrid Quadrupole-Orbitrap Mass Spectrometer (ThermoFisher Scientific). The mass spectrometer cycle was programmed to collect one full MS scan followed by 20 data dependent MS/MS scans. The MS scans (400-1600  $m/z$  range,  $3 \times 10^6$  AGC target, 100 ms maximum ion time) were collected at a resolution of 70,000 at  $m/z$  200 in profile mode. The HCD MS/MS spectra (1.6  $m/z$  isolation width, 28% collision energy,  $1 \times 10^5$  AGC target, 100 ms maximum ion time) were acquired at a resolution of 17,500 at  $m/z$  200. Dynamic exclusion was set to exclude previously sequenced precursor ions for 30 s. Precursor ions with +1, and +7, +8 or higher charge states were excluded from sequencing. Mass spectrometry protocols previously outlined [28, 31].

### **Protein Identification and Quantification:**

MS Raw files were uploaded into MaxQuant software (version 2.4.9.0), where HEK-293 data were searched against the human Uniprot 2017 database (90412 proteins), and BV-2 data was searched against the 2020 mouse Uniprot proteome database (91441 proteins), both of which were modified to contain target sequences for TurboID. Methionine oxidation, protein N-terminal acetylation, and deamination were variable modifications; carbamidomethyl was a fixed modification; the maximum number of modifications to a protein was 5. Label Free Quantification (LFQ) minimum ratio count was set to 1. Re-quantification, a process in Maxquant to double check peptides, was used. The minimum peptide length was set to 6 amino acids, with a maximum peptide mass of 6000 Da. Identifications were matched between runs. For protein quantification, the label minimum ratio count was set to 1, peptides were quantified using unique and razor peptides. Fourier transformed MS (FTMS) match tolerance was set to 0.05Da and Ion Trap MS was set to 0.6Da. The false discovery rate (FDR) was set to 1%. The Maximum number of missed cleavages is set to 1.

For both the enriched samples and cell lysates, Maxquant intensities were uploaded into Perseus (version 1.6.15). Categorical variables, such as potential contaminants, reverse peptides, and samples only identified by one site were all removed. Data were log<sub>2</sub> transformed and filtered for missingness such that at least two samples had non-missing values within an experimental group. After this threshold, missing data were imputed based on normal distribution and matched to uniprot gene names (Supp. datasheet 1 and 2). In enriched samples, protein groups were normalized to TurboID abundance (Supp. Datasheet 3 and 4). The same process was applied to all cell types and conditions described below.

### **Data analysis:**

Analysis of TurboID biotinylated proteomes of HEK-293 cells

The analysis was divided into 4 groups which are “Control”, “Cterm”, “Nterm”, and “TurboID” each with a n=3 and a final dataset of 2122 proteins. The C-term fusion  $\Delta$ PDZ was excluded from analysis due to inconsistent labeling. Principal component analysis (PCA) of affinity purified data was performed. Furthermore, to identify genes of interest that were differentially abundant, we performed a one-way analysis of variance (ANOVA) on all samples (n = 12), comparing the groups are “Control”, “Cterm”, “Nterm”, and “TurboID” (n = 3 each). The code for the one-way ANOVA analysis was adapted from the "parANOVA" repository on GitHub (<https://github.com/edammer/parANOVA>). Volcano plot comparisons were generated for the following data. The proteins which have a raw p-value of  $\leq 0.05$  and a Log2FC of  $\pm 1$  are considered statistically significant.

#### Analysis of TurboID biotinylated proteomes of BV-2 cells

The finalized data set of 1412 proteins were identified. A smaller number of proteins were identified in BV-2s likely just because there were less proteins biotinylated. We performed principal component analysis (PCA) for analyzing high-dimensional datasets which helped to distinguish patterns, relationships in the dataset and identify the main sources of variation.

Differential enrichment analysis (DEA) was performed. Significantly differentially abundant proteins were identified with an unadjusted p-value  $\leq 0.05$  (nominal p values are widely accepted for volcano analysis and hence were chosen for this analysis over BH corrected to avoid over filtering of genes and data) and a Log2FC of  $\pm 1$  for up and decreased proteins considered statistically significant respectively. Following the roadmap for statistical analysis, the "parANOVA" repository on GitHub (<https://github.com/edammer/parANOVA>) was referenced for the one-way ANOVA code and was implemented. Volcano plots were created to represent results from differential abundance analyses. Morpheus (Morpheus,

<https://software.broadinstitute.org/morpheus>) was used to create visual heat maps of proteins abundance. Individual proteins were colored based on z-score, where the darker shades of red indicate +1 and the darker shades of blue indicates -1. Hierarchical clustering arranged proteins based on groups.

### Analysis of whole BV-2 Cell Lysates

The input data was loaded and shared in the supplemental file. Post processing the finalized dataset identified 4152 observations or proteins. To distinguish patterns, relationships in the dataset and identify the main sources of variation, we performed principal component analysis (PCA) for analyzing high-dimensional datasets.

Differential enrichment analysis was performed. Significantly differentially enriched proteins were identified via unadjusted p-value  $\leq 0.05$  and log<sub>2</sub> fold change of +/-1. The "parANOVA" repository on GitHub (<https://github.com/edammer/parANOVA>) was referenced for the one-way ANOVA code and was implemented for analysis. The PBS Group was compared to the LPS Group with a n=5 of each and Volcano plot was generated for the comparison. "KCNA3" and "TurboID" were highlighted as significant proteins to clarify biological insight from the pertinent dataset.

### **Gene Set Enrichment Analysis**

#### HEK-293 cells:

Gene set enrichment analysis (GSEA) was performed utilizing the software AltAnalyze (version 2.1.4)[32, 33]. Z-score of higher than 1.96 was used to identify significantly enriched genes. In the HEK-293 cells, the DEA comparison between N-terminal and C-terminal were used to create an input list that was unique to the N-terminus of Kv1.3 and a list of proteins enriched with the

C-terminus of Kv1.3. These lists were compared to all of the proteins captured normalized to TurboID abundance. The most abundant genes were listed along with the STRING analysis.

#### BV-2 microglial cells:

Gene set enrichment analysis (GSEA) was performed utilizing the software AltAnalyze (version 2.1.4)[32, 33]. Z-score of higher than 1.96 was used to identify significantly enriched genes. The DEA comparison of both N and C termini compared to global TurboID presence was used to calculate an input list of all microglial Kv1.3 interactors. The DEA comparison between N and C termini was used to create an input list specifically for Kv1.3 N-terminal interactors. For the LPS conditions, the DEA comparison for the C-terminal fusion with PBS or LPS was used to create lists of proteins more abundant in the PBS conditioned media or LPS conditioned media. Lists were created for proteins that are enriched and depleted with the deletion of the PDZ binding domain on the C-terminus. Lists were referenced to all proteins abundant in mass spectrometry data that were normalized to TurboID abundance. The top 10 genes lists were selected based on highest z-score. The GSEA results were plotted with a bar graph of z-score and colored based on type of process using PRISM (Version 10.1.0).

#### **Protein-protein interaction network analysis (STRING):**

##### HEK-293 cells:

Interacting networks were made using the STRING analysis software[34]. Network nodes represent proteins. Node Color represents gene term member, where dark colors indicate significant z-score in GSEA list and light color indicates not significant. Disconnected nodes were excluded from String network. Edges represent protein-protein association, where edge

thickness indicates confidence, thickest line indicates highest confidence (0.900) while thinnest line indicates low confidence (0.150).

#### BV-2 cells:

Interacting networks were made using the STRING analysis software [34]. Network nodes represent proteins of Kv1.3 interactors or Kv1.3 interactors overlapping with MITOCARTA. Node Color represents GSEA list. Disconnected nodes were excluded from String network. Edges represent protein-protein association, where edge thickness indicates confidence, thickest line indicates highest confidence (0.900) while thinnest line indicates low confidence (0.150).

#### **Experimental Design and Statistical rational:**

Sample conditions were prepared by cell type (either BV-2 or HEK\_293), inflammatory challenge (LPS, PBS), Type of TurboID (control – absent of turboID, Kv1.3 with a N-terminal fusion of TurboID, Kv1.3 with a C-terminal fusion of TurboID, Truncated Kv1.3 with the PDZ-binding domain removed and a C-terminal fusion of TurboID), and biotin enrichment (Streptavidin Affinity purified or Lysate). For mass spectrometry, AP samples were run in three biological replicates and lysates were pooled for each experimental condition. Overall, a total of 46 samples were analyzed and described in the results. Maximum number of samples was based on budget allowance, an a priori power analysis was not performed. Sample acquisition order was randomized by non-biotinylated samples followed by biotin-containing samples, as to prevent contamination of biotin-labeled proteins. Statistical rational and analysis is further described in the “Data analysis”, “Gene Set Enrichment Analysis, and “Protein-protein network interactions analysis (STRING)”.

#### **Luminex assays:**

BV-2 cells were grown at 50,000 cells/well in 12-well plates and allowed to adhere to bottom of plate for 24 h. Cells were then treated with LPS (100 ng/mL) for 24 h and then exposed to IFN- $\gamma$  (100 ng/mL) for 60 min. Lysates were prepared in 8 M Urea as previously described [28].

Complement proteins and MAPK phosphoproteins were quantified using multiplexed Luminex immunoassays; these have been previously used without cross reactivity [31]. The analytes measured with the human complement panel are complement C1q, complement C3, complement C3b/iC3B, complement C4, complement factor B, and complement factor H. To determine cross-species reactivity between the human complement panel analytes and the murine cell line lysates, linear ranging was performed. Only analytes obeying a linear response were evaluated. Analytes detected with the MAPK panel are pATF2 (Thr71), pErk (Thr185/Tyr187), pHSP27 (Ser78), pJNK (Thr183/Tyr185), p-c-Jun (Ser73), pMEK1 (Ser222), pMSK1 (Ser212), p38 (Thr180/Tyr182), p53 (Ser15) and pSTAT1 (Tyr701). Standard protocols from the manufacturer were followed, with quarter volume loading of reagents to reduce excess antigen. Sample loadings were normalized to total protein via Pierce BCA. To identify samples biotinylated in vitro, an adapted Luminex protocol was followed as previously reported[31]. The overarching mechanism in the standard protocol is an analyte is immobilized using a magnetic bead specific to the analyte. The analytes are then tagged with specific biotinylated antibodies and biotinylation is detected with a streptavidin fluorophore; streptavidin-phycoerythrin. The adapted assay protocol utilizes the biotin-ligated proteome and thus omits the biotinylated antibody. Appropriate protein loadings for both standard and adapted assays were determined following a linear ranging to ensure signal above noise/background levels and to mitigate potential impact of the hook effect (false negatives) [31]. Average Net MFI values were utilized; negative values

were imputed to zero. Statistical significance was calculated based on unpaired t-test and graphed in PRISM (Version 10.1.0).

### **Preparation of Mitochondrial Enriched Fractions from BV-2 microglia cells**

Method for mitochondrial enrichment was adapted from Wieckowski MR, et al. [36].

The BV-2 cell lines described previously: BV-2, TurboID, N-terminal fusion, C-terminal fusion, and the C-terminal fusion  $\Delta$ PDZ were cultured at 5% CO<sub>2</sub> in DMEM-F12 (10%FBS, 1% Penn/Strep). Untransduced cells were removed by adding 2  $\mu$ g/mL puromycin to the complete medium. After 5-7 days of selection, all cell lines were seeded in 150 mm Petri dishes and allowed to grow until 90% of confluency in complete medium. Cells were exposed to 200  $\mu$ M biotin for 24 h before harvesting. Approximately 40-million cells were used to generate mitochondrial enriched fractions by differential centrifugation as described previously [36]. Experiments were performed in triplicates at the same time. Briefly, cells were detached by trypsinization, then washed with cold 1XPBS and pelleted at 800xg for 10 min at 4°C. After aspirating PBS, pellets were resuspended in 1.6 mL IB-1 buffer (225 mM mannitol, 75 mM sucrose, 0.1 EGTA and 30 mM Tris-HCl pH 7.4) with HALT protease and phosphatase inhibitor cocktail and homogenized using a Teflon potter homogenizer with 25 strokes on ice. Total homogenates (Fraction A0) were transferred to a clean tube, and then centrifuged twice at 600xg for 5 min at 4 °C, pellets containing unbroken cells, nuclei, and heavy membranes were fraction A1. Supernatants were pelleted at 7,000xg for 10 min at 4°C and the resulting pellets (Fraction A2) correspond to heavy membrane organelles, likely containing the largest presence of Kv1.3. Pellets were washed in 200  $\mu$ L 1B-2 buffer (225 mM mannitol, 75 mM sucrose, 30 mM Tris-HCl pH 7.4) and centrifuged at 7,000xg for 10 min at 4°C, resulting pellets are crude mitochondria (Fraction A3). For each fraction, pellets and homogenates were diluted in 200  $\mu$ L

of 8 M urea buffer and sonicated (5 s on–off pulses, Amplitude 30%) for 45 s, and then centrifuged at 21,130xg for 10 min at 4°C. Supernatants were collected, and protein concentration was determined by BCA assay. 10 µg of protein were used to verify mitochondrial enrichment (HSP60, 1:1000), TurboID fusion (anti-V5 tag, 1:250, IRDye800, 1:10,000) by western blot.

### Evaluating changes in STAT1 phosphorylation with Kv1.3 blockade

N-terminal KV1.3 -TurboID BV-2 cells were seeded in a six well plate at a density of 1 million cells in DMEM-F12 (10 %FBS, 1 %P/S) for 24 h. Media was changed and PAP-1 (1 µM) was added for 30 min followed by induction with IFN-γ (10 ng/ml) in the same media for 30 min. Cells were washed in chilled PBS and harvested in urea lysis buffer with protease and phosphatase inhibitor cocktail. After cell lysis protein quantification was performed using BCA colorimetric assay. Samples were then subjected to western blot with 30 µg loading per well as described earlier. Blots were probed for pSTAT1 Tyr701(1:1000), total STAT1(1:1000) and β-actin (1:10000) as loading control. Band density was analyzed using Image J. software.

TABLES:

**Table 1. Constructs Designed for experiments conducted.**

Constru ct	Restriction Sites	Primer Sequences
MetRS	NheI/BstBI	5'- ctagagctagcgccaccatgggcaagcccatccccaaccccctgctgggcctg gacagcaccAGACTGTTTCGTGAGCGAGGGTTCCCC-3' 5'-gatcgttcgaaTCACTTTTTCTTCTTGCCTTTAGGAGTT-3'

TurbolD	BstBI/Bam HI	5'- gcgctactctagagctagcgaattcgaagccaccatgggcaagcccatcccc aa-3' 5'- agaaggcacagtcggcggccgcgatccttagtccagggtcaggcgctccag ggg-3'
Kv1.3 N-term Fusion	Xbal/Agel	5'- CAGGTCGACTCTAGagccaccatgggcaagcccatccccaaccccct gct-3' 5'- gtggcaccggtGCTGCCACCGCCACCGCTTCCACCCCGC CTGAGCCCCCTCCGCCcttttcggcagaccgcagactgatttc-3'
Kv1.3 C-term Fusion	BamHI/Bsr GI	5'- ACTTAAGCTTGGTACCGAGCTCGGATCCgccaccatgaccgt ggtgcccggggaccacct-3' 5'- tggtgtacaAGGCCCGGGGTTGCTCTCAACATCTCCAGC CAATTTCAAGAGAGCATAGTTAGTACACTGcttttcggcagac cgcagactgattt-3'
Kv1.3 C-term Fusion ΔPDZ	NheI/Bam HI	5'- ACTTAAGCTTGGTACCGAGCTCGGATCCgccaccatgaccgt ggtgcccggggaccacct-3' 5'- ctgttcgccactatggaactcgcc-3'

**Table 2. Reagents List**

<b>Reagent</b>	<b>Manufacturer</b>	<b>Catalog #</b>
Dulbecco's Modified Eagle Medium (DMEM-F12)	Gibco	11965-092
Penicillin-Streptomycin	Gibco	15140-122
Fetal Bovine Serum (FBS)	Gibco	26140-079
JETPRIME	Polyplus transfection	101000046
Lipopolysaccharide (LPS)	Sigma-Aldrich	L4391, 1 mg
Polybrene	Sigma-Aldrich	S2667
Puromycin	Gibco	A11138-02
Recombinant mouse IFN- $\gamma$	R&D Systems	485-MI-100
0.05% Trypsin-EDTA	Gibco	253000054
Biotin	Sigma-Aldrich	B4639-100mg
Trizol	Invitrogen	15596018
10x RT buffer	Applied Biosystems	4319981
Multiscribe reverse transcriptase	Applied Biosystems	4308228
dNTP mix	Applied Biosystems	4367381
10x RT random Primers	Applied Biosystems	4319979
Taqman Universal Master Mix II, no UNG	Applied Biosystems	4440040
MicroAmp Fast-96-well Reaction Plate	Applied Biosystems	4346907

MicroAmp Optical Adhesive Film	Applied Biosystems	4311971
<i>Kcna3</i> qPCR primer	Applied Biosystems	Mm00434599_s1
<i>Gapdh</i> qPCR primer	Applied Biosystems	Mm99999915_g1
Rabbit Anti-V5 tag	Abcam	ab206566
Donkey anti-Rabbit, FITC	Invitrogen	A16030
Streptavidin-594 antibody	Invitrogen	21842
DAPI	Sigma-Aldrich	10236276001
Prolong Diamond	Invitrogen	p36970
1x fixation buffer	eBioscience	00-8222-49
1x permeabilization buffer	eBioscience	00-8333-56
Streptavidin, Alexa-Fluor 488 conjugate	Invitrogen	21832
Unstained OneComp ebeads compensation beads	eBioscience	01-111-42
HALT protease & phosphatase inhibitor cocktail	Thermofisher	1861284
BCA colorimetric assay	Thermofisher	23227
Bovine Serum Albumin Standards	Thermofisher	23208
4x laemmli buffer	Bio-Rad	1610747
BOLT 4%-12% Bis-Tris Gels	Invitrogen	NW04125BOX
250kDa Protein Ladder	BioLabs	P7719S
iBLOT mini stack system	Invitrogen	IB23002

StartingBlockT20	Thermofisher	37543
Streptavidin, Alexa-Fluor 680 conjugate	Invitrogen	S32358
Silverstain	Thermofisher	24612
lysyl endopeptidase	Wako	125-05061
Trypsin	Promega	V5111
HLB columns	Oasis	186003908
Reagent A	Thermofisher	23222
Reagent B	Thermofisher	23224
Complement proteins Luminex immunoassay	Millipore	HCMP2MAG-19K-06
MAPK phosphoproteins Luminex immunoassay	Millipore	48-660MAG
HSP60, 60KDa heat-shock protein	Cell Signaling	12165
$\beta$ -actin	Santa Cruz Biotechnology	sc-47778
IRDye800	LI-COR	925-32211
HRP anti-mouse	Jackson ImmunoResearch	115-035-033
PAP-1	Synthesized in Wulff lab as described [37]	N/A
Anti pSTAT1	Cell Signaling	9167S
Anti STAT1	Cell Signaling	14994

## v. RESULTS

### **Validation of N and C terminus TurboID fusion constructs for mapping the Kv1.3 interactome in HEK-293 cells.**

To identify Kv1.3 interacting proteins, we employed proximity labeling via TurboID, wherein TurboID was fused to the N-terminus or C-terminus of Kv1.3 and then expressed in mammalian cells *in vitro* for proteomic labeling and mass spectrometry-based quantification of biotinylated proteins. TurboID is a biotin ligase that rapidly and promiscuously biotinylates proteins within a 10-30 nm radius [24]. TurboID constructs were generated such that TurboID was fused to the N-terminus or C-terminus of Kv1.3 with an intervening 15 amino acid linker, and a V5 tag (**Fig. 1A and B**). A construct that globally expresses TurboID in the cytoplasm was used as a positive control. Transfection with plasmid containing an unrelated V5 tagged protein (MetRS) with an otherwise identical plasmid, was a transfection control. These constructs were inserted into plasmids and transfected into human embryonic kidney (HEK-293) cells. After 24 h of transfection, cells were then exposed to biotin for 24 h (**Fig. 1B**). We specifically chose HEK-293 cells based on their negligible basal levels of Kv1.3 channel expression, providing an optimal system for initial validation of the TurboID-Kv1.3 fusion constructs [35].

We conducted electrophysiological studies on transfected HEK-293 cells using the whole-cell patch-clamp technique to confirm the functional expression of recombinant Kv1.3 channels at the cell surface. The current amplitude produced by the transiently transfected fusion constructs was similar to that of the transfected WT Kv1.3, indicating that the fusion with TurboID on either the N-terminus or C-terminus had no effect on trafficking and insertion of the channel into

the plasma membrane. (**Fig. 1C and Supp. Fig. 1A**). At 10 nM, PAP-1, a selective Kv1.3 blocker, potently inhibited more than 90% of Kv1.3 currents in HEK-293 cells over-expressing WT Kv1.3 or Kv1.3-TurboID fusions, confirming that all currents detected were indeed associated with transfected Kv1.3 (**Fig. 1C and Supp. Fig. 1A**). Interestingly, both constructs fused with TurboID exhibited a small shift in the voltage-dependence of activation towards more positive potentials (**Fig. 1D and 1G**), a delayed decay of use-dependent current upon repeated stimulation (**Fig. 1E and 1G**), and slower inactivation decay (**Fig. 1F and 1G**). The C-terminal fused Kv1.3 showed delayed activation kinetics compared to positive controls of HEK-293 cells transfected with unmodified Kv1.3 (**Fig. 1D and 1G**). Overall, these studies highlighted that our Kv1.3-TurboID fusion constructs are properly inserted and retained functional and pharmacological properties at the cell surface but exhibit minor changes in activation/inactivation kinetics [36].

Immunofluorescence microscopy was performed to confirm Kv1.3 channel localization to the cell surface and inside the cell, along with colocalization with biotinylated proteins (**Fig. 1H**). Transfection control, with a non-TurboID plasmid, showed a presence of the V5-tagged MeTRS and no biotinylation (**Fig. 1H** control row). The N-terminal construct and the C-terminal construct showed similar localization of V5 and biotinylation to the cell surface, which confirmed localization of Kv1.3 and biotinylation of membrane-associated proteins that was comparable across Kv1.3 TurboID-fusion constructs. In contrast with Kv1.3-TurboID fusion constructs, we also over-expressed cytosolic TurboID (TurboID-NES not fused to any protein) [24] in HEK-293 cells, which showed expected V5 localization and biotinylation to the cytosol. These indicated that the expression of the Kv1.3 channel is likely on the plasma membrane and that the biotinylation of proteins corresponded with membrane localization of Kv1.3 channels.

Cells were then lysed in 8 M Urea lysis buffer, and biotinylated proteins were affinity purified using streptavidin magnetic beads. Western blot of inputs (before streptavidin affinity purification [AP]) and after AP showed a higher level of biotinylated proteins in N-terminal and C-terminal fusions compared to negative control (**Fig 1I and Supp. Fig. 1B and C**). In contrast, the biotinylation pattern of cytosolic TurboID transfected cells was distinct from that of the Kv1.3-TurboID fusion transfected cells (**Fig 1I and Supp. Fig. 1B and C**). These experiments established that Kv1.3 is present and functional on the surface, and that TurboID is able to biotinylate proteins in HEK-293 cells in a pattern distinct from global cytosolic TurboID expression. We proceeded with MS of biotinylated proteins to identify Kv1.3 N-terminal and C-terminal interacting proteins in HEK-293 cells.

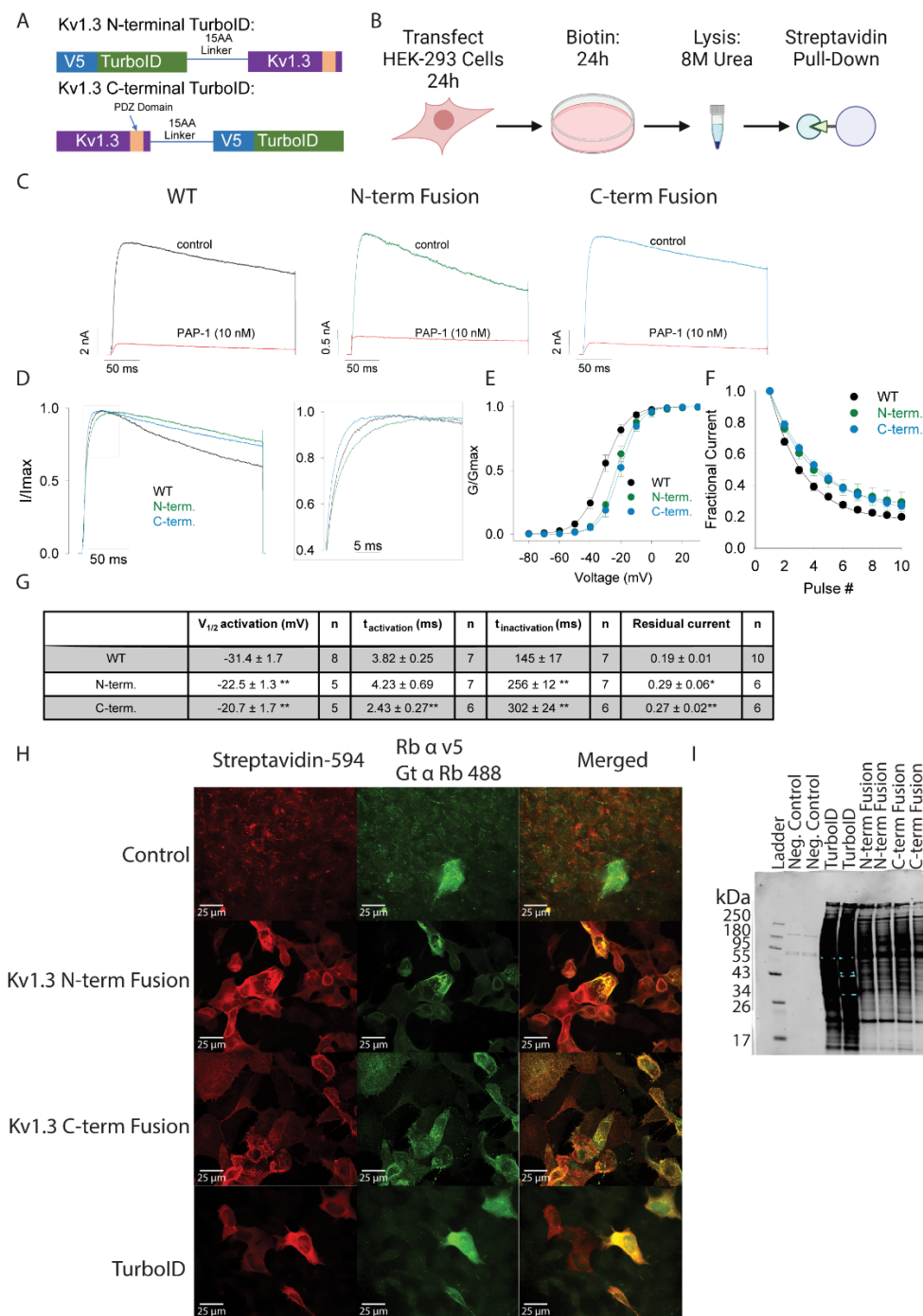


**Figure 1: Transfected cells show Kv1.3 channel activity and biotinylation of proximal proteins. (A)** Schematic of experimental design. HEK-293 cells were transfected with Kv1.3-

turboID fusion constructs for 24 h then exposed to biotin for 24 h. Cells were then lysed in 8 M urea and pulled-down using magnetic beads fused to streptavidin prior to mass spectrometry. **(B)** Constructs of Kv1.3 fusion with TurboID. Each fusion construct contains TurboID, a 15 amino acid linker, a V5 tag and Kv1.3. The N-terminal fusion, has TurboID located on the N-terminus of Kv1.3, and the C-terminal fusion has TurboID located on the C-term of Kv1.3. **(C)** Electrophysiology of HEK-293 cells transfected with Kv1.3-TurboID constructs shows similar biophysical properties and pharmacological responses to the Kv1.3 inhibitor PAP-1. **(D)** Averaged current traces showing N-terminal and C-terminal fusions induce a slight slowing of current inactivation while the C-terminal fusion enhances the activation compared to WT control. **(E)** The voltage-dependence of activation of Kv1.3 channels fused to TurboID shows a small shift in the depolarized direction compared to the WT control. **(F)** TurboID fusing reduces use-dependent inactivation. **(G)** Table highlighting changes in biophysical properties with TurboID fusion to Kv1.3. Statistical significance denotes  $p < 0.05$  (\*) and  $p < 0.01$  (\*\*). **(H)** Immunofluorescence (IF) of HEK-293 cells transfected with Kv1.3-TurboID Constructs. IF highlights colocalization of biotinylated proteins (tagged with Streptavidin) with V5 tagged TurboID. **(I)** Streptavidin (680) Western blot shows high biotin labeling with presence of TurboID. n=3.

### **Kv1.3 Amino and Carboxyl terminal fusions with TurboID identifies distinct domain-interacting proteins in HEK-293 cells.**

After confirmation of Kv1.3 channel activity and TurboID biotinylation of proteins, we wanted to evaluate which proteins were interacting with Kv1.3. Affinity purified (AP) proteins were assessed by silver stain and Western Blot to check for quality of proteins available and efficiency

of AP, a higher efficiency meaning less overall protein in controls in the silver stain (**Supp. Fig 1C**). To evaluate the Kv1.3 interactome, AP proteomes from all Kv1.3-TurboID fusion transfections were first normalized to TurboID protein abundance to account for any uneven transfection or efficiency of SA-enrichment. These normalized data were visualized using Principal component analysis (PCA). Principal Component 1 (PC1) accounted for 79% variance and clearly separated samples containing biotinylated proteins via TurboID, from non-TurboID controls (**Fig. 2A**). PC1 therefore represents proteins that were labeled by TurboID across all experimental conditions.

We then performed differential enrichment analysis (DEA) to identify proteins that interact with Kv1.3 that appear both in the N and C terminal proteomes (*i.e.* proteins within labeling radius of TurboID) as well as proteins that show selective interactions with the N or C terminus of Kv1.3. Differential enrichment showed 1,681 N-terminal interacting proteins (**Fig. 2B**) and 1716 C-terminal interacting proteins (**Fig. 2C**). A large proportion of these N-terminal and C-terminal interactomes overlapped (**Supp. Fig. 1**), probably indicative of general Kv1.3 channel protein interactors that were within the 10-20nm labeling radius of TurboID, regardless of N-terminus or C-terminus. While the N and C terminus of one Kv1.3 monomer may be separated in space, N and C termini of the adjacent Kv1.3 monomers in the tetrameric complex are likely closer to each other potentially explaining this overlap. The surprisingly large numbers of Kv1.3 interactors is also likely due to TurboID biotinylating proteins at all steps of Kv1.3 being processed, through the ER before being localized to the cell membrane. Accordingly, many of the interactors listed were associated with ER processing of proteins (*e.g.* SEC24A, SEC16A, HSPA5).

Although the majority of the N-terminal and C-terminal interactomes of Kv1.3 overlapped, some proteins were uniquely enriched in a domain-specific manner. DEA comparing N-terminal and C-terminal interactors directly, showed 32 proteins associated with the N-terminus of Kv1.3 and 40 proteins associated with the C-terminus of Kv1.3 (**Fig. 2D**). Gene set enrichment analysis (GSEA) highlighted biological processes associated with the N-terminus, involved in metabolic processing (*e.g.* TNXL1, ACSL1, and EPHX2) (**Fig. 2D**). The proteins that interacted with the N-terminus were likely associated with processing proteins to the ER such as some of the key metabolic interactors. In contrast, the C-terminal-specific interactome of Kv1.3 was enriched in proteins associated with signal transduction (*e.g.* SMAD3, RAC1, and CNOT1) (**Fig. 2D**). We also used Search Tool for the Retrieval of Interacting Genes/Proteins (STRING), to visualize known protein-protein interactions (PPIs) within these domain-specific Kv1.3 interactors (**Fig. 2E and F**). STRING analysis showed that Kv1.3 N-terminal interactors were involved in processing of proteins from the endoplasmic reticulum to the cell membrane. SRRM2, NACA, and TXNL1(**Fig. 2E**). Kv1.3 C-terminal interactors were largely associated with cell signaling (**Fig. 2F**). These results in HEK-293 cells indicate that distinct protein interactors of Kv1.3 channels can be defined using N and C terminal TurboID fusion, without significant disruption of channel physiology. Our analyses of both the protein lists and GSEA suggest that the N-terminus of Kv1.3 is primarily associated with protein processing whereas the C-terminus is associating with signaling proteins. Based on these studies in HEK-293 cells, we next applied TurboID-based proximity labeling to examine Kv1.3 channel interactomes in microglia.

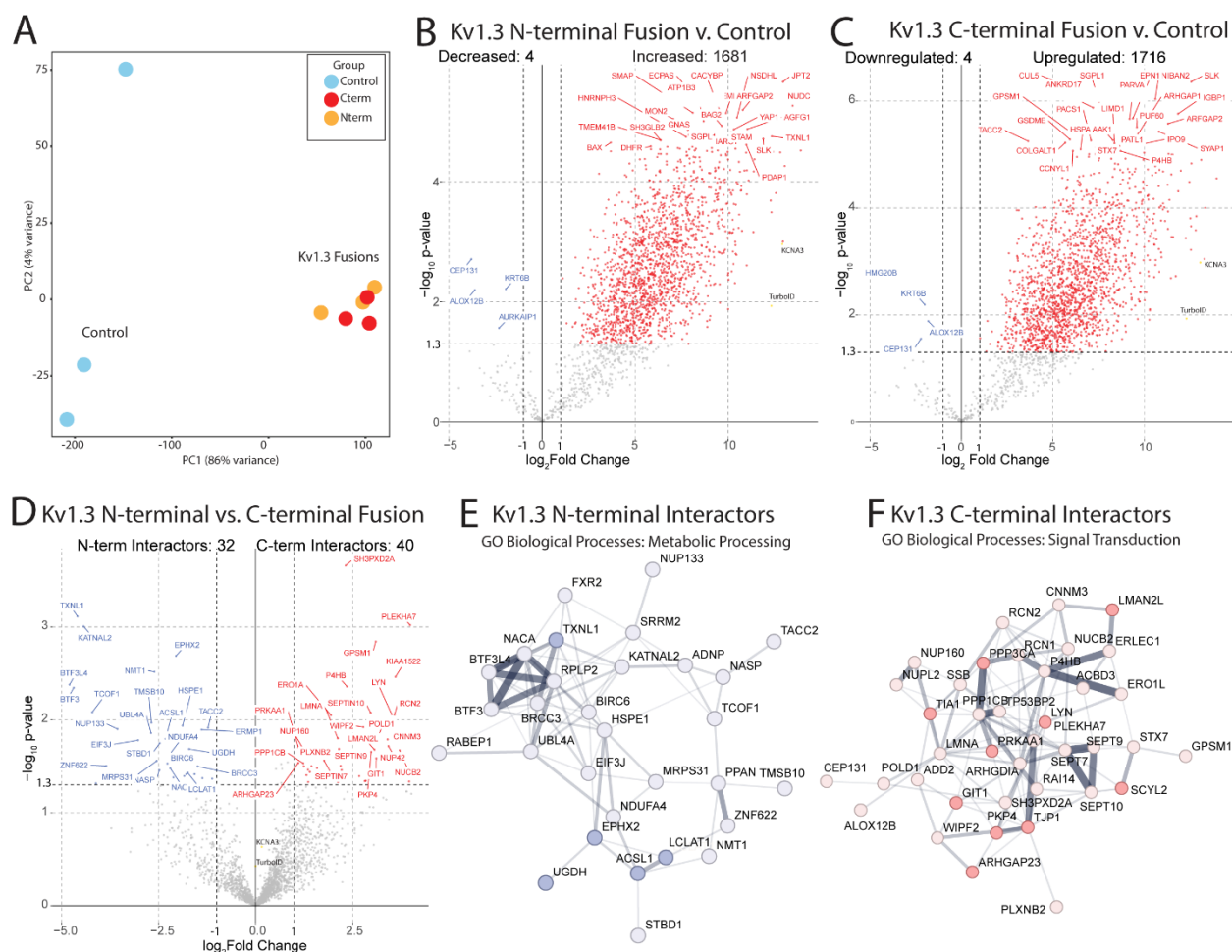


**Figure 2: Kv1.3 interactors in HEK-293 Cells show that the N-terminus is associated with protein processing and the C-terminus is involved in signaling. (A)** Principal Component Analysis (PCA) of mass spectrometry of biotinylated proteins shows distinct separation between control and Kv1.3-TurboID transfected cells. **(B)** Differential Abundance Analysis of N-terminal interactors shows about 1600 protein interacting with Kv1.3. **(C)** Differential Abundance Analysis of C-terminal interactors shows about 1700 proteins interacting with Kv1.3. **(D)** Differential Abundance Comparison between N and C terminal interactors shows 32 proteins interacting more with the N-terminus of Kv1.3 and 40 proteins interacting with the C-terminus of Kv1.3. **(E)** String analysis shows close associations with N-terminal interactors. Gene Ontology highlights that many of these proteins are associated with metabolic processing. **(F)** String

Analysis and GSEA analysis show that many of the C-terminal interactors are associated with signal transduction. Darker colors represent statistical significance in GSEA results, lighter color indicates an interactor that is not present in GSEA lists but interacting with Kv1.3, and edge thickness represents confidence of interactions based on literature. Differential Abundant proteins were calculated using paired t-test, where  $\log P\text{-value} > 1.3$  and  $\text{Log}_2 \text{Fold Change (FC)}$  of  $\pm 1$  were considered significant.  $n=3$  \*\* $p < 0.01$ , \*\*\*  $p < 0.001$

### **Generation and validation of stably transduced BV-2 microglial lines expressing N and C term Kv1.3-TurboID fusions**

We chose the mouse-derived immortalized BV-2 microglial cell line as a model system to first identify proteins that interact with Kv1.3 channels in a N and C term-specific manner, and then test whether these domain-specific interactions were altered when microglia adopt pro-inflammatory phenotypes. BV-2 cells were transduced for 24 h with lentiviruses (LV) or no LV for control, encoding one of three constructs confirmed in HEK-293 cells: a Kv1.3 Fusion protein with TurboID on the N-terminus, Kv1.3 fusion with TurboID on the C-terminus, and an Kv1.3-TurboID C-terminal fusion with the PDZ-binding domain removed (**Fig. 3A**). TurboID globally expressed in the cytoplasm was used as a positive control and untransduced BV-2 cells were utilized as a negative control. Following puromycin selection for seven days, transduced cell lines were either exposed to lipopolysaccharide (LPS, 100 ng/mL) or PBS for 24 h and then exposed to biotin for 1 h to increase the stringency of the interactomes of Kv1.3 (**Fig. 3A**). LPS induction was used to induce a pro-inflammatory like state in BV-2 microglia. We first performed qRT-PCR and confirmed that *Kcna3* mRNA was highly and comparably transcribed across all three lines as compared to sham transduced/control BV-2 cells (**Fig. 3B**). Western blot

and flow cytometry showed biotinylation in Kv1.3-TurboID transduced microglia, which was absent in control BV-2 cells (**Fig. 3C and D**).

To determine whether stably transduced BV-2 lines exhibited functional Kv1.3 channel currents on the cell surface, we performed electrophysiological studies confirming that comparable and high Kv1.3 current densities were present across all cell lines (**Fig. 3E**). Similar to results observed in HEK-293 cells, BV-2 cells transduced with either of the three constructs fused with TurboID exhibited a positive shift in the voltage-dependence of activation, less use-dependent current decay, and delayed inactivation kinetics (**Fig. 3G-J**). The C-terminal fused Kv1.3 also showed enhanced activation kinetics compared to positive controls of HEK-293 cells transfected with unmodified Kv1.3 (**Fig. 3G and J**). PAP-1 also blocked Kv1.3 currents [37] (**Fig. 3I and Sup. Fig. 2A**) confirming the identity of the overexpressed Kv1.3 channels in BV-2 cells. These experiments showed that Kv1.3 is functionally active at comparable levels across all BV-2 Kv1.3-TurboID cell lines, with small, yet significant, increase in current with BV-2 cells transduced with Kv1.3 compared to a HEK-293 cell. These studies therefore lay the foundation for proteomic assessments of Kv1.3 channel interactomes in microglia using the proximity-labeling approach.

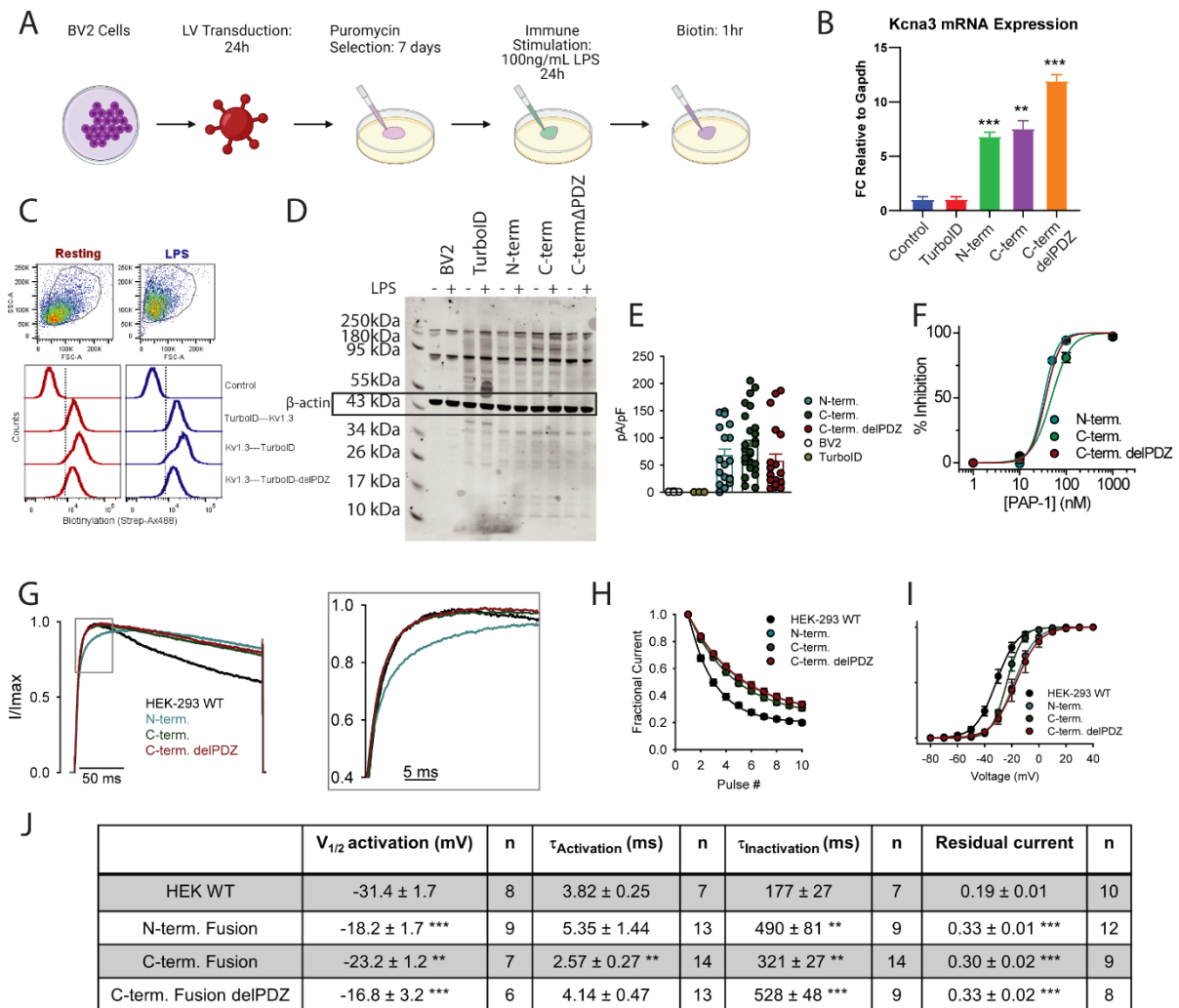


**Figure 3: BV-2 cells transduced with Kv1.3-TurboID constructs show presence of biotinylation and channel activity. (A)** Schematic of experimental design. BV-2 cells were transduced with Kv1.3 constructs described in Fig 1B and selected for plasmid uptake using puromycin. Cells were then exposed to LPS to induce an inflammatory response and biotin to allow for biotinylation of proximal proteins. **(B)** qRT-PCR of Kcna3 transcript shows increased Kcna3 mRNA expression in Kv1.3-TurboID transduced cell lines compared to control and Gapdh. **(C)** Flow cytometry of biotinylated proteins using Streptavidin-488 shows high biotinylation in Kv1.3-TurboID transduced cell lines independent of LPS exposure. **(D)** Western blot depicting streptavidin-680 labeling, which highlights biotinylation increase in the presence

of TurboID. Ponceau staining shows no change in protein concentration across samples. **(E)** Scattered plot shows increased channel density in BV-2 cells transduced with Kv1.3-TurboID constructs. **(F)** Inhibition of Kv1.3 by PAP-1, a Kv1.3-selective small molecule inhibitor, following transduction of Kv1.3-TurboID constructs. **(G)** Exemplifying current traces showing changes in inactivation and activation kinetics in transduced Kv1.3-TurboID cells. **(H)** Fractional currents show reduced use-dependent current reduction of Kv1.3 currents in Kv1.3-TurboID transduced cells. **(I)** Voltage-dependent activation of Kv1.3 is shown to be shifted in the depolarized direction in cells transduced by Kv1.3-TurboID constructs. **(J)** Table summarizing electrophysiology results. Statistical significance denotes  $p < 0.05$  (\*),  $p < 0.01$  (\*\*), and  $p < 0.001$  (\*\*\*)).

### **Identification of Kv1.3 channel domain-specific protein interactors and molecular pathways in BV-2 microglia**

In order to evaluate proteins that interact with Kv1.3 in microglia, biotinylated proteins were enriched from whole cell lysates of BV-2 lines by affinity purification with streptavidin magnetic beads. Affinity purified proteins were verified by Western Blot and silver stain (**Supp. Fig 2B**). Via PCA of the cell lysates, we confirmed that LPS induction accounted for 23% of the variance of proteins in the total samples, whereas the addition of Kv1.3 did not alter variance within the samples (**Supp. Fig. 3A**). This indicated that overexpression of Kv1.3 did not significantly alter proteins present in each sample. DEA of proteins present in the cell lysates highlighted that LPS induced an increase of proteins associated with a neuroinflammatory response, including TLR2, IL-1 $\alpha$ , and STAT1 (**Supp. Fig. 3B**). TurboID-normalized AP samples (n=3) were clustered using Principal component analysis (PCA). PC1 accounted for 65% variance and separated the samples

with TurboID present from the un-transduced BV-2 controls as well as N-terminal fusions from C-terminal fusions (**Fig. 4A**). Separation of controls and all TurboID samples indicated that both biotinylation and enrichment was successful. PC2 accounted for 10% of the variance and separated the different cell types: overexpression of Kv1.3, un-transduced control, and global TurboID, which acts as a positive control for biotinylation but does not have Kv1.3 attached (**Fig. 4A**). This finding highlighted that the proteins biotinylated in BV-2 cells transduced with Kv1.3 are unique compared to un-transduced controls or the biotinylated proteome of BV-2 cells with global (cytosolic) TurboID localization.

We hypothesized that Kv1.3 would have distinct interactors between the N and C termini of the channel in microglia. There were many proteins present in the samples transduced with Kv1.3-TurboID that were absent in the untransduced controls (**Fig. 4B**). In total 991 proteins interacted either with the N or C terminus of Kv1.3 and were distinctly present in Kv1.3-TurboID transduced (**Fig. 4B and Supp. Fig. 3 C-E**). GSEA and STRING analyses of these Kv1.3-specific interactors identified protein localization/transport, metal ion transporters, cholesterol metabolism, amino acid transporters, N-glycan biosynthesis and immune/defense proteins (**Fig. 4C**). The most represented pathway in the Kv1.3 interactome in KEGG 2021 was protein processing in endoplasmic reticulum (corrected  $p$  4.84E-22). These include ER translocon and translocation machinery, such as SEC61A1, SEC61B, SEC61G, SEC63, HSPA5. The largest interaction groups with Kv1.3 in general were associated with cholesterol metabolism (*e.g.* NPC1 and ABCA1) and protein localization/transport (*e.g.* Tmem165 and MAGT1) (**Fig. 4C**). We also identified an immune/defense response cluster of Kv1.3 channel interactors including integrins (ITGB1, ITGAX), TLRs (TLR2, TLR13), receptor tyrosine phosphatases (*e.g.* PTPRC/CD45), lysosomal protein CD68 and Alzheimer's disease related proteins (*e.g.* SORL1,

ITGAX) (**Fig. 4C**). Next, we compared how Kv1.3 terminal interactors differ between the termini.

Comparing the Kv1.3 N-terminus to C-terminus in BV-2 transduced cells, identified 284 proteins that preferentially interacted with the Kv1.3 N-terminus. These included proteins like TIMM50, a mitochondrial translocase protein, and NUDC and TXNL1, associated with protein processing (**Fig. 4D**). In comparison, far fewer exclusive C-terminal interactors were identified, including SNX3 and MYO6, both associated with intracellular processing (**Fig. 4D**). GSEA of the Kv1.3 N-terminal interactors show processes associated with calcium ion transport and oxidoreductase activity (**Fig. 4E**). In contrast to N and C terminal interactors in HEK-293 cells (albeit human), the N terminal interactome of Kv1.3 in BV-2 cells was much larger while the C terminal interactome was smaller. Our analyses in BV-2 cells identified the distinct Kv1.3 N-terminal and C-terminal interactors, among which the C terminal interactome was most impacted by LPS treatment of BV-2 cells, indicative of context-dependent changes of the Kv1.3 channel interactome.

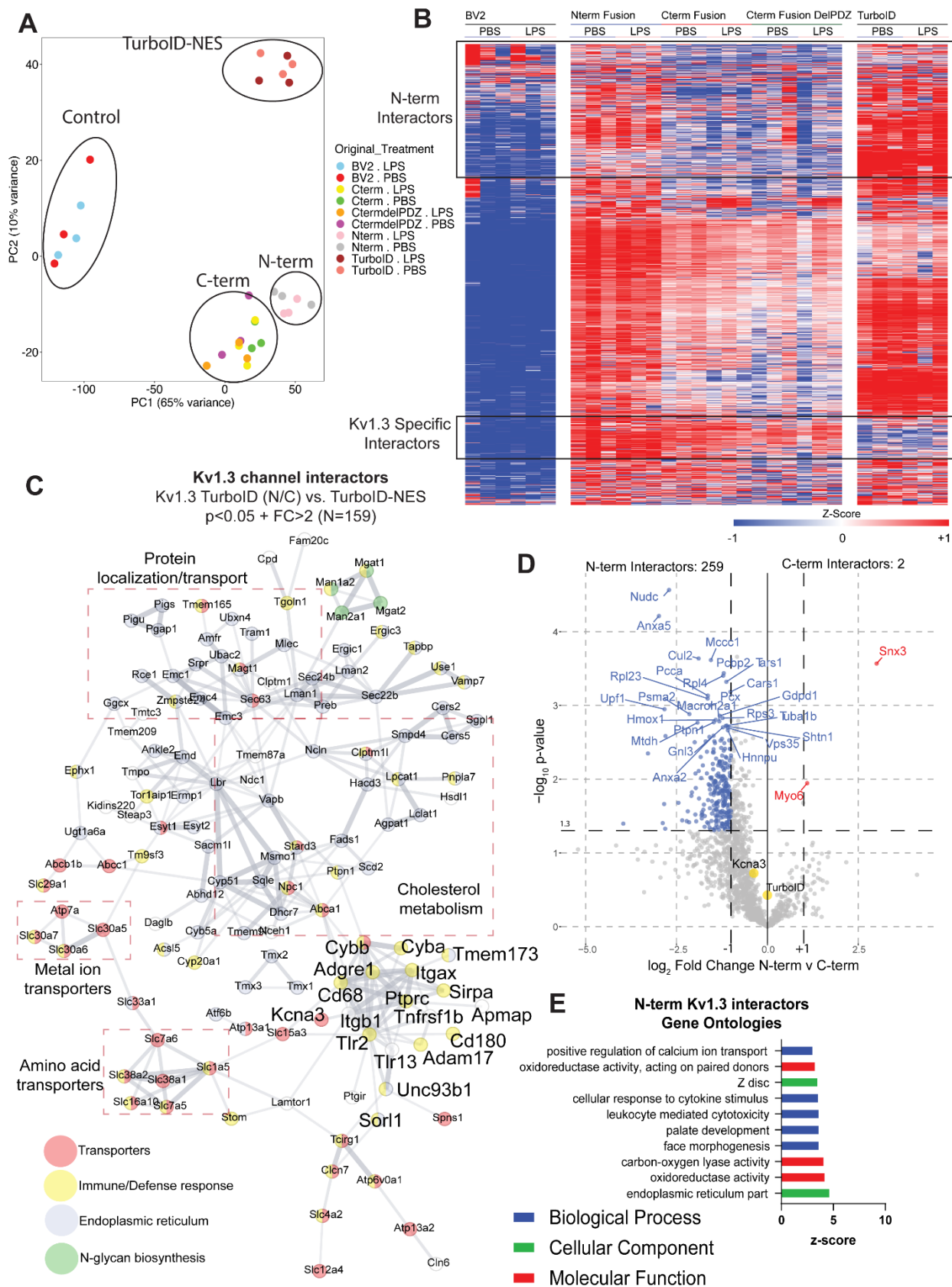


**Figure 4: Microglial Kv1.3 have distinct N-terminal and C-terminal interactors. (A)**

Principal Component Analysis (PCA) of mass spectrometry of biotinylated proteins show distinct clustering of controls, TurboID, Kv1.3 N-term fusion, and Kv1.3 C-term fusion. **(B)** Heat map of biotinylated proteins, designed by Morpheus, show distinct clusters of Kv1.3 specific interactors, Kv1.3 N-terminal specific interactors, and Kv1.3 C-terminal interactors. Individual proteins were colored based on z-score, where the darker shades of red indicate +1 and the darker shades of blue indicates -1. Hierarchical clustering arranged proteins based on groups. **(C)** STRING analysis highlights proteins differentially interacting with Kv1.3 over global TurboID expression. Color indicates protein type. Associated protein groups are boxed. **(D)** Differential Enrichment Analysis (DEA) of proteins enriched with Kv1.3 N-terminal fusion and Kv1.3 C-terminal fusion indicates about 250 N-terminal interactors and 2 C-terminal interactors. **(E)** Gene set enrichment analysis (GSEA) analysis shows most of the interacting proteins with the N-terminus of Kv1.3 appear to be a part of calcium transport and oxidoreductase activity. Differential Abundant proteins were calculated using paired t-test, where  $\log P\text{-value} > 1.3$  and  $\text{Log}_2 \text{Fold Change (FC)}$  of  $\pm 1$  were considered significant.  $n=3$

**Pro-inflammatory activation preferentially modifies the C-terminal interactome of Kv1.3 channels in microglia**

Microglia are well known to adopt distinct inflammatory profiles when exposed to immune stimuli, and their cellular functions are context-dependent [38, 39]. We therefore next assessed whether LPS pro-inflammatory activation impacted the Kv1.3 channel interactome in a domain-specific manner. We found that there were many LPS-induced C-terminal interactors that were also highly abundant in cells with a LPS response, although the N-terminal interactome was not

impacted by LPS treatment (**Fig. 4B**). In the presence of LPS, we hypothesized the interactors of Kv1.3 would shift towards inflammatory signaling. DEA showed negligible effects of LPS on the Kv1.3 N-terminal interactome, even though LPS effects were noted on the whole cell proteome (**Fig. 5A**). DEA showed in the presence of LPS there were 36 proteins increased and 27 proteins decreased in the C-terminal interactome (**Fig. 5B**). Proteins with increased interaction with the C terminus upon LPS activation included STAT1, C3, and TLR2, often associated with a proinflammatory response in microglia, whereas the decreased proteins include SNX3 and HSPA9. GSEA showed the C-terminal proteins that interacted with Kv1.3 in the absence of LPS, associated with the ER and transport (**Fig. 5C**). In the presence of LPS, Kv1.3 C-terminal interactors transitioned towards inflammatory proteins and immune effector processes (**Fig. 5D**). This increase in C terminal interactors by LPS cannot be explained by increased total protein abundance itself, because this increase was largely absent in the N-terminus as well as in the global TurboID conditions. In addition, what makes this interactome even more interesting is that there is a paucity of secreted proteins in the unstimulated Kv1.3 interactome which suggested that these results may be selective. In fact, the overlap between the Kv1.3 interactome and the human secretome is just 63 proteins. Therefore, we conclude that the pro-inflammatory context of microglial activation specifically modifies the C-terminal interactome of Kv1.3 channels, potentially linking channel function with immune signaling machinery.

### **Kv1.3 C-terminal inflammatory interactors dependent on the PDZ binding domain**

The Kv1.3 PDZ-binding domain has been shown to be essential to Kv1.3 function [23]. Since the C-terminus of Kv1.3 interacted with signaling proteins across two mammalian cell lines, we

hypothesized that deletion of the PDZ binding domain of the C-terminus of Kv1.3 would result in a reduction of interacting proteins with the C-terminus. DEA identified 70 Kv1.3 C-terminus interacting proteins with reduced interactions with the C-terminus upon deletion of the PDZ-binding domain, including SNX3, ND3, and NSF. Conversely, we found 16 proteins with increased interactions with the C-terminus when the PDZ-binding domain was removed, including GBA, NRP2, and CRTAC1 (**Fig. 5E**). GSEA of the proteins that interacted with the C-terminus in a PDZ-dependent manner (proteins with reduced interactions with Kv1.3 upon PDZ-binding domain removal), showed an association with the cellular component of coated vesicles and the biological processes of antigen processing and presentation and immune-response-regulating signaling pathway (**Fig. 5F**). Proteins that showed increased C-terminal interaction upon PDZ-binding domain removal were enriched in ontologies related to lipid biosynthesis and alcohol metabolic processing (**Fig. 5G**). These results highlighted several proteins and pathways related to the C-terminal Kv1.3 channel interactome that require the PDZ binding domain to interact with Kv1.3.

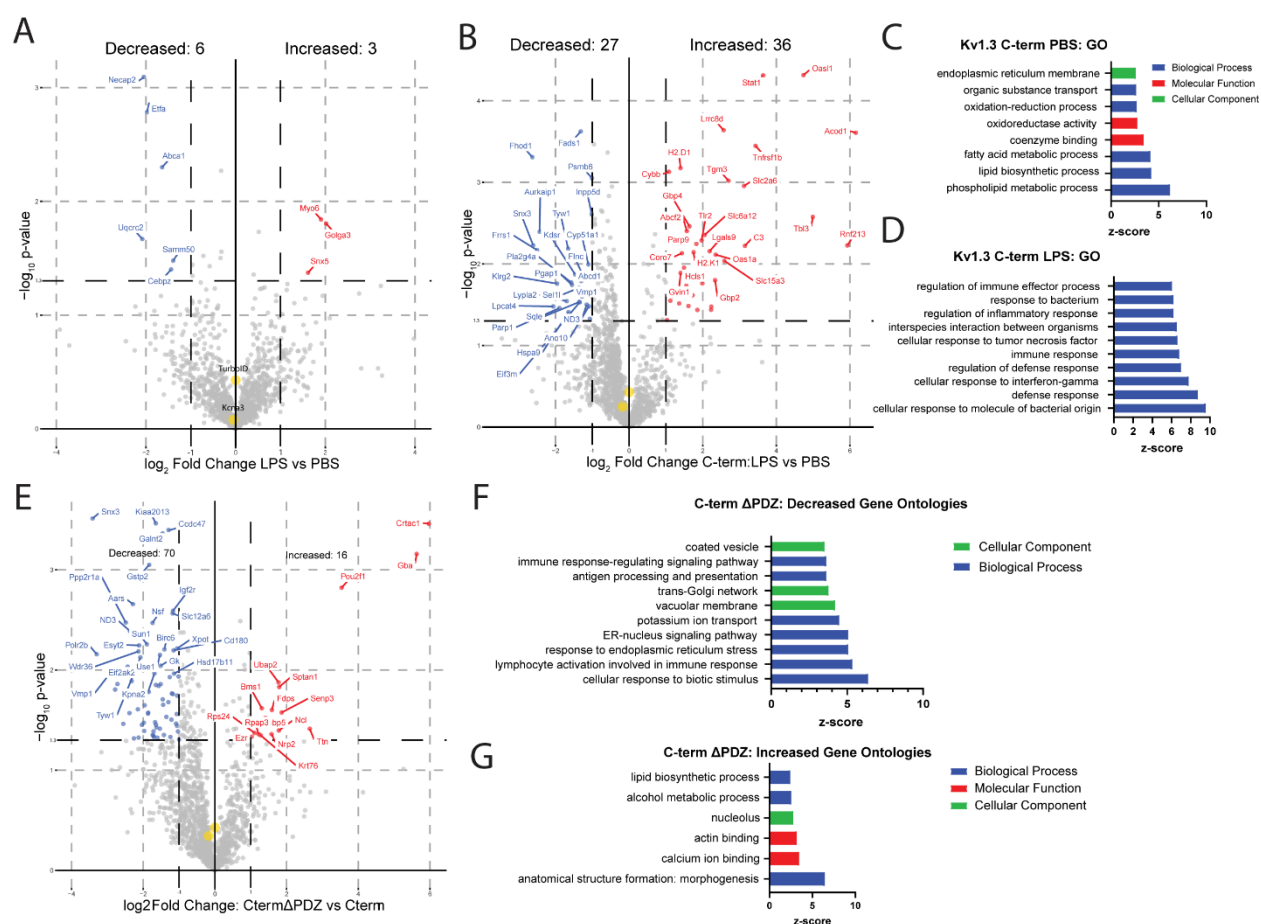


**Figure 5: Inflammatory exposure results in a PDZ-binding domain dependent interactions with the C-terminus of Kv1.3. (A)** Differential Enrichment Analysis (DEA) between N-terminal interactors and N-terminal interactors with LPS exposure highlights minimal change in N-terminal interactors with LPS exposure. **(B)** DEA between C-terminal interactors and C-terminal interactors show 27 proteins interacting with the C-term of Kv1.3 during homeostasis and 36 proteins interacting with the C-terminus during an LPS-induced inflammatory response. **(C)** Gene Set Enrichment Analysis (GSEA) analysis shows protein transport and processing terms downregulated during an LPS response. **(D)** GSEA shows an upregulation of immune signaling terms associated with the C-terminus of Kv1.3 during LPS immune stimulation. **(E)** DEA comparison of Kv1.3 C-terminal interactors and C-terminal interactors with the PDZ-

binding domain removed shows 70 proteins downregulated and 16 upregulated with deletion of the PDZ-binding domain. **(F)** GSEA analysis of proteins downregulated with the deletion of the PDZ-binding domain are mostly associated with immune-signaling response and protein packaging. **(G)** GSEA analysis of proteins upregulated with deletion of the Kv1.3 C-terminal PDZ-binding domain shows terms associated with lipid biosynthesis and alcohol metabolism. Differential Abundant proteins were calculated using paired t-test, where  $\log P\text{-value} > 1.3$  and  $\text{Log}_2 \text{Fold Change (FC)}$  of  $\pm 1$  were considered significant.

### **Kv1.3 channel is present in mitochondria-enriched fractions in microglia**

The Kv1.3 channel can be detected at the plasma as well as the inner mitochondrial membranes in lymphocytes and cancer cells [15, 40, 41]. To assess the presence of Kv1.3 in mitochondria from BV-2 cells transduced with Kv1.3-TurboID constructs, we prepared subcellular fractions from total cell homogenates (Fraction 0) by sequential centrifugation. Fraction A1 contained light membranes, Fraction A2 contained crude mitochondria, and Fraction A3 was enriched in mitochondria (**Fig. 6A**). Western blot analysis of the mitochondrial marker HSP60 showed that HSP60 levels were increased in Fractions A3 compared to Fractions 0, confirming mitochondrial enrichment of fraction A3 was successful (**Fig. 6B**). Next, Western blot analysis of these fractions, probed for V5 (fused to Kv1.3-TurboID or to TurboID), detected V5 bands that corresponded to the predicted molecular weights of fusion proteins in all subcellular fractions from BV-2 cells transduced with Kv1.3-TurboID constructs (N-term, C-term, and C-term  $\Delta$ PDZ), including the mitochondria-enriched fractions A3 (**Fig. 6C**). Small variabilities between V5-tagged N-terminus and C-terminus intensities may be due to small variability in TurboID expression. No bands were detected in un-transduced BV-2 cells (Neg. Control) (**Fig. 6C**).

STRING analysis of Kv1.3 interactors that are present in the MITOCARTA 3.0 database data show 73 proteins associated with the mitochondria (**Fig. 6D**). These include proteins associated with transport of proteins to the mitochondria and mitochondrial ribosomal machinery (*e.g.* TIMM50, MRPS30, and TMX1). Our results provide evidence for mitochondrial Kv1.3 protein presence in mitochondrial fractions from BV-2 cells transduced with Kv1.3-TurboID constructs.

### **Verification of interactions of Kv1.3 with C3 and pSTAT1 via the C terminal domain**

Among the immune-related protein interactors of Kv1.3 that were measured by our MS studies, we nominated C3 and STAT1 as proteins of interest to be validated by Luminex based on their known role in several neuroinflammatory and neurodegenerative diseases [42-47]. The standard Luminex approach immobilizes the protein of interest on to a bead via capture antibody, and then uses a biotinylated detection antibody followed by streptavidin-fluorophore conjugate to quantify abundance of the target protein [31]. We adapted this approach by omission of the detection antibody, so that all C3/pSTAT1 would be captured but only their biotinylated forms would be detected, which proved a direct quantification of the biotinylated forms of these proteins from a total cell lysate without enrichment (**Fig. 6E**).

The adapted assay was able to detect biotinylated C3 in cell lysates from the C-term TurboID Kv1.3 BV-2 cells, regardless of LPS stimulation, confirming the MS result of an interaction between the C-terminus of Kv1.3 and C3 (**Fig. 6F**). In comparison to the adapted assay which only detects biotinylated C3 in cell lysates, the standard assay for C3 also showed an overall increased level of C3 in C-terminus Kv1.3 independent of global expression of TurboID (**Fig. 6G**). This finding can be explained by either increased C3 protein abundance in microglia when

Kv1.3 is over-expressed, or, an increased C3 signal due to detection of the protein via the capture antibody as well as detection of the biotinylated C3 via streptavidin-fluorophore. Importantly, the adapted C3 levels detected in cell lysates from Kv1.3 transduced BV-2 cells, were greater than 50% of the C3 signal from the standard assay. This suggested that majority of C3 in BV-2 TurboID cells is biotinylated by TurboID, consistent with C3 being identified as an important Kv1.3 interactor. Since C3 is not traditionally a membrane-attached protein, this result most likely represents an interaction between Kv1.3 and C3 in the processing stage of C3 before its secretion, potentially at the stage of processing in the ER translocon. This was consistent with several other ER translocon proteins identified as Kv1.3 interactors (*e.g.* SEC61A1, SEC61B, SEC61G, SEC63, HSPA5), and enrichment of protein processing in the ER, as a major over-represented pathway in the Kv1.3 interactome.

We also measured levels of phosphorylated Stat1 (pStat1 Tyr 701) to reflect activated Stat1 in BV-2 cells. Stat1 phosphorylation is triggered by type 1 and 2 interferons, leading to activation of interferon-related gene expression which are important in anti-viral immune responses, as well as in neurological diseases [48]. Previously, a functional relationship between Kv1.3 channel activity and pStat1 phosphorylation was also suggested [9]. Our MS studies suggested that the C-terminus of Kv1.3 interacts with STAT1. We utilized the Luminex assay to detect pStat1 levels in cell lysates from BV-2 cells exposed to LPS and IFN- $\gamma$ , a pro-inflammatory conditioning stimulus and a activator of Type II interferon signaling, respectively. We also examined whether the PDZ-binding domain is required for this interaction. Standard Luminex measurements of pStat1 showed that IFN- $\gamma$  treated BV-2 cells, regardless of pre-incubation with LPS, responded

via increased pStat1 levels to IFN- $\gamma$ , and this effect of IFN- $\gamma$  was decreased by half when the PDZ-binding domain of the C-terminus Kv1.3 was deleted (**Fig. 6H**).

Since our Luminex data indicated the role of Kv1.3 in the regulation of STAT1 phosphorylation, we also investigated the effect of inhibition of Kv1.3 channel on STAT1 phosphorylation levels post interferon induction. PAP-1, a small molecule inhibitor of KV1.3 was used for channel blockade in N terminal Kv1.3 -TurboID BV-2 cells followed by IFN- $\gamma$  induction. IFN-  $\gamma$  induction resulted in a significant increase in pSTAT1, while the total STAT1 was unchanged (**Fig. 6I-K and Supp. Fig. 5**). Blockade of Kv1.3 significantly reduced STAT1 Tyr 701 phosphorylation (**Fig. 6I and J**). However, the total STAT1 level did not show significant changes upon treatment (**Fig. 6I and K**). This result supported an important role of the C-terminal domain, particularly the PDZ-binding domain, in the regulation of the interaction between Kv1.3 and STAT1 signaling proteins in microglia.

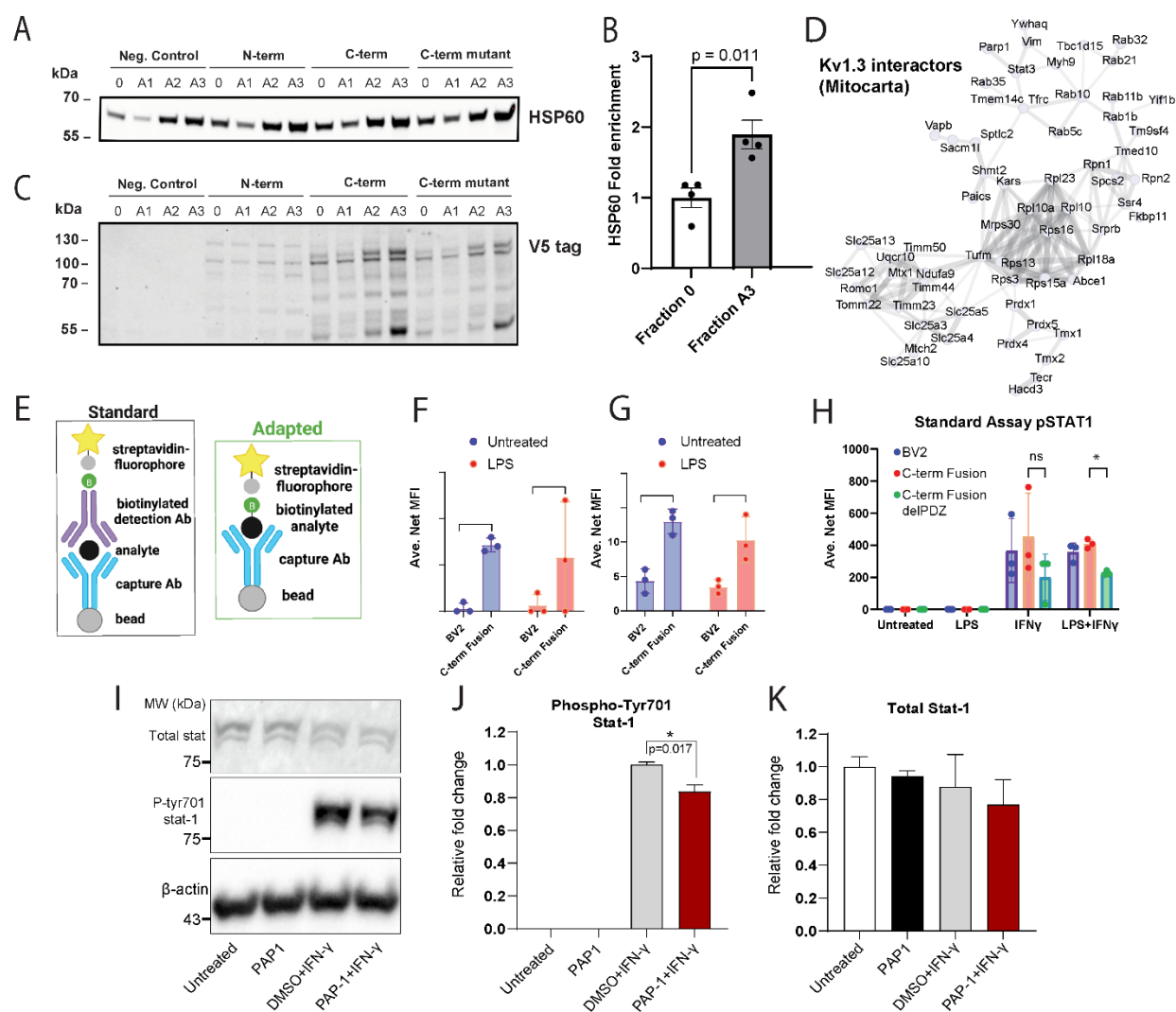


**Figure 6. Confirmation of Kv1.3 interactions with mitochondria and immune signaling. (A)**

Validation of mitochondria-enrichment in the subcellular fractions obtained during the isolation process from untransduced BV-2 cells (Neg. control) and BV-2 cells transduced with Kv1.3-TurboID constructs (N-term, C-term, and C-term $\Delta$ PDZ). Total homogenates (0) were fractionated to heavy membranes (A1), crude mitochondria (A2), and mitochondria-enriched fractions (A3) by sequential centrifugation; and then analyzed by Western blot using HSP60 as a mitochondrial marker. **(B)** Quantification of HSP60 comparing total homogenates (0) to mitochondria-enriched fractions (A3). P-value for two-sided unpaired T-test is indicated. **(C)**

Representative blot of V5 tag (TurboID fusion) in fractions 0 – A3 from BV-2 cells transduced with Kv1.3-TurboID constructs. **(D)** STRING analysis of Kv1.3 interactors cross referenced to MITOCARTA 3.0 database highlights many proteins interacting with Kv1.3 associated with the mitochondria and the functional and physical interactions. **(E)** Schematic of standard and adapted Luminex assay. Standard assay includes a bead attached to a capture antibody that binds to the protein of interest, then a biotinylated antibody binds to the protein of interest to form a sandwich. Streptavidin with a fluorophore binds to the biotin. This estimates how much of a protein is in a sample. The adapted assay includes a capture antibody with bead and then adds streptavidin with the fluorophore directly to the protein of interest. The adapted assay captures abundance of proteins interacting with Kv1.3 directly. **(F)** Adapted Luminex assay of intracellular C3 shows an increased interaction with Kv1.3 at a resting state. **(G)** Standard Luminex assay of proteins isolated from BV-2 cells transduced with Kv1.3-TurboID highlights an increase in intracellular C3 with the overexpression of Kv1.3, independent of LPS exposure. **(H)** Standard Luminex assay of pSTAT1 shows activation of pSTAT1 in the presence of IFN- $\gamma$ , a known activator of the STAT1 signaling pathway. In the presence of LPS and IFN- $\gamma$ , the removal of the PDZ-binding domain in Kv1.3 leads to a decrease in the presence of pSTAT1. **(I)** Western blot analysis of whole cell lysate from BV-2 cells expressing N-terminal Kv1.3 - TurboID shows reduced STAT1 phosphorylation upon induction with IFN- $\gamma$  post Kv1.3 blockade with PAP-1. No changes were observed in the total STAT level. **(J)** Quantification of pSTAT1 shows decrease of IFN - $\gamma$  response with PAP-1 exposure using densitometry. **(K)** Densitometry analysis shows total STAT1 is unchanged by IFN- $\gamma$  exposure or PAP-1 exposure. Significance was calculated utilizing unpaired t-test. \*  $p < 0.05$ , \*\* $p < 0.01$ , \*\*\* $p < 0.001$ , \*\*\*\* $p < 0.0001$ .  $n=3$

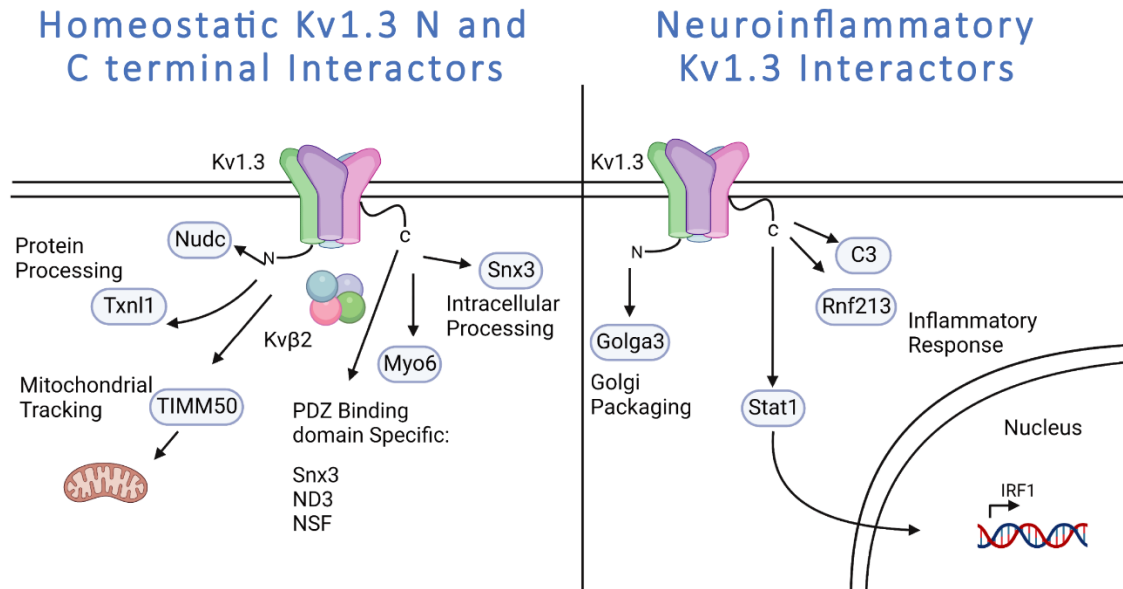


**Figure 7. Schematic of Kv1.3 interactors in microglia during homeostatic and neuroinflammatory states.** During homeostasis, many of the interactors of Kv1.3 are shared. The N-terminus appears to be responsible for protein processing and tracking to the mitochondria, whereas the C-terminus has some PDZ-binding domain specific interactors that are largely associated with intracellular processing. During LPS stimulation of an immune response, the N-terminus of Kv1.3 has very little change in the interacting partners, whereas the C-terminus has PDZ-binding domain dependent interactors associated with immune signaling.

## vi. DISCUSSION

### **Kv1.3 interacts with immune signaling proteins in microglia, exhibiting domain-specific as well as context-dependent interaction patterns**

Among several immune targets for neuroimmune modulation in neurological diseases, the Kv1.3 channel has emerged as a promising target that is highly expressed in pro-inflammatory subsets of disease-associated microglia (DAM). To address gaps in our current understanding of how Kv1.3 channels regulate immune functions of microglia, we applied a proximity-labeling approach to label the protein-protein interactome of Kv1.3 channels in mammalian cells, including mouse microglia *in vitro*. The TurboID proximity labeling technique has emerged as a tool to determine what proteins are interacting with in a close proximity to other proteins. By fusing the biotin ligase TurboID to the C- or N-terminus of Kv1.3 channels in microglia, we labeled the C- and N-terminal interactomes of Kv1.3 and used MS to quantify these biotinylated proteins after streptavidin-based enrichment. We identified over 900 proteins that interact with Kv1.3 channels in both HEK-293 cells and BV-2 microglia.

Using a combination of electrophysiology, biochemical and immunofluorescence microscopy approaches, we confirmed that fusion of TurboID to the N- or C-terminal domains of Kv1.3 via a flexible linker, has minimal impact on channel localization and biophysical properties. During a homeostatic state in HEK-293 and BV-2 cells, it appears that the majority of interactors with Kv1.3 are indistinguishable between the N-terminus and the C-terminus but distinct from a global exposure to TurboID. LPS acts through TLRs, which are involved in pathogenesis of both AD and PD [26, 27]. Using LPS allows a more precise, pathway-specific Kv1.3 interactome analysis. The Kv1.3 interactors are strongly associated with many disease-associated signaling

pathways, including proteins like TLR2 and ITGAX, many of which are associated with immune responses and the DAM phenotype of microglia neurodegeneration [26, 27, 49]. Within MS-quantified Kv1.3 interacting proteins, we identified distinct groups of proteins that preferentially interact with N and C terminal domains of Kv1.3. It appears that the N-terminus is responsible primarily for interacting with proteins associated with protein processing, while the C-terminus interacts with signaling proteins (**Fig. 7**).

Given the context-dependency of microglial states and functions in disease, we assessed whether the Kv1.3 channel interactome is altered when microglia adopt pro-inflammatory states, using LPS as a well-known pro-inflammatory stimulus [38, 39]. We found that while the N-terminal interactome was not impacted by LPS, the C-terminal interactome underwent significant reorganization, such that immune and signaling proteins showed higher levels of interaction, indicative of a domain-specific and context-specific effect of LPS. The proteins with higher interaction with the C-terminus during LPS activation included immune signaling proteins and immune proteins that are part of the TLR and MHC complex, as well as STAT1 and C3 (**Fig. 7**). It is very likely that the presence and activation of the Kv1.3 increases pSTAT1 activity and aids in the induction of an inflammatory response in microglia. Similarly, in HEK-293 cells, the C-terminus of Kv1.3 also interacts with key signaling proteins such as MEK, a kinase that activates ERK signaling. We also found that a large fraction of the C-terminal interactome is dependent on the PDZ binding domain [50]. Removal of the PDZ binding domain resulted in a reduction of immune signaling protein interactions, suggesting that this binding domain is necessary for physical interactions between Kv1.3 and these proteins (**Fig. 7**). Proteins such as STAT1 and C3 are independent of the PDZ-binding domain, whereas others like, CD190 and SUN1 are PDZ-binding domain dependent. While both status and the PDZ-binding domain interacting proteins

are involved in signaling, the PDZ-binding regulation does not influence the interaction of proteins during an activate state. This means that other domains of Kv1.3 on the C-terminus (or another intermediary interactor) may be determining how immune status impacts C-terminal interactions.

These traits of Kv1.3 provide insight into how Kv1.3 may regulate microglial immune functions, and how regulation of the Kv1.3 channel might be useful as a therapeutic target. Perhaps, the observed beneficial effects of blocking Kv1.3 channels in a plethora of neurological disease models may be explained in part by the interaction between Kv1.3 channels and immune signaling proteins that co-assemble in activated microglia.

### **Kv1.3 presence in the mitochondria in microglia.**

Our MS-based studies also suggested an interaction between Kv1.3 and mitochondrial proteins. Specifically, we found that the N terminal interactome of Kv1.3 includes proteins such as TIMM50, suggesting that some Kv1.3 channels in microglia are transported to the mitochondria, where they are likely present in the inner membrane [15, 51]. To validate this biochemically, we performed mitochondrial fractionation from whole cell lysates and found that Kv1.3 protein (detected via the V5 tag fused to Kv1.3) was indeed enriched in the mitochondrial fractions along with a known canonical mitochondrial marker (HSP60). Our finding of Kv1.3 protein presence in mitochondria of microglia aligns with prior observations that Kv1.3 channels can localize to the mitochondria in T cells, where they may regulate apoptosis, mitochondrial potential and proton flux. Future proteomics studies of the Kv1.3 channel interactome specifically in microglial mitochondria, and mechanistic studies investigating the functional implications of these interactors, are therefore warranted. These functional implications include,

how Kv1.3 in the mitochondria is changed during LPS exposure and how Kv1.3 could regulate mitochondrial function during inflammation.

**Kv1.3 potassium channels may regulate immune function of microglia via protein-protein interactions.**

Microglia in neurological diseases have a higher expression of Kv1.3 [5, 7, 52]. Kv1.3 potassium channel activity is increased when membrane potential is reduced by the influx of calcium into microglia during an inflammatory response [53]. Activity of Kv1.3 clearly plays an important role in regulating immune function in microglia; however, it appears that Kv1.3 is also directly interacting with immune proteins independent of its channel activity. This is evident by the fact that Kv1.3 has multiple binding locations including the SH3 binding region located on the N-terminus and the PDZ binding domain located on the C-terminus [30]. Previous studies have shown some immune signaling proteins directly interacting with Kv1.3, including MEK, a necessary part of the ERK activation pathway [50]. The ERK activation pathway is strongly linked to neurological diseases and is a necessary step in the activation of microglia.

Our findings strengthen previous connections between Kv1.3 and immune interactors specifically highlighting the potential for physical interactors of Kv1.3 with the TLR proteins in an immune stimulation complex. Prior work in mouse microglia cells (MMC), a murine cell line endogenously expressing Kv1.3, and primary microglia shows that blockade of Kv1.3 using Shk-223 results in p38 and MAPK regulation [9, 54]. The current manuscript describes that pStat1 is regulated by the C-terminus, cooperating with our previous data showing that Stat1 phosphorylation is regulated by Kv1.3 function in BV-2, and Kv1.3 may interact with TLR [11]. This work highlights that the C-terminal interactome has several immune proteins including TLR2, MHC proteins and STAT1, further supporting previous predictions[9]. These data and

previous reports highlight that Kv1.3 channels may regulate or be functionally coupled with type 1/2 IFN signaling in microglia. IFN signaling is important in neuroinflammatory diseases like AD and aging, and in microglia, where IFN-based signatures have been identified in human brain [55, 56]. The data presented in this manuscript provides rationale for further evaluation of Kv1.3 influence in immune signaling *in vivo* and *in vitro*. Based on interactions with anchoring proteins (e.g. cortactin, integrins etc.), Kv1.3 likely becomes a part of a much larger macromolecular complex of proteins that come together as an immune complex.

### **Limitations of this study.**

There are many desirable benefits to utilizing an *in vitro* system to gain insights into Kv1.3's interactomes, including complete control over both the concentration and duration of stimulus in a highly pathway-specific manner; however, this model system does present some limitations.

While BV-2 cells retain many properties of primary mouse microglia, they are not a physiological replicate of *in vivo* microglia. In general, BV-2 cells are known to have adopted a more reactive phenotype compared to primary microglia, but do have similar inflammatory responses [46]. Endogenously, BV-2 cells and HEK-293 cells express minimal Kv1.3, however, we utilized transduced or transiently-transfected overexpression models of Kv1.3. There is an inherent risk that the overexpression model itself impacts levels of proteins that could be interacting with Kv1.3 channels, compared to cells that inherently express Kv1.3 channels.

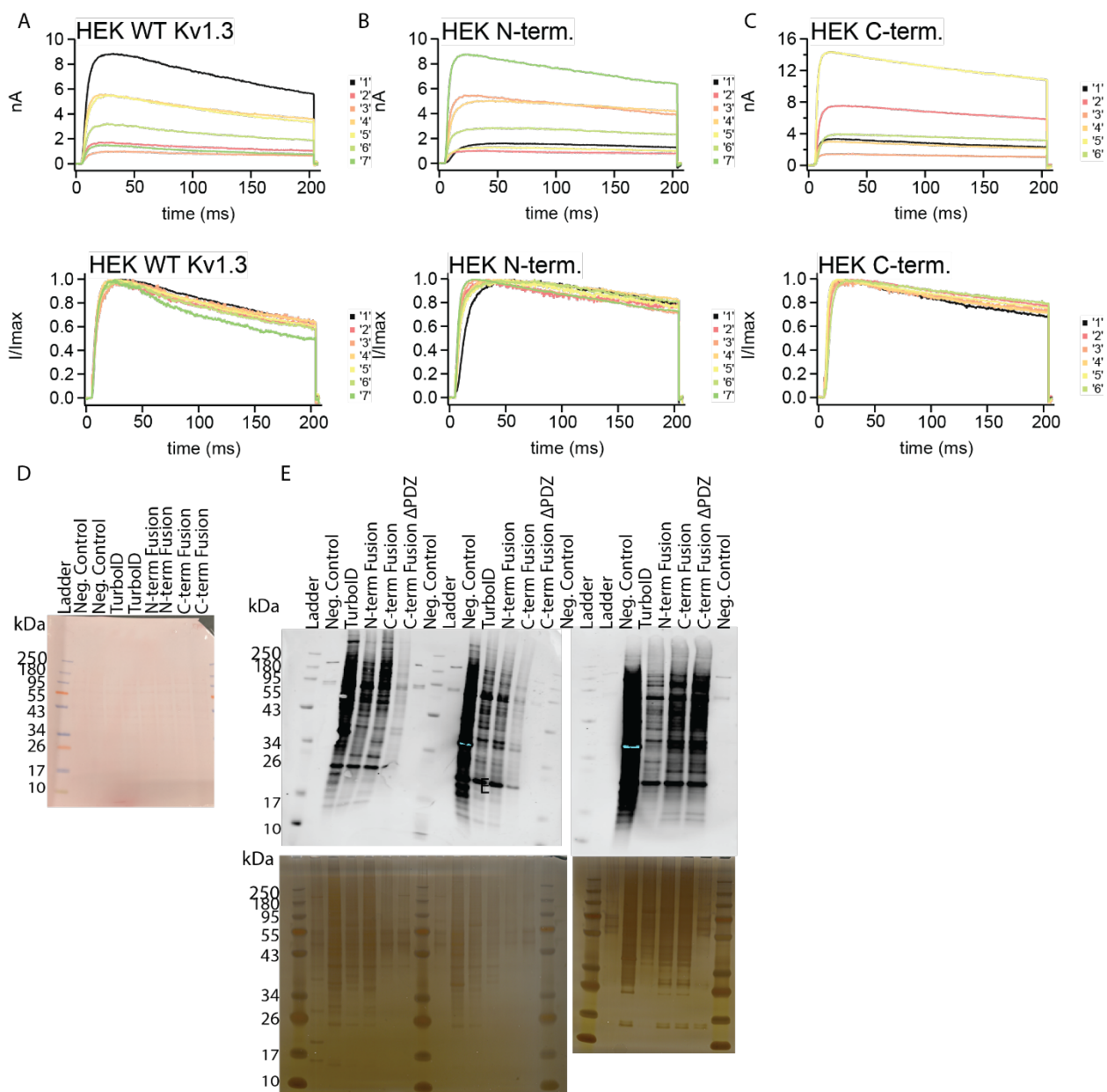
TurboID is a proximity labeling technique, meaning that biotinylation of proteins can occur as long as it's within the 10-30 nm radius of labeling [24]. As a result, TurboID can biotinylate proteins that are just within proximity and not physically interacting with Kv1.3. Fortunately, the radius of labeling for TurboID fused with Kv1.3 should be within the range of direct and immediate interactors, including those are transient or fixed interactors. In addition, TurboID can

biotinylate proteins that are near Kv1.3 as it's being packaged to the cell surface, such as labeling while Kv1.3 is present in the ER, which could explain the interactions observed with secreted proteins such as C3 [24]. In support of this, we found ER translocon/chaperone proteins such as HSP90 and HSPA5 as interactors of Kv1.3. It will be important to determine whether these interactions are dependent or independent of K<sup>+</sup> conductance via the pore of Kv1.3 channels. It is necessary to ascertain whether the Kv1.3 initiates the formation of the immune signaling complex or activates in responses to the formation of the immune signaling complex. With the establishment of the potential interactors of Kv1.3 in microglia, future studies are needed to determine how regulation of Kv1.3 alters in immune and disease response of microglia *in vivo* and how the directionality of immune interactions can be determined.

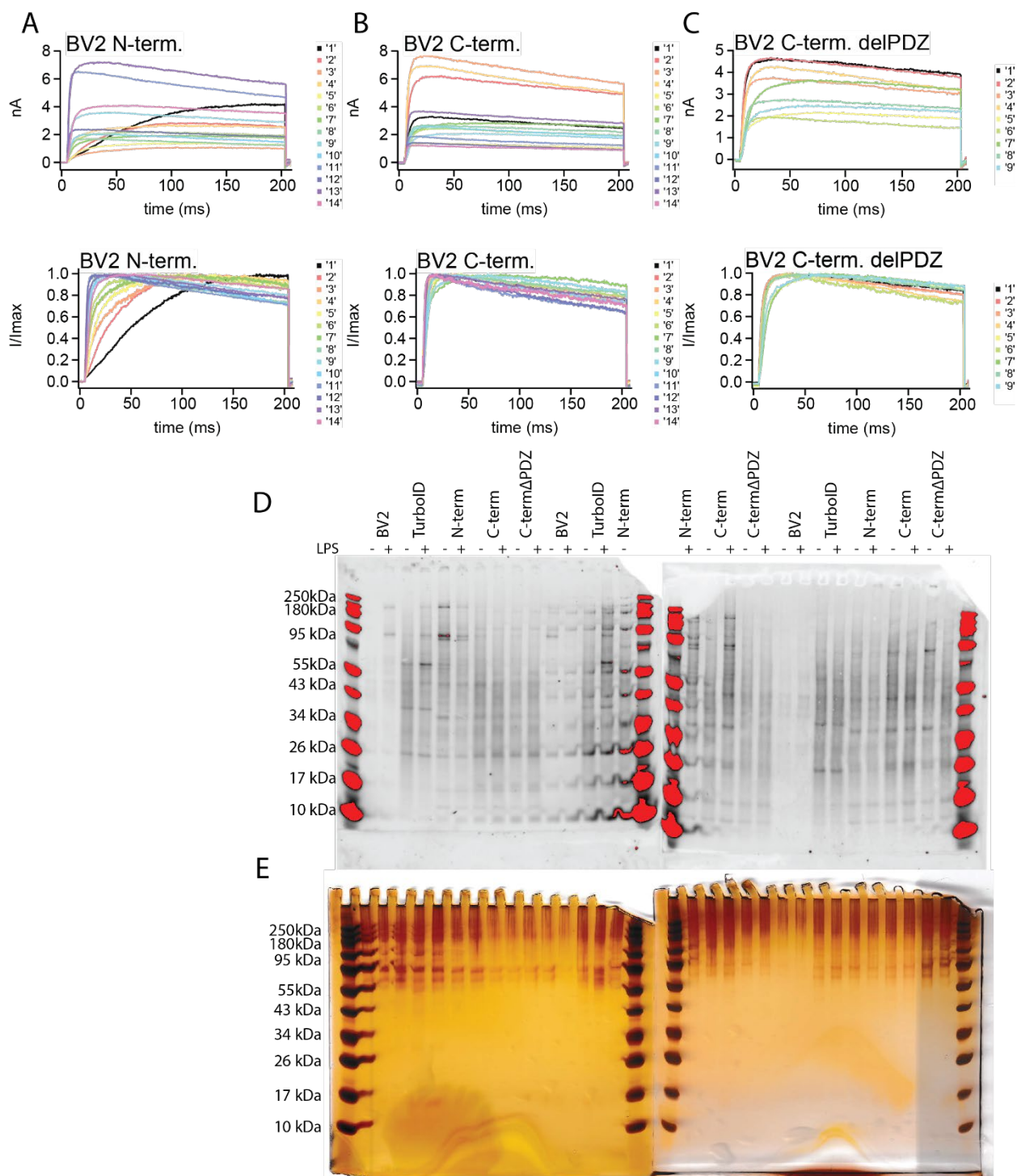
## **vii. CONCLUSIONS**

We used proximity-based proteomics to identify the interactome of Kv1.3 channels, which is a critical regulator of microglial function. Our analysis revealed several novel protein interactors of Kv1.3 channels in BV-2 microglia, including domain specific interactors of the N-terminus (*e.g.* TIMM50) and C-terminus (*e.g.* STAT1 and C3) of the channel. While the N-terminal interactome is larger and includes anchoring, localization and metabolic processing related proteins, the C-terminal interactome is enriched in immune signaling proteins, and many of these are directly governed by the immune status of microglia, and some are dependent on the PDZ-binding domain. Collectively, our data emphasize the pleiotropic nature of Kv1.3 and highlight its relevance as a therapeutic target for modulating microglial function.

## viii. SUPPLEMENTAL Figures



**Supplemental Figure 1: Confirmation of Hek-293 cell Kv1.3 function and TurboID activity. (A)** Traces of Kv1.3 electrophysiology of HEK-293 transfected with WT Kv1.3. **(B)** Traces of Kv1.3 activity of HEK-293 cells transfected with TurboID fused to the N-terminus of Kv1.3. **(C)** Traces of Kv1.3 activity of HEK-293 cells transfected with TurboID fused to the C-terminus of Kv1.3. **(D)** Ponceau staining of HEK-293 showing even protein loading across western blots prior to affinity purification. **(E)** Post-affinity purification western blot and silverstain show streptavidin labeling of proteins transfected with TurboID and proper affinity purification. **(F)** DEA comparison of HEK-293 Kv1.3 interactors on the N-terminus and C-terminus. Differential Abundant proteins were calculated using paired t-test, where  $\log P\text{-value} > 1.3$  and  $\text{Log}_2 \text{Fold Change (FC)}$  of  $\pm 1$  were considered significant.  $n=3$

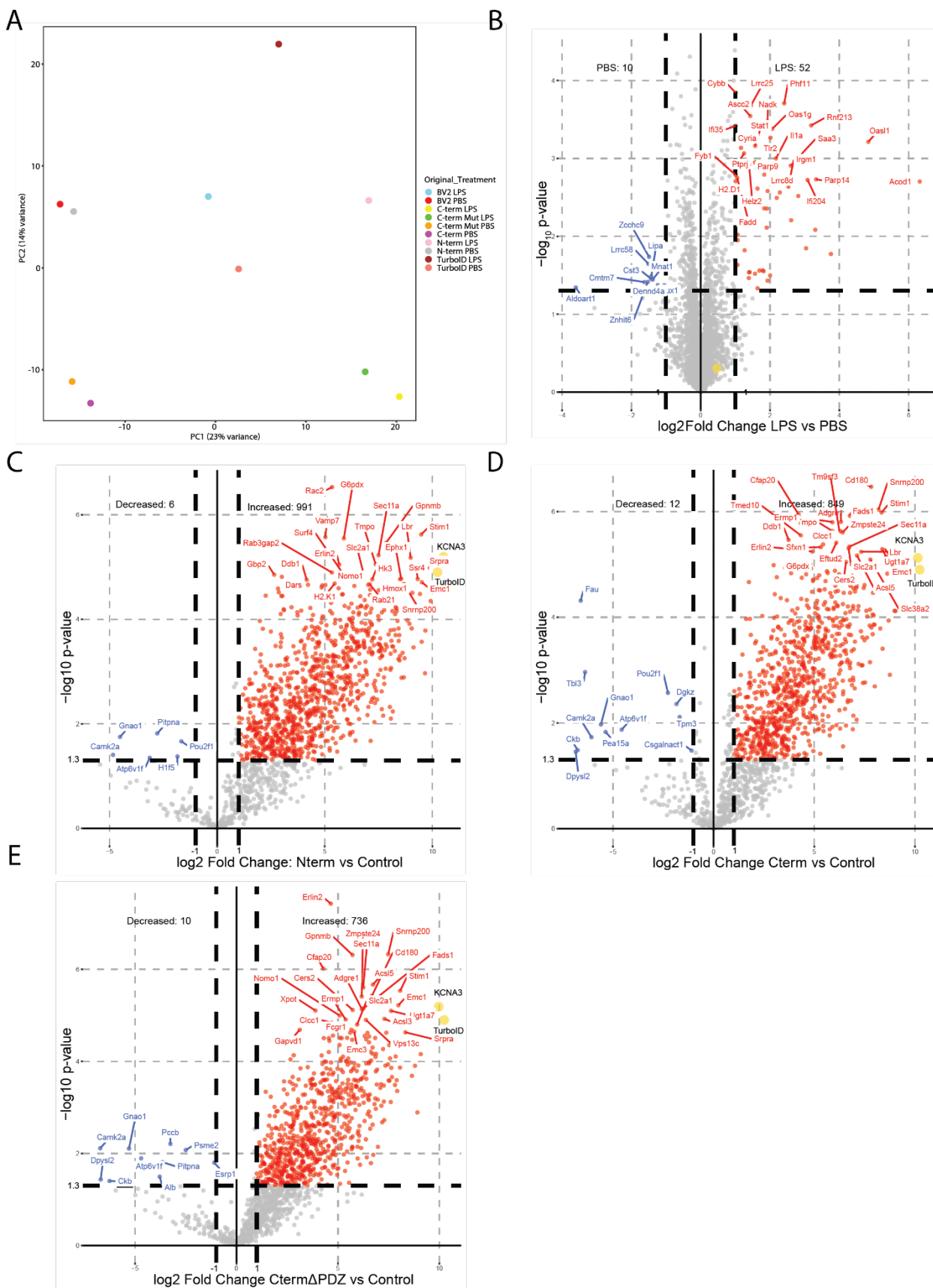


**Supplemental Figure 2: Confirmation of BV-2 cell Kv1.3 function and TurbolID**

**activity. (A)** Traces of Kv1.3 electrophysiology of BV-2 cells transduced with

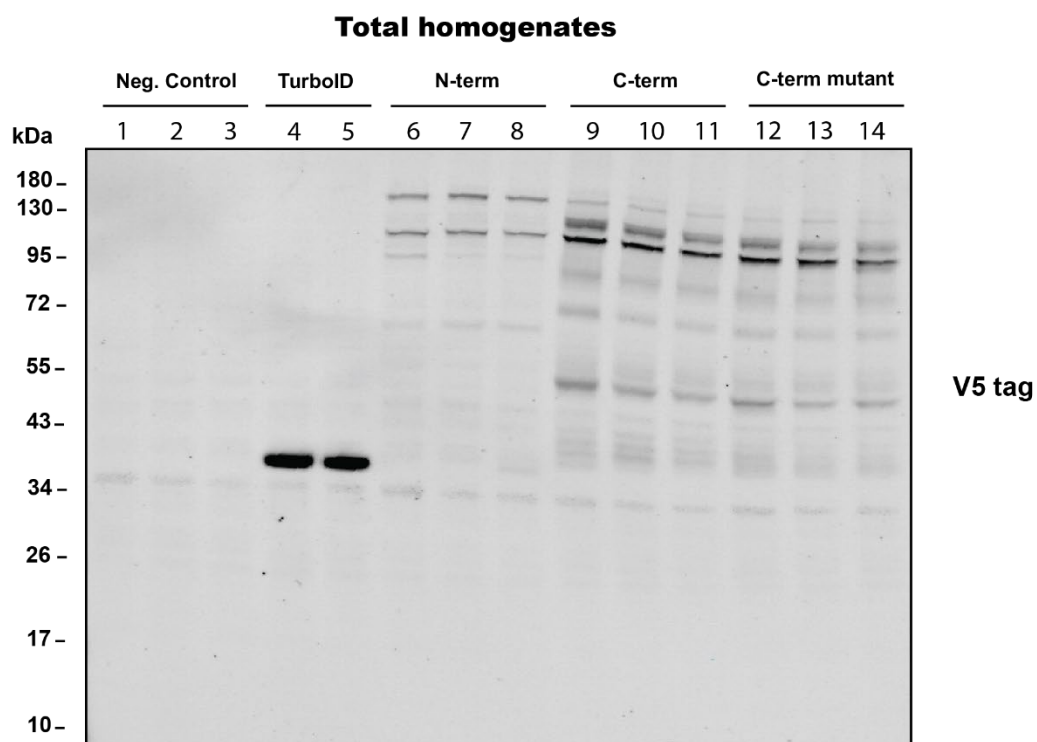
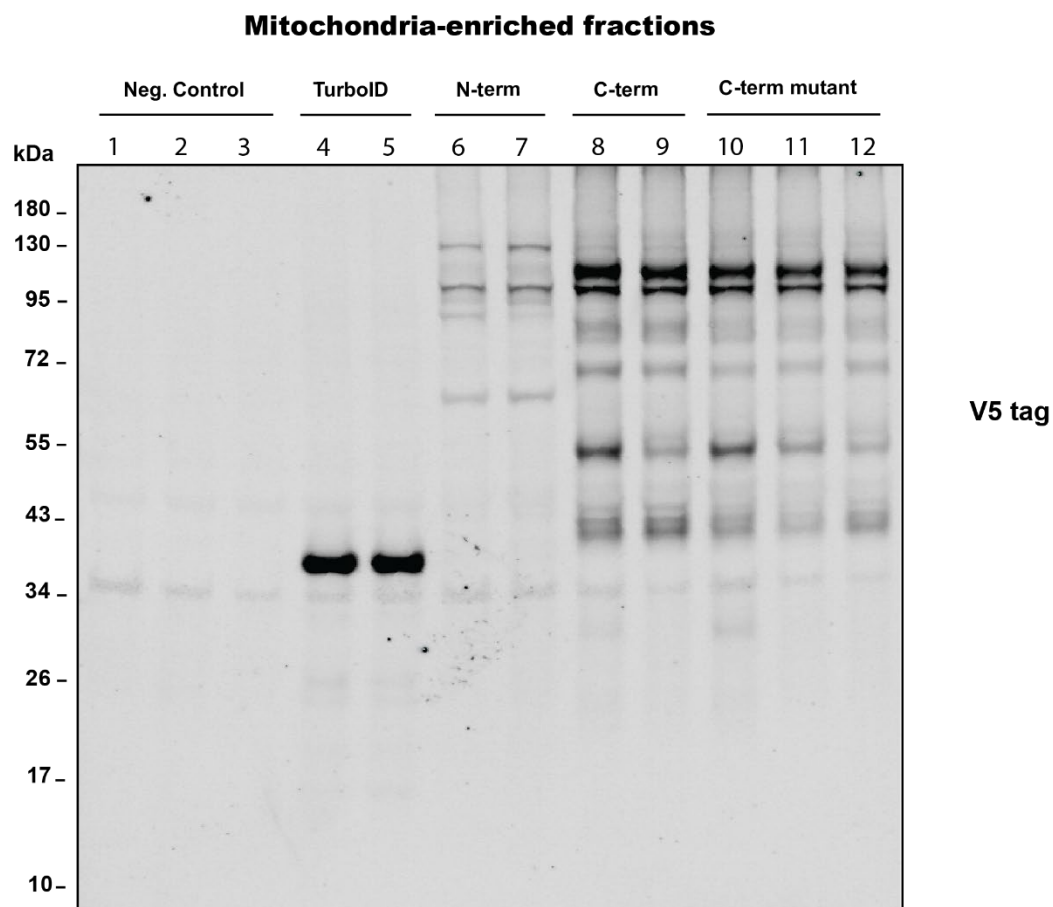
TurbolID fused to the N-terminus of Kv1.3. **(B)** Traces of Kv1.3 activity of BV-2 cells

transduced with TurboID fused to the C-terminus of Kv1.3. **(C)** Traces of Kv1.3 activity of BV-2 cells transduced with TurboID fused to the C-terminus of Kv1.3 with the PDZ-binding domain removed. **(D)** Post-affinity purification western blot and silverstain show streptavidin labeling of proteins transfected with TurboID and proper affinity purification. n=3

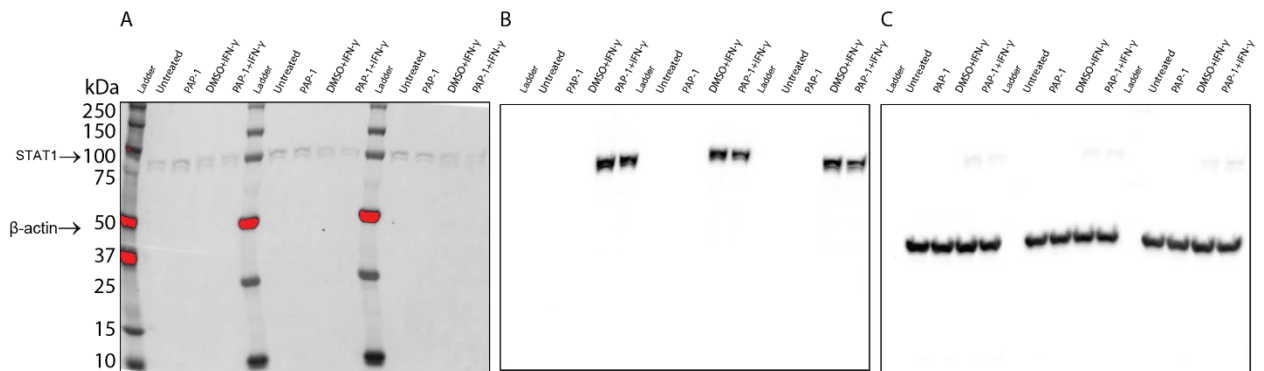


**Supplemental Figure 3: BV-2 cells successfully produce inflammatory responses and cells transduced with Kv1.3 have distinct interactors. (A)**

Principal Component Analysis (PCA) of mass spectrometry of BV-2 cell lysates shows distinct separation between cells exposed to LPS compared to PBS. There is little variance explained in the cell lysate proteomes that show difference between overexpression of Kv1.3. **(B)** DEA of whole cell lysates of BV-2 cells induced with LPS have increased presence of key inflammatory proteins. **(C)** DEA of affinity purified BV-2 cells with an N-terminal fusion of TurboID to Kv1.3 compared to controls shows presence of proteins interacting with the Kv1.3 channel. **(D)** DEA of affinity purified BV-2 cells with an C-terminal fusion of TurboID to Kv1.3 compared to controls shows presence of proteins interacting with the Kv1.3 channel. **(E)** DEA of affinity purified BV-2 cells with an C-terminal fusion of TurboID to Kv1.3 with a deletion of the PDZ-binding domain compared to controls shows presence of proteins interacting with the Kv1.3 channel. Differential Abundant proteins were calculated using paired t-test, where  $\log P\text{-value} > 1.3$  and  $\text{Log}_2 \text{Fold Change (FC)}$  of  $\pm 1$  were considered significant.  $n=3$

**A****B**

**Supplemental Figure 4: Full-length Western blot images of V5 tag in total homogenates (A) and mitochondria-enriched fractions (B).** Fractionation experiments were run in triplicates and TurboID was included as positive control for anti-V5 tag antibody.



**Supplemental Figure 5: Full-length WB images of STAT1(A), pSTAT1(B), β-actin (C).** The molecular weights of STAT1, pSTAT1, and β-actin are 84kDa, 84kDa, and 45kDa, respectively. Triplicate experiment showing the western blot analysis of whole cell lysate from BV-2 cells expressing N-terminal KV1.3 -TurboID. There is a consistent reduction of STAT1 phosphorylation upon induction with IFN-γ post KV1.3 blockade with PAP1 in all three experiments.

### **III. CHAPTER III: DISCUSSION AND FUTURE DIRECTIONS**

Neuroinflammatory diseases have risk factors that associate microglia with a shift toward increased disease pathology. Microglia act as the immune cell of the brain. During an inflammatory response, microglia shift toward a disease associated microglia state referred to as DAM [27]. During this shift, microglia have a massive influx of calcium to assist in calcium-dependent immune signaling. Regulation of calcium influx has been shown to regulate microglial function; however, in addition to calcium, potassium efflux has been well described during an immune response [93]. During this inflammatory response, Kv1.3 localization and activity increase at the cell membrane [85]. In mouse models of neuroinflammation, blockade of Kv1.3 changes the immune response of microglia, resulting in a reduction of the proinflammatory genes and an increase in phagocytic properties of microglia [85, 124].

Ion channels like Kv1.3 can potentially regulate immune functions via K conductance-dependent mechanisms and regulating calcium flux and membrane potential. Potassium and calcium channels are known to regulate chemotaxis, ROS production, effector functions such as neuronal killing [95]. Less studied conductance-independent mechanisms could also potentially regulate immune function; where membrane depolarization results in conformational change in Kv1.3, which then impacts proteins interacting with Kv1.3 channels and alters their activity. Both these mechanisms functionally link Kv1.3 to other proteins/complexes/pathways, providing avenues to Kv1.3 to regulate cellular function. Therefore, defining these interactions specifically in microglia is important for biological insights, and developing new therapeutic approaches/applications. The work presented in this dissertation establish a comprehensive

protein-protein interactome of Kv1.3 channels in microglia using the TurboID proximity-labeling method in an in vitro model. This identified known as well as several previously unknown Kv1.3 channel interactors including transporters, immune signaling proteins, lysosomal proteins and mitochondrial proteins. This approach further identified novel protein interactors and potential mechanisms associated with the N and C termini of Kv1.3 channels in microglia, emphasizing domain-specific functions of Kv1.3 channels. We also found that a large fraction of the C-terminal interactome depends on the PDZ-binding domain of the channel. Interestingly, with pro-inflammatory microglial activation, we found that the interactome of the C-terminus but not the N-terminus undergoes significant re-organization whereby immune signaling and inflammatory proteins are associated with Kv1.3 channels, allowing Kv1.3 channels to regulate immune pathways such as STAT1 signaling.

### **i. Kv1.3 interactions in microglia**

Microglia have a high level of Kv1.3 channel expression during disease-like conditions. Blockade of these channels changes the immune response of microglia, where there is a reduction of the inflammatory state and an increase in the phagocytic state. However, how Kv1.3 interacts with the immune response was previously unknown. The purpose of our project was to establish what proteins are interacting with Kv1.3 and how that could be regulating an immune response. Our lab hypothesized that Kv1.3 is likely interacting directly with key immune signaling proteins. We fused a biotin ligase, TurboID to Kv1.3 to determine which proteins interact with Kv1.3 in microglia. We then confirmed that the function of both the channel and TurboID were unaltered by overexpression of either. Then, we utilized mass

spectrometry to evaluate which proteins were biotinylated by TurboID and thus interacting with Kv1.3. Finally, we completed functional assays to evaluate the presence of Kv1.3 in the mitochondria as well as its alteration of phosphorylation of STAT1. When utilizing proximity labeling of Kv1.3 interactors, we showed that the N-terminus of Kv1.3 interacts with protein processing and mitochondrial trafficking. Whereas, the C-terminus of Kv1.3 has several interactors with the PDZ-binding domain, some of which are associated with an immune response. During an LPS-induced inflammatory response, the C-terminus of Kv1.3 interacts with key immune signaling proteins, such as STAT1 and C3. Overall, these data highlight that Kv1.3 likely interacts directly with the immune signaling complex in microglia.

### **Kv1.3 is associated with cell signaling in HEK-293 cells.**

Due to the fact that TurboID is a relatively newer biotin-ligase, we started our work in HEK-293 cells. These human embryonic kidney cells were utilized in the original TurboID paper and are easily transfected. This enabled us to gather an initial Kv1.3 interactome in human cells, while also checking to make sure this process would work well in our lab. We transfected constructs with Kv1.3 fused to TurboID into HEK-293 cells; an N-terminal fusion and a C-terminal fusion. We confirmed that TurboID does not alter the functionality of the Kv1.3 channel in HEK-293 cells and produces active channels on the surface of the cell. Utilizing western blots, we evaluated that TurboID is still actively biotinylating proteins, and these proteins appear to be in close proximity to Kv1.3. The vast majority of Kv1.3 interactors are shared between the N-terminus and the C-terminus. However, the N-terminus appears to interact with proteins that are associated with metabolic and protein processing. The C-terminus of Kv1.3 interacts with proteins associated with signal transduction. Previously in the field there is evidence that Kv1.3

influences signaling; however, this is the first time showing a physical interaction between Kv1.3 and key signaling proteins. Establishing Kv1.3 interactions with signaling proteins progressed the desire to evaluate Kv1.3 interactors in an immune cell model.

Following similar procedures established in HEK-293 cells, we then transitioned to creating Kv1.3-TurboID overexpression stabilized microglial cell lines. Using the same constructs, we created a lenti virus to transduce BV-2 cells with the Kv1.3-TurboID constructs. After determining minimal alteration to the function of either Kv1.3 or TurboID, we then evaluated what proteins were potentially in the interactome of Kv1.3 via mass spectrometry. We collected and evaluated data based on the Kv1.3 N-terminal interactome, the C-terminal interactome, and the C-terminal interactome with the PDZ-binding domain removed.

### **Proximity labeling shows that Kv1.3 interacts with many endoplasmic reticulum associated proteins.**

When evaluating the proteins that were in the Kv1.3 interactome both in HEK-293 and BV-2 Cells, many were associated with the endoplasmic reticulum. This finding indicates that Kv1.3 is being processed in the cell similarly to other transmembrane proteins. The majority of transmembrane proteins at the cell surface are processed in the endoplasmic reticulum (ER) before being directed to the cell surface. Previous studies show the presence of Kv1.3 in both the ER and being packaged in the Golgi apparatus [112]. Whether ER-localized Kv1.3 can have functional importance, is not well known, although one can suspect that ER Kv1.3 channels are likely to be functionally active. Removal of the PDZ-binding domain of Kv1.3 has also been shown to result in a reduction of the Golgi apparatus localization of Kv1.3 [91]. When evaluating

the proteins interacting with Kv1.3, we showed that many of the proteins that were labeled with biotin were ER associated or processed in the ER. These included proteins associated with the ER translocon machinery (*e.g.* SEC61A1, SEC61B, SEC61G, SEC63, HSPA). These data highlight the presence of Kv1.3 in the ER. We also found that deletion of the PDZ-binding domain resulted in decreased biotinylation of several proteins, enriched in ER and Golgi related functions, confirming the importance of this domain in Kv1.3 localization to this compartment. Furthermore, this shows that Kv1.3 is being processed and inserted into the membrane as previously described in literature. The ER was not the only organelle that had many proteins interacting with Kv1.3. In addition to the ER, there were many Kv1.3 interacting proteins that are localized to the cell surface as well as the mitochondria.

**Proximity labeling of proteins interacting with Kv1.3 highlight the presence of Kv1.3 in the mitochondria.**

There is some evidence that Kv1.3 likely is located in the inner mitochondrial membrane of cells and contributes to changes in cellular respiration of immune cells. Biophysical evidence of Kv1.3 in the inner mitochondrial membrane shows the Kv1.3 is likely present and functionally relevant in the mitochondria [96]. In lymphocytes, mitochondrial Kv1.3 contributes to the apoptotic ability of the cells [97, 127]. This regulation of apoptosis of lymphocytes is primarily through Kv1.3 interactions with BAX, a known pro-apoptotic protein located on the mitochondrial membrane [97, 127]. Recent studies describe the mechanism of Kv1.3 trafficking to the mitochondria in lymphocytes via the Kv1.3 binding to the TIMM23 nonconical mechanism [94]. As part of evaluating the interactome of Kv1.3, we wanted to determine how

many of the previously described interactors would be present. In addition, our goal was to evaluate the types of mitochondrial proteins that may interact with Kv1.3,

Our studies show that Kv1.3 interacts with 73 proteins associated with the mitochondria in microglia cells. Many of the proteins interacting with Kv1.3 in the mitochondria are associated with transport of proteins to the mitochondria and mitochondrial ribosomal machinery (*e.g.* BAX, TIMM50, and RPL23). Furthermore, utilizing the v5 tag, we show that Kv1.3 presence is increased in mitochondrial fractions compared to cytoplasm. With these studies, we further establish Kv1.3 presence in mitochondria in microglia. It is likely that Kv1.3 contributes to the respiration changes that microglia undergo during an inflammatory response; since Kv1.3 is known to change cellular respiration and microglia are dependent on respiration transitions during an inflammatory response [98, 128]. Among the proteins labeled were VDAC1 which raises the possibility that proton flux and mitochondrial potential may be potentially regulated by Kv1.3 channels in microglia. These studies indicate that Kv1.3 may assist in regulation of respiration across the inner mitochondrial membrane but there need to be functional assays to determine what role the channel could have on function. Supported by my results, our lab intends to continue to evaluate Kv1.3 presence in mitochondria and how the channel may be influencing the microglial ability to undergo a bioenergetic shift during an inflammatory response. Recently, we optimized protocols to purify mitochondria from BV-2 microglia expressing Kv1.3-TurboID fusions, and performed biotinylated protein enrichment from mitochondrial fractions, the proteomics studies of which are being executed. In addition to localization of Kv1.3 in microglia, we also performed these assays to evaluate functional interactions between structures on Kv1.3, such as the PDZ-binding domain, and immune signaling proteins.

### **Kv1.3 interactome contains proteins that are dependent on the PDZ-binding domain to interact with Kv1.3.**

The Kv1.3 PDZ-binding domain is located at the C-terminus of Kv1.3 [88]. The PDZ-binding domain likely interacts with PSD-95, which is associated with an immune response [90]. The goal of this portion of the study was to determine how much of the interactions with Kv1.3 are dependent on the PDZ-binding domain. We hypothesized that many of the C-terminal interacting proteins were PDZ-binding domain dependent. However, our study showed that there were about 70 proteins that dependent on the PDZ-binding domain for interacting with the C-terminus. Gene set enrichment shows that these proteins were associated with an immune response, but very few of these proteins were changed during an LPS-induced inflammatory response. This indicates that proteins that interact with the C-terminus during an LPS response are likely not dependent on the PDZ-binding domain. That being said, when evaluating phosphorylation of STAT1 in particular, the absence of the PDZ-binding domain reduces the phosphorylation of STAT1, suggesting that the PDZ-binding domain may still contribute to the immune signaling component of the C-terminus. Overall, these studies indicate that the PDZ-binding domain of Kv1.3 is likely important to the immune response of microglia. Establishing that the PDZ-binding domain can alter the proteins interacting with Kv1.3 is relatively novel component to the field. Since, we see alterations to Kv1.3 result in changes in immune response, we then evaluated how Kv1.3 interactomes change during induction of an immune response utilizing LPS.

## **The C-termini of Kv1.3 interacts with key immune signaling during LPS stimulation in microglia.**

Blockade and KO of Kv1.3 shows a reduction in the inflammatory response of microglia. Studies show a there is a reduction of key proinflammatory cytokines including STAT-1, TLR2, and C3 with such blockade of Kv1.3 in stroke and AD models [85, 124]. Our goal for this portion of the study was to evaluate how the Kv1.3 interactome is altered during LPS induction. We hypothesized that Kv1.3 interacts directly with early signaling proteins such as TNF and STAT1 during an inflammatory response. Utilizing proximity labeling, we determined that during an LPS-induced inflammatory response, the N-terminal Kv1.3 interactors remain unchanged; however there are 36 C-terminal interactors that are dependent on an LPS response. Gene set enrichment shows these proteins are associated with an immune response and antigen presentation. These include proteins such as STAT1 and C3. Luminex and western blots highlight that phosphorylation of STAT1 is dependent on Kv1.3 activity, where removal of the PDZ-binding domain or blockaded of reduces pSTAT1 activity. Furthermore, the presence of Kv1.3 leads to an increase in intracellular C3 in microglia, thus indicating expression of Kv1.3 contributes to activation of the C3 signaling response. Overall, these data show both a physical and functional interactions of Kv1.3 with key immune signaling functions in microglia. This is an important contribution to the field because this starts to highlight a pathway in which Kv1.3 could be directly influencing signaling. Our lab aims to evaluate how Kv1.3 may contribute to the phosphorylation of key signaling proteins in future experiments.

### **Implications of Kv1.3 interactors in microglia.**

The goal of our study was to establish the interacting proteins with Kv1.3 in microglia during an immune response. In addition, we set out to evaluate how regions of the channel (the N-terminus, C-terminus, and PDZ-binding domain) change the interactions with Kv1.3. These data highlight that Kv1.3 likely has interactions with proteins beyond the activity of the channel in microglia. The N-terminus of Kv1.3 is largely responsible for protein processing and directing Kv1.3 either to the cell membrane or the mitochondria. The C-terminus primarily interacts with inflammatory signaling proteins during an LPS-induced inflammatory response, some of which are dependent on the PDZ-binding domain. This further grasps at the mechanism by which Kv1.3 likely influences inflammatory responses in microglia. We hypothesize that Kv1.3 works in close complex with key signaling proteins during an immune response that enables the further induction of a proinflammatory response in microglia. Based on our results, we are also considering the possibility that Kv1.3 channel state may also determine the proteins that the channel interacts with. To do this, the laboratory will be undertaking studies to see how Kv1.3 blockade by Kv1.3 pore blockers, and persistent inactivation of Kv1.3 channels by increasing extracellular K<sup>+</sup> concentrations, impacts the Kv1.3 channel interactome.

### **Limitations of TurboID-based proximity labeling for Kv1.3 channel interactome studies.**

The proteomics studies performed to gather these data captures transient and stable interactors and proteins in close proximity with Kv1.3. This indicates that there is an increased risk of non-specific interactions being captured. To reduce this issue, we utilized a global TurboID not fused to Kv1.3 to compare. In addition, we limited biotinylation to one hour to minimize the risk of

excessive biotinylation. To further increase specificity, the laboratory is also undertaking proteome studies where biotinylation occurs only when the channel is assembled and localized to the cell surface. To do this, we are using the split-TurboID approach, described in the next section.

## **ii. FUTURE APPLICATIONS**

### **Establishing KV1.3 Potassium Channel interactors in T-cells.**

There are strong indicators that Kv1.3 acts as an immunomodulator for T-cells and other lymphocytes. Blockade and KO of the channel in T-cells shows a reduction of the proliferation of T-cells as well as a reduction of their response [103, 105]. The purpose of evaluating T-cell Kv1.3 interactome is to determine how macrophages and T-lymphocyte interactions with Kv1.3 may differ. Our lab utilized the TurboID-Kv1.3 constructs to transduce Jurkat T-cells and evaluate the interacting proteins within T-cells. We hypothesize that the Kv1.3 interacting complex overlaps some between microglia and T-cells but each cell type will have proteins that only interact with Kv1.3 in that cell type. Furthermore, we hypothesize that Kv1.3 likely also forms a complex with key immune signaling proteins in T-cells.

### **Utilizing the Split-TurboID method to further evaluate interactors with the Kv1.3 complex in microglia.**

In order to reduce the risk of TurboID labeling indiscriminately, we hope to utilize the split-TurboID system to establish closer interactions with Kv1.3. The Kv1.3 complex forms a homotetramer with Kv $\beta$ 2 within microglia in order to form an active potassium channel. The disadvantage with TurboID is that it is endogenously active as soon as it is translated by the ribosome; this means it can indiscriminately biotinylate proteins [126]. The Ting lab created a split-TurboID construct where the catalytic portion of TurboID is split into two separate constructs; thus, biotinylation only occurs when both components of TurboID interact [126]. We added one component of split-TurboID to Kv1.3 and another component to Kv $\beta$ 2 to evaluate how many proteins interact with the complex compared to Kv1.3 or Kv $\beta$ 2 individually. We hypothesize that the interacting proteins with the Kv1.3 channel complex will be distinct from Kv1.3 or Kv $\beta$ 2. These studies will add establish the interactors with the channel that are dependent on channel activity; this will add specificity to the Kv1.3 interactome that is currently absent in the field. In addition to evaluating the interactome, it is also necessary to evaluate how blockade of the Kv1.3 channel could alter immune function.

### **Pharmacological blockade of Kv1.3 influences microglial inflammatory response.**

Several studies indicate that blockade of Kv1.3 reduces the proinflammatory response of microglia. These include both extracellular blockade utilizing the peptide, ShK-223, and intracellular blockade utilizing the small molecule, PAP-1 [85, 129]. These studies highlight a reduction of the transcripts of key proinflammatory genes such as *Ilr* and *Tnfa* [85, 119]. In

addition, the microglial phenotype transitions toward an increase in phagocytosis [85]. However, these studies don't directly compare intracellular and extracellular blockade. Furthermore, none of these studies evaluate how these blockades influence different cell types. The goal of this study is to evaluate how different blockades of the Kv1.3 influences individual cell types in AD mouse models. We hypothesize that small molecule and peptide blockade of Kv1.3 will have different effects *in vivo* for different cell types.

To determine how different blockades of Kv1.3 influences AD pathology, our lab treated 5xFAD mice age 3 or 6 months old with either Shk-223 or PAP-1 for 3 months. We evaluated their behavior, total A $\beta$  presence, accumulation of A $\beta$  plaques, brain proteomics, and brain snRNAseq. Preliminary data highlights that a reduction of the AD-like behavior and a reduction of A $\beta$  plaques was associated with both forms of blockade of Kv1.3. However, snRNAseq highlights that ShK-223 and PAP-1 behave different at the cell-type level, both of which still reducing an inflammatory response in microglia. We look forward to further evaluating the proteomics and snRNAseq of these mice, studies which will be completed beyond the scope of my dissertation.

Overall, determining which Kv1.3 blockade strategy will be more effective in reducing AD pathology is essential. In addition to determining efficiency, determine the mechanism by which each of these blockades influence microglial inflammatory response is extremely useful for the development of potential AD treatments. Establishing the function of Kv1.3 further enables us to evaluate new treatments for AD and potential biomarkers to evaluate. In addition to blockade in models, establishing which cell types are influenced by Kv1.3 the most is best done through KO models.

### **Developing a microglial-specific Kv1.3 conditional Knock Out.**

Knock out models of Kv1.3 highlight that there's a reduction of immune cell response, particularly T-cells [120]. Microglia isolated from Kv1.3 KO mice have a reduction of key proinflammatory cytokines, including TNF- $\alpha$  and IL-1 $\beta$  [119]. In addition, these mice have reduced metabolism [100]. While global KO models of Kv1.3 are useful at evaluating how the overall gene expression of Kv1.3 influences inflammatory responses including those of microglia. However, these studies cannot evaluate the individual cell gene expression of Kv1.3 influences the inflammatory response in the brain. The goals of these studies is to determine how much microglial Kv1.3 contributes to changes in the brain. We hypothesize that microglial expression of Kv1.3, particularly changes the ability for the brain and for the microglia to produce an inflammatory response. Furthermore, we hypothesize that by a reduction of microglial Kv1.3, there will be a reduction of the DAM phenotype in stroke and AD mouse models.

Our lab developed a mouse where the *Kcna3* gene is flanked by LoxP sites (*Kcna3*-fl/fl). We then crossed these *Kcna3*-fl/fl mice with either a CMV-cre, a cre with a global promotor or *Tmem-119*-cre-ert2, which is an inducible cre expressed exclusively in microglia [43, 130]. The cross of the *Cmv*-cre mice allows for a development of a global KO of Kv1.3 in all cell types, referred to as Kv1.3 KO mice. In contrast, the *Tmem-119*-Cre-ert2 x *Kcna3*-fl/fl approach allows for recombination of the *Kcna3* gene in microglia only in the presence of Tamoxifen.

Preliminary data from our lab shows a reduction in brain, microglia and liver in the Kv1.3 KO mice. In mice with the *Tmem119*-cre cross, preliminary qPCR data shows a reduction in *Kcna3* only in microglia. We hope to further evaluate how Kv1.3 KO models both globally and in

microglia alone would influence the inflammatory response by crossing with 5xFAD mice or using MCAO to mimic stroke.

Overall, determining how much Kv1.3 reduction of neuroinflammatory responses is cell-type specific is essential to determining how Kv1.3 influences neuroinflammation. Also, it would further determine how microglial Kv1.3 specifically could alter the disease progression of many neuroinflammatory diseases. Understanding the mechanism by which Kv1.3 could be influencing these diseases further progresses the knowledge of biomarkers and potential treatment options.

#### IV. CHAPTER IV: REFERENCES

1. Mass, E., et al., *Tissue-specific macrophages: how they develop and choreograph tissue biology*. Nature Reviews Immunology, 2023. **23**(9): p. 563-579.
2. del Rio-Hortega, P., *Cytology & [and] cellular pathology of the nervous system*. 1932: Hoeber.
3. Ginhoux, F., et al., *Fate mapping analysis reveals that adult microglia derive from primitive macrophages*. Science, 2010. **330**(6005): p. 841-5.
4. Abe, N., et al., *Microglia and Macrophages in the Pathological Central and Peripheral Nervous Systems*. Cells, 2020. **9**(9): p. 2132.
5. Gautier, E.L., et al., *Gene-expression profiles and transcriptional regulatory pathways that underlie the identity and diversity of mouse tissue macrophages*. Nat Immunol, 2012. **13**(11): p. 1118-28.
6. Alliot, F., I. Godin, and B. Pessac, *Microglia derive from progenitors, originating from the yolk sac, and which proliferate in the brain*. Brain Res Dev Brain Res, 1999. **117**(2): p. 145-52.
7. Stremmel, C., et al., *Yolk sac macrophage progenitors traffic to the embryo during defined stages of development*. Nat Commun, 2018. **9**(1): p. 75.
8. Chitu, V., et al., *Emerging Roles for CSF-1 Receptor and its Ligands in the Nervous System*. Trends Neurosci, 2016. **39**(6): p. 378-393.
9. Easley-Neal, C., et al., *CSF1R Ligands IL-34 and CSF1 Are Differentially Required for Microglia Development and Maintenance in White and Gray Matter Brain Regions*. Front Immunol, 2019. **10**: p. 2199.
10. Butovsky, O., et al., *Identification of a unique TGF- $\beta$ -dependent molecular and functional signature in microglia*. Nat Neurosci, 2014. **17**(1): p. 131-43.
11. Schafer, D.P., et al., *Microglia sculpt postnatal neural circuits in an activity and complement-dependent manner*. Neuron, 2012. **74**(4): p. 691-705.
12. Li, Q. and B.A. Barres, *Microglia and macrophages in brain homeostasis and disease*. Nature Reviews Immunology, 2018. **18**(4): p. 225-242.

13. Keren-Shaul, H., et al., *A Unique Microglia Type Associated with Restricting Development of Alzheimer's Disease*. *Cell*, 2017. **169**(7): p. 1276-1290.e17.
14. Zabel, M.K., et al., *Microglial phagocytosis and activation underlying photoreceptor degeneration is regulated by CX3CL1-CX3CR1 signaling in a mouse model of retinitis pigmentosa*. *Glia*, 2016. **64**(9): p. 1479-91.
15. Stevens, B., et al., *The classical complement cascade mediates CNS synapse elimination*. *Cell*, 2007. **131**(6): p. 1164-78.
16. Maksour, S. and L. Ooi, *Innovations advancing our understanding of microglia in Alzheimer's disease: From in vitro to in vivo models*. *Journal of Neurochemistry*, 2023. **166**(3): p. 497-516.
17. Flowers, A., et al., *Proteomic analysis of aged microglia: shifts in transcription, bioenergetics, and nutrient response*. *Journal of Neuroinflammation*, 2017. **14**(1): p. 96.
18. Hammond, T.R., et al., *Single-Cell RNA Sequencing of Microglia throughout the Mouse Lifespan and in the Injured Brain Reveals Complex Cell-State Changes*. *Immunity*, 2019. **50**(1): p. 253-271.e6.
19. Hattori, Y., *The microglia-blood vessel interactions in the developing brain*. *Neuroscience Research*, 2023. **187**: p. 58-66.
20. Foulquier, S., et al., *The role of receptor MAS in microglia-driven retinal vascular development*. *Angiogenesis*, 2019. **22**(4): p. 481-489.
21. Kim, J.-S., et al., *A Binary Cre Transgenic Approach Dissects Microglia and CNS Border-Associated Macrophages*. *Immunity*, 2021. **54**(1): p. 176-190.e7.
22. Haruwaka, K., et al., *Dual microglia effects on blood brain barrier permeability induced by systemic inflammation*. *Nature Communications*, 2019. **10**(1): p. 5816.
23. Thurgur, H. and E. Pinteaux, *Microglia in the Neurovascular Unit: Blood–Brain Barrier–microglia Interactions After Central Nervous System Disorders*. *Neuroscience*, 2019. **405**: p. 55-67.
24. Paolicelli, R.C., et al., *Microglia states and nomenclature: A field at its crossroads*. *Neuron*, 2022. **110**(21): p. 3458-3483.
25. Shmuel-Galia, L., et al., *Intramembrane attenuation of the TLR4-TLR6 dimer impairs receptor assembly and reduces microglia-mediated neurodegeneration*. *J Biol Chem*, 2017. **292**(32): p. 13415-13427.
26. Kettenmann, H., et al., *Cultured microglial cells have a distinct pattern of membrane channels different from peritoneal macrophages*. *J Neurosci Res*, 1990. **26**(3): p. 278-87.
27. Rangaraju, S., et al., *Identification and therapeutic modulation of a pro-inflammatory subset of disease-associated-microglia in Alzheimer's disease*. *Molecular Neurodegeneration*, 2018. **13**(1): p. 24.
28. Au - Sarkar, S., et al., *Rapid and Refined CD11b Magnetic Isolation of Primary Microglia with Enhanced Purity and Versatility*. *JoVE*, 2017(122): p. e55364.
29. Giulian, D. and T.J. Baker, *Characterization of amoeboid microglia isolated from developing mammalian brain*. *J Neurosci*, 1986. **6**(8): p. 2163-78.
30. Bohlen, C.J., et al., *Diverse requirements for microglial survival, specification, and function revealed by defined-medium cultures*. *Neuron*, 2017. **94**(4): p. 759-773. e8.
31. Chhor, V., et al., *Characterization of phenotype markers and neuronotoxic potential of polarised primary microglia in vitro*. *Brain Behav Immun*, 2013. **32**: p. 70-85.
32. Blasi, E., et al., *Immortalization of murine microglial cells by a v-raf / v-myc carrying retrovirus*. *Journal of Neuroimmunology*, 1990. **27**(2): p. 229-237.
33. Henn, A., et al., *The suitability of BV2 cells as alternative model system for primary microglia cultures or for animal experiments examining brain inflammation*. *Altex*, 2009. **26**(2): p. 83-94.

34. Moss, D.W. and T.E. Bates, *Activation of murine microglial cell lines by lipopolysaccharide and interferon- $\gamma$  causes NO-mediated decreases in mitochondrial and cellular function*. European Journal of Neuroscience, 2001. **13**(3): p. 529-538.
35. Liu, Y., et al., *Beta-amyloid activates NLRP3 inflammasome via TLR4 in mouse microglia*. Neuroscience Letters, 2020. **736**: p. 135279.
36. Lu, W., Z. Chen, and J. Wen, *Flavonoids and ischemic stroke-induced neuroinflammation: Focus on the glial cells*. Biomedicine & Pharmacotherapy, 2024. **170**: p. 115847.
37. Singh, N., et al., *BACE-1 inhibition facilitates the transition from homeostatic microglia to DAM-1*. Sci Adv, 2022. **8**(24): p. eabo1286.
38. Horvath, R.J., et al., *Differential migration, LPS-induced cytokine, chemokine, and NO expression in immortalized BV-2 and HAPI cell lines and primary microglial cultures*. Journal of Neurochemistry, 2008. **107**(2): p. 557-569.
39. Lloyd, A.F., et al., *Deep proteomic analysis of human microglia and model systems reveal fundamental biological differences of *in vitro* and *ex vivo* cells*. bioRxiv, 2022: p. 2022.07.07.498804.
40. Sarkar, S., et al., *Characterization and comparative analysis of a new mouse microglial cell model for studying neuroinflammatory mechanisms during neurotoxic insults*. NeuroToxicology, 2018. **67**: p. 129-140.
41. Halle, A., et al., *The NALP3 inflammasome is involved in the innate immune response to amyloid- $\beta$* . Nature Immunology, 2008. **9**(8): p. 857-865.
42. Sarkar, S., et al., *Molecular Signatures of Neuroinflammation Induced by  $\alpha$ Synuclein Aggregates in Microglial Cells*. Frontiers in Immunology, 2020. **11**.
43. Janabi, N., et al., *Establishment of human microglial cell lines after transfection of primary cultures of embryonic microglial cells with the SV40 large T antigen*. Neurosci Lett, 1995. **195**(2): p. 105-8.
44. Etemad, S., et al., *A novel in vitro human microglia model: characterization of human monocyte-derived microglia*. J Neurosci Methods, 2012. **209**(1): p. 79-89.
45. Muffat, J., et al., *Efficient derivation of microglia-like cells from human pluripotent stem cells*. Nat Med, 2016. **22**(11): p. 1358-1367.
46. Monzón-Sandoval, J., et al., *Lipopolysaccharide distinctively alters human microglia transcriptomes to resemble microglia from Alzheimer's disease mouse models*. Disease Models & Mechanisms, 2022. **15**(10).
47. Haenseler, W., et al., *A Highly Efficient Human Pluripotent Stem Cell Microglia Model Displays a Neuronal-Co-culture-Specific Expression Profile and Inflammatory Response*. Stem Cell Reports, 2017. **8**(6): p. 1727-1742.
48. Xu, R., et al., *Human iPSC-derived mature microglia retain their identity and functionally integrate in the chimeric mouse brain*. Nat Commun, 2020. **11**(1): p. 1577.
49. Hedegaard, A., et al., *Honing the Double-Edged Sword: Improving Human iPSC-Microglia Models*. Front Immunol, 2020. **11**: p. 614972.
50. Batista, C.R.A., et al., *Lipopolysaccharide-Induced Neuroinflammation as a Bridge to Understand Neurodegeneration*. Int J Mol Sci, 2019. **20**(9).
51. Okun, E., et al., *Toll-like receptors in neurodegeneration*. Brain Res Rev, 2009. **59**(2): p. 278-92.
52. Zhan, X., et al., *Gram-negative bacterial molecules associate with Alzheimer disease pathology*. Neurology, 2016. **87**(22): p. 2324-2332.
53. Hickman, S., et al., *Microglia in neurodegeneration*. Nature Neuroscience, 2018. **21**(10): p. 1359-1369.
54. Song, W.M. and M. Colonna, *The identity and function of microglia in neurodegeneration*. Nature Immunology, 2018. **19**(10): p. 1048-1058.

55. Ising, C., et al., *NLRP3 inflammasome activation drives tau pathology*. Nature, 2019. **575**(7784): p. 669-673.
56. Gustin, A., et al., *NLRP3 Inflammasome Is Expressed and Functional in Mouse Brain Microglia but Not in Astrocytes*. PLOS ONE, 2015. **10**(6): p. e0130624.
57. Asai, H., et al., *Depletion of microglia and inhibition of exosome synthesis halt tau propagation*. Nat Neurosci, 2015. **18**(11): p. 1584-93.
58. Al Mamun, A., et al., *Interferon regulatory factor 4/5 signaling impacts on microglial activation after ischemic stroke in mice*. European Journal of Neuroscience, 2018. **47**(2): p. 140-149.
59. Qin, C., et al., *Dual Functions of Microglia in Ischemic Stroke*. Neuroscience Bulletin, 2019. **35**(5): p. 921-933.
60. Qin, C., et al., *Fingolimod Protects Against Ischemic White Matter Damage by Modulating Microglia Toward M2 Polarization via STAT3 Pathway*. Stroke, 2017. **48**(12): p. 3336-3346.
61. Song, S., et al., *Selective role of Na(+)/H(+) exchanger in Cx3cr1(+) microglial activation, white matter demyelination, and post-stroke function recovery*. Glia, 2018. **66**(11): p. 2279-2298.
62. De Strooper, B. and E. Karran, *The Cellular Phase of Alzheimer's Disease*. Cell, 2016. **164**(4): p. 603-15.
63. Jack, C.R., Jr., et al., *Tracking pathophysiological processes in Alzheimer's disease: an updated hypothetical model of dynamic biomarkers*. Lancet Neurol, 2013. **12**(2): p. 207-16.
64. Braak, H. and K. Del Tredici, *The pathological process underlying Alzheimer's disease in individuals under thirty*. Acta Neuropathologica, 2011. **121**(2): p. 171-181.
65. Yasuno, F., et al., *Increased binding of peripheral benzodiazepine receptor in mild cognitive impairment-dementia converters measured by positron emission tomography with [<sup>11</sup>C]DAA1106*. Psychiatry Res, 2012. **203**(1): p. 67-74.
66. Gray, S.C., K.J. Kinghorn, and N.S. Woodling, *Shifting equilibriums in Alzheimer's disease: the complex roles of microglia in neuroinflammation, neuronal survival and neurogenesis*. Neural Regen Res, 2020. **15**(7): p. 1208-1219.
67. Smith, A.M., et al., *Diverse human astrocyte and microglial transcriptional responses to Alzheimer's pathology*. Acta Neuropathol, 2022. **143**(1): p. 75-91.
68. Yin, Z., et al., *Immune hyperreactivity of Aβ plaque-associated microglia in Alzheimer's disease*. Neurobiology of Aging, 2017. **55**: p. 115-122.
69. Zhou, Y., et al., *Human and mouse single-nucleus transcriptomics reveal TREM2-dependent and TREM2-independent cellular responses in Alzheimer's disease*. Nat Med, 2020. **26**(1): p. 131-142.
70. Krasemann, S., et al., *The TREM2-APOE Pathway Drives the Transcriptional Phenotype of Dysfunctional Microglia in Neurodegenerative Diseases*. Immunity, 2017. **47**(3): p. 566-581.e9.
71. Griciuc, A., et al., *Alzheimer's disease risk gene CD33 inhibits microglial uptake of amyloid beta*. Neuron, 2013. **78**(4): p. 631-43.
72. Rangaraju, S., et al., *Potassium Channel Kv1.3 Is Highly Expressed by Microglia in Human Alzheimer's Disease*. Journal of Alzheimer's Disease, 2015. **44**: p. 797-808.
73. Sunna, S., et al., *Advances in proteomic phenotyping of microglia in neurodegeneration*. Proteomics, 2023. **23**(13-14): p. e2200183.
74. Oakley, H., et al., *Intraneuronal beta-amyloid aggregates, neurodegeneration, and neuron loss in transgenic mice with five familial Alzheimer's disease mutations: potential factors in amyloid plaque formation*. J Neurosci, 2006. **26**(40): p. 10129-40.
75. Jankowsky, J.L., et al., *Mutant presenilins specifically elevate the levels of the 42 residue beta-amyloid peptide in vivo: evidence for augmentation of a 42-specific gamma secretase*. Hum Mol Genet, 2004. **13**(2): p. 159-70.
76. Boza-Serrano, A., et al., *Innate immune alterations are elicited in microglial cells before plaque deposition in the Alzheimer's disease mouse model 5xFAD*. Scientific Reports, 2018. **8**(1): p. 1550.

77. Althafar, Z.M., *Targeting Microglia in Alzheimer's Disease: From Molecular Mechanisms to Potential Therapeutic Targets for Small Molecules*. *Molecules*, 2022. **27**(13).
78. Lian, H., et al., *NFκB-activated astroglial release of complement C3 compromises neuronal morphology and function associated with Alzheimer's disease*. *Neuron*, 2015. **85**(1): p. 101-115.
79. Shi, Q., et al., *Complement C3 deficiency protects against neurodegeneration in aged plaque-rich APP/PS1 mice*. *Sci Transl Med*, 2017. **9**(392).
80. Srinivasan, K., et al., *Alzheimer's Patient Microglia Exhibit Enhanced Aging and Unique Transcriptional Activation*. *Cell Rep*, 2020. **31**(13): p. 107843.
81. Deczkowska, A., et al., *Disease-Associated Microglia: A Universal Immune Sensor of Neurodegeneration*. *Cell*, 2018. **173**(5): p. 1073-1081.
82. Rangaraju, S., et al., *Kv1.3 potassium channels as a therapeutic target in multiple sclerosis*. *Expert Opinion on Therapeutic Targets*, 2009. **13**(8): p. 909-924.
83. Sarkar, S., et al., *Kv1.3 modulates neuroinflammation and neurodegeneration in Parkinson's disease*. *The Journal of Clinical Investigation*, 2020. **130**(8): p. 4195-4212.
84. Gao, T., et al., *Temporal profiling of Kv1.3 channel expression in brain mononuclear phagocytes following ischemic stroke*. *Journal of Neuroinflammation*, 2019. **16**(1): p. 116.
85. Ramesha, S., et al., *Unique molecular characteristics and microglial origin of Kv1.3 channel-positive brain myeloid cells in Alzheimer's disease*. *Proceedings of the National Academy of Sciences*, 2021. **118**(11): p. e2013545118.
86. Chen, X., et al., *Structure of the full-length Shaker potassium channel Kv1.2 by normal-mode-based X-ray crystallographic refinement*. *Proc Natl Acad Sci U S A*, 2010. **107**(25): p. 11352-7.
87. Long, S.B., et al., *Atomic structure of a voltage-dependent K<sup>+</sup> channel in a lipid membrane-like environment*. *Nature*, 2007. **450**(7168): p. 376-382.
88. Selvakumar, P., et al., *Structures of the T cell potassium channel Kv1.3 with immunoglobulin modulators*. *Nature Communications*, 2022. **13**(1): p. 3854.
89. Pérez-Verdaguer, M., et al., *Caveolin interaction governs Kv1.3 lipid raft targeting*. *Scientific Reports*, 2016. **6**(1): p. 22453.
90. Marks, D.R. and D.A. Fadool, *Post-synaptic density perturbs insulin-induced Kv1.3 channel modulation via a clustering mechanism involving the SH3 domain*. *J Neurochem*, 2007. **103**(4): p. 1608-27.
91. Doczi, M.A., D.H. Damon, and A.D. Morielli, *A C-terminal PDZ binding domain modulates the function and localization of Kv1.3 channels*. *Exp Cell Res*, 2011. **317**(16): p. 2333-41.
92. Chun, B.J., et al., *Simulation of P2X-mediated calcium signalling in microglia*. *The Journal of Physiology*, 2019. **597**(3): p. 799-818.
93. Nguyen, H.M., et al., *Biophysical basis for Kv1.3 regulation of membrane potential changes induced by P2X4-mediated calcium entry in microglia*. *Glia*, 2020.
94. Capera, J., et al., *The Mitochondrial Routing of the Kv1.3 Channel*. *Frontiers in oncology*, 2022. **12**: p. 865686-865686.
95. Pérez-García, M.T., P. Ciudad, and J.R. López-López, *The secret life of ion channels: Kv1.3 potassium channels and proliferation*. *American Journal of Physiology-Cell Physiology*, 2018. **314**(1): p. C27-C42.
96. Szabò, I., et al., *A novel potassium channel in lymphocyte mitochondria*. *J Biol Chem*, 2005. **280**(13): p. 12790-8.
97. Gulbins, E., et al., *Role of Kv1.3 mitochondrial potassium channel in apoptotic signalling in lymphocytes*. *Biochim Biophys Acta*, 2010. **1797**(6-7): p. 1251-9.
98. Styles, F.L., et al., *Kv1.3 voltage-gated potassium channels link cellular respiration to proliferation through a non-conducting mechanism*. *Cell Death Dis*, 2021. **12**(4): p. 372.

99. Upadhyay, S.K., et al., *Selective Kv1.3 channel blocker as therapeutic for obesity and insulin resistance*. Proc Natl Acad Sci U S A, 2013. **110**(24): p. E2239-48.
100. Xu, J., et al., *The voltage-gated potassium channel Kv1.3 regulates energy homeostasis and body weight*. Human Molecular Genetics, 2003. **12**(5): p. 551-559.
101. Fadool, D.A., K. Tucker, and P. Pedarzani, *Mitral Cells of the Olfactory Bulb Perform Metabolic Sensing and Are Disrupted by Obesity at the Level of the Kv1.3 Ion Channel*. PLOS ONE, 2011. **6**(9): p. e24921.
102. Fadool, D., et al., *Kv1.3 channel gene-targeted deletion produces "Super-Smeller Mice" with altered glomeruli, interacting scaffolding proteins, and biophysics*. Neuron, 2004. **41**(3): p. 389-404.
103. Levite, M., et al., *Extracellular K<sup>+</sup> and Opening of Voltage-Gated Potassium Channels Activate T Cell Integrin Function: Physical and Functional Association between Kv1.3 Channels and  $\beta$ 1 Integrins*. Journal of Experimental Medicine, 2000. **191**(7): p. 1167-1176.
104. Toldi, G., et al., *The effects of Kv1.3 and IKCa1 potassium channel inhibition on calcium influx of human peripheral T lymphocytes in rheumatoid arthritis*. Immunobiology, 2013. **218**(3): p. 311-316.
105. Zhu, J., et al., *T-lymphocyte Kv1.3 channel activation triggers the NLRP3 inflammasome signaling pathway in hypertensive patients*. Exp Ther Med, 2017. **14**(1): p. 147-154.
106. Vicente, R., et al., *Association of Kv1.5 and Kv1.3 Contributes to the Major Voltage-dependent K<sup>+</sup> Channel in Macrophages \**. Journal of Biological Chemistry, 2006. **281**(49): p. 37675-37685.
107. Olivencia, M.A., et al., *KV1.3 channels are novel determinants of macrophage-dependent endothelial dysfunction in angiotensin II-induced hypertension in mice*. British Journal of Pharmacology, 2021. **178**(8): p. 1836-1854.
108. Kan, X.-H., et al., *Kv1.3 potassium channel mediates macrophage migration in atherosclerosis by regulating ERK activity*. Archives of Biochemistry and Biophysics, 2016. **591**: p. 150-156.
109. Schmidt, K., et al., *Heterogeneous expression of voltage-gated potassium channels of the shaker family (Kv1) in oligodendrocyte progenitors*. Brain Research, 1999. **843**(1): p. 145-160.
110. Liu, H., et al., *IL-17 Inhibits Oligodendrocyte Progenitor Cell Proliferation and Differentiation by Increasing K<sup>+</sup> Channel Kv1.3*. Frontiers in Cellular Neuroscience, 2021. **15**.
111. Liu, H., et al., *Human immunodeficiency virus protein Tat induces oligodendrocyte injury by enhancing outward K<sup>+</sup> current conducted by KV1.3*. Neurobiology of Disease, 2017. **97**: p. 1-10.
112. Zhu, J., J. Yan, and W.B. Thornhill, *The Kv1.3 potassium channel is localized to the cis-Golgi and Kv1.6 is localized to the endoplasmic reticulum in rat astrocytes*. The FEBS Journal, 2014. **281**(15): p. 3433-3445.
113. Bozic, I., et al., *Voltage Gated Potassium Channel Kv1.3 Is Upregulated on Activated Astrocytes in Experimental Autoimmune Encephalomyelitis*. Neurochemical Research, 2018. **43**(5): p. 1020-1034.
114. Kotecha, S.A. and L.C. Schlichter, *A Kv1.5 to Kv1.3 Switch in Endogenous Hippocampal Microglia and a Role in Proliferation*. The Journal of Neuroscience, 1999. **19**(24): p. 10680-10693.
115. Pannasch, U., et al., *The potassium channels Kv1.5 and Kv1.3 modulate distinct functions of microglia*. Molecular and Cellular Neuroscience, 2006. **33**(4): p. 401-411.
116. Anton, R., et al., *Potassium Channels Kv1.3 and Kir2.1 But Not Kv1.5 Contribute to BV2 Cell Line and Primary Microglial Migration*. International Journal of Molecular Sciences, 2021. **22**(4): p. 2081.
117. Rangaraju, S., et al., *A systems pharmacology-based approach to identify novel Kv1.3 channel-dependent mechanisms in microglial activation*. Journal of Neuroinflammation, 2017. **14**(1): p. 128.

118. Fordyce, C.B., et al., *Microglia Kv1.3 channels contribute to their ability to kill neurons*. J Neurosci, 2005. **25**(31): p. 7139-49.
119. Di Lucente, J., et al., *The voltage-gated potassium channel Kv1.3 is required for microglial pro-inflammatory activation in vivo*. Glia, 2018. **66**(9): p. 1881-1895.
120. Gocke, A.R., et al., *Kv1.3 deletion biases T cells toward an immunoregulatory phenotype and renders mice resistant to autoimmune encephalomyelitis*. The Journal of Immunology, 2012. **188**(12): p. 5877-5886.
121. Pennington, M., et al., *Development of Highly Selective Kv1.3-Blocking Peptides Based on the Sea Anemone Peptide ShK*. Marine Drugs, 2015. **13**(1): p. 529-542.
122. Schmitz, A., et al., *Design of PAP-1, a Selective Small Molecule Kv1.3 Blocker, for the Suppression of Effector Memory T Cells in Autoimmune Diseases*. Molecular Pharmacology, 2005. **68**(5): p. 1254-1270.
123. Lai, I.K., et al., *Blocking Kv1.3 potassium channels prevents postoperative neuroinflammation and cognitive decline without impairing wound healing in mice*. British Journal of Anaesthesia, 2020. **125**(3): p. 298-307.
124. Chen, Y.-J., et al., *Inhibition of the potassium channel Kv1.3 reduces infarction and inflammation in ischemic stroke*. Annals of Clinical and Translational Neurology, 2018. **5**(2): p. 147-161.
125. Bowlby, M.R., et al., *Modulation of the Kv1.3 Potassium Channel by Receptor Tyrosine Kinases*. Journal of General Physiology, 1997. **110**(5): p. 601-610.
126. Cho, K.F., et al., *Proximity labeling in mammalian cells with TurboID and split-TurboID*. Nature Protocols, 2020. **15**(12): p. 3971-3999.
127. Szabo, I., et al., *Mitochondrial potassium channel Kv1.3 mediates Bax-induced apoptosis in lymphocytes*. Proceedings of the National Academy of Sciences, 2008. **105**(39): p. 14861-14866.
128. Lauro, C. and C. Limatola, *Metabolic Reprogramming of Microglia in the Regulation of the Innate Inflammatory Response*. Frontiers in Immunology, 2020. **11**(493).
129. Maezawa, I., et al., *Kv1.3 inhibition as a potential microglia-targeted therapy for Alzheimer's disease: preclinical proof of concept*. Brain, 2017. **141**(2): p. 596-612.
130. Kaiser, T. and G. Feng, *Tmem119-EGFP and Tmem119-CreERT2 Transgenic Mice for Labeling and Manipulating Microglia*. eNeuro, 2019. **6**(4): p. ENEURO.0448-18.